

Oxidative stress-induced cell death in paediatric cancer cell lines

Dissertation

Zur Erlangung des Doktorgrades
der Naturwissenschaften

vorgelegt am Fachbereich 14
der Johann Wolfgang Goethe-Universität
in Frankfurt am Main

von

Jasmin Dächert
aus Seeheim-Jugenheim

Frankfurt am Main 2018

(D30)

vom Fachbereich 14 der

Johann Wolfgang Goethe-Universität als Dissertation angenommen.

Dekan: Prof. Dr. Clemens Glaubitz

Erster Gutachter: Prof. Dr. Volker Dötsch

Zweiter Gutachter: Prof. Dr. Simone Fulda

Datum der Disputation:

Table of contents

Table of contents	I
List of abbreviations	V
List of figures	X
List of tables	XII
1 Abstract	1
2 Introduction	3
2.1 Paediatric cancer entities	3
2.1.1 Acute lymphoblastic leukaemia	3
2.1.2 Rhabdomyosarcoma	4
2.2 Reactive oxygen species and oxidative stress	5
2.2.1 Sources of ROS	6
2.2.2 ROS detoxification systems	8
2.2.3 ROS-inducing compounds	9
2.2.4 ROS in cancer	10
2.3 Ferroptosis	11
3 Aim of the study	16
4 Materials and methods	17
4.1 Materials	17
4.1.1 Paediatric cell lines	17
4.1.2 Packaging cell lines	17
4.1.3 Primary acute lymphoblastic leukaemia samples	18
4.1.4 Cell culture materials	18
4.1.5 Cell death-inducing compounds	19
4.1.6 Cell death inhibitors, antioxidants and ROS scavengers	19
4.1.7 Fluorescent dyes used for FACS and microscope measurements	20
4.1.8 Plasmids	20
4.1.9 siRNA oligonucleotides	21
4.1.10 Primary western blot antibodies	21
4.1.11 Secondary western blot antibodies	21
4.1.12 Oligonucleotides for qRT-PCR	22
4.1.13 General reagents, chemicals, consumable material	22
4.1.14 Kits	25
4.1.15 Equipment	25
4.1.16 Software	27
4.2 Methods	28
4.2.1 Cell biology methods	28

4.2.1.1	Cell culture	28
4.2.1.2	Freezing and thawing of cells	28
4.2.1.3	Cell counting, seeding and treatment	28
4.2.1.4	Preparation of primary ALL cells	29
4.2.1.5	Retroviral transduction	29
4.2.1.6	Transient siRNA transfection.....	30
4.2.1.7	Determination of cell death using flow cytometry (forward/sideward scatter).....	30
4.2.1.8	Determination of cell death using PI-staining.....	31
4.2.1.9	Determination of caspase 3/7 activity	31
4.2.1.10	Determination of GSH depletion	31
4.2.1.11	Determination of cellular ROS production and lipid peroxidation ...	31
4.2.1.12	Determination of lipid peroxidation.....	32
4.2.2	Molecular biology methods	32
4.2.2.1	Cell lysis, SDS Page and western blot analysis.....	32
4.2.2.2	Isolation of RNA, cDNA synthesis and qRT-PCR	33
4.2.2.3	Statistical analysis	33
5	Results.....	34
5.1	Oxidative cell death in acute lymphoblastic leukaemia cells.....	34
5.1.1	Lipoxygenase inhibitors protect against ferroptotic cell death in acute lymphoblastic leukaemia cells.....	34
5.1.1.1	RSL3 induces cell death in ALL cells which can be classified as ferroptosis	34
5.1.1.2	RSL3-induced ferroptosis is independent of caspases and RIP1 ...	36
5.1.1.3	Lipoxygenases are involved in ferroptotic signalling	37
5.1.1.4	GPX4 protein levels are not affected by lipoxygenase inhibitors.....	38
5.1.1.5	Lipoxygenases are not regulated on mRNA level in ALL	39
5.1.2	RSL3 and Erastin differentially promote redox-based Smac mimetic-induced cell death.....	40
5.1.2.1	BV6 potentiates RSL3- and Erastin-induced cell death	40
5.1.2.2	RSL3/BV6- but not Era/BV6-induced cell death is iron-dependent .	41
5.1.2.3	Pharmacological and genetic inhibition of lipid peroxide formation rescue from RSL3/BV6- and Era/BV6-generated lipid peroxidation, whereby only RSL3/BV6-induced cell death is blocked	42
5.1.2.4	RSL3/BV6- or Era/BV6-induced cell death is independent of caspases, RIP1 and RIP3	44
5.1.2.5	α -Tocopherol depletes RSL3/BV6- and Era/BV6-generated ROS production, whereby Fer-1 only blocks RSL3/BV6-triggered ROS production	47
5.1.2.6	Erastin as single agent does not induce ferroptosis in ALL cells.....	48

5.1.2.7	RSL3 or Erastin cooperate with BV6 to generate ROS-dependent cell death in primary ALL blasts.....	49
5.2	Oxidative cell death in rhabdomyosarcoma cells.....	51
5.2.1	Erastin induces cell death in several RMS cell lines	51
5.2.2	Erastin-induced cell death shows characteristic features of ferroptosis, which is blocked through the addition of NOX inhibitors.....	53
5.2.3	Erastin leads to GSH depletion, accompanied by ROS and lipid peroxide formation	55
5.2.4	Erastin-induced ROS production and lipid peroxidation is decreased through ferroptosis and NOX inhibitors	57
5.2.5	Genetic silencing of NOX4 rescues from Erastin-induced cell death.....	59
5.2.6	Bim1, a broad PKC inhibitor, decreases Erastin-induced cell death, ROS accumulation and lipid peroxidation	60
5.2.7	The α and β selective PKC inhibitor Gö6976 reduces Erastin-induced cell death and lipid peroxidation.....	62
5.2.8	Genetic silencing of PKC α attenuates Erastin-triggered cell death	64
6	Discussion.....	65
6.1	Oxidative cell death mechanisms in ALL cells	65
6.1.1	Lipoxygenases are involved in ROS-mediated ferroptotic signalling upon RSL3 stimulation in ALL cells	65
6.1.1.1	Specific activation of LOX remains unclear in ALL	65
6.1.1.2	LOX play a central role in cell death mechanisms, especially in ferroptosis	66
6.1.2	RSL3 and Erastin in combination with BV6 differentially modulate ROS-induced cell death in ALL cells.....	68
6.1.2.1	Erastin and RSL3 differ in their mode of action	69
6.1.2.2	Era/BV6 does not trigger ferroptosis, neither apoptosis nor necroptosis.....	70
6.1.2.3	Possible modulators of Erastin-induced cell death in ALL cells which negatively regulate ferroptosis onset	70
6.2	RMS cells display classical features of ferroptosis.....	72
6.2.1	Ferroptosis sensitivity is independent on RAS and xCT expression level..	72
6.2.2	NOX are involved in ferroptosis as a ROS-generating enzyme	73
6.2.3	The activation of NOX in RMS remains unclear	74
6.2.4	PKC, an upstream regulator of NOX, are involved in ferroptotic signalling in RMS.....	75
6.2.5	Different PKC might be differently activated through Erastin-induced ROS in RMS	75
7	Outlook.....	79
8	Deutsche Zusammenfassung	80

References	88
Appendix	102
Acknowledgement	106
Eidesstattliche Versicherung	107
Curriculum Vitae	108

List of abbreviations

AA	Arachidonic acid
AIF	Apoptosis inducing factor
ALL	Acute lymphoblastic leukaemia
APS	Ammonium persulphate
aRMS	Alveolar rhabdomyosarcoma
ATCC	American type culture collection
α -TOC	α -Tocopherol
Bai	Baicalein
BCA	Bicinchoninic acid
BHA	Butylated hydroxyanisole
Bim1	Bisindolylmaleimide I
BSA	Bovine serum albumin
BSO	L-Buthionine-S,R-sulphoximine
cAMP	Cyclic adenosine monophosphate
COX	Cyclooxygenase
Cys	Cysteine
Cu	Copper
DAG	Diacylglycerol
DFO	Deferoxamine
DMEM medium	Dulbecco's modified eagle medium
DMSO	Dimethyl sulphoxide
DNA	Deoxyribonucleic acid
DPI	Diphenyleneiodonium
DSMZ	Deutsche Sammlung
DTT	Dithiothreitol
e.g.	Exempli gratia (latin) for example
ECL	Enhanced chemiluminescence
EDTA	Ethylenediaminetetraacetate
ER	Endoplasmatic reticulum
Era	Erastin (eradicator of RAS and ST-ex-
ERK	Extracellular signal-regulated kinase
eRMS	Embryonal rhabdomyosarcoma
ETR2	Agonistic antibody against TRAIL recep-

EV	Empty vector
FACS	Fluorescent activated cell sorter
FADD	Fas associated death domain protein
FCS	Foetal calf serum
FDA	US food & drug Association
Fe ²⁺ /Fe ³⁺	Ferrous/ferric iron
Fer-1	Ferrostatin-1
FOXO1	Forkhead box protein O1
FSC	Forward scatter
GAPDH	Glyceraldehyde-3-phosphate dehydro-
GCL	Glutamate cysteine ligase
GPX	Glutathione peroxidase
GR	Glutathione reductase
GSS	Glutathione synthetase
GSH	Glutathione
GSSG	Glutathione disulphide
GST	Glutathione S-transferase
HCC	Hepatocellular carcinoma
HCL	Hydrogen chloride
HIF-1	Hypoxia-inducible factor 1
HPETE	Hydroperoxyeicosatetraenoic acid
H ₂ O ₂	Hydrogen peroxide
cm-H ₂ DCFDA	Chlormethylderivat- dichlordihydrofluo-
HEPES	Hydroxyethyl
HRP	Horseradish peroxidase
HS-	Thiol-
HSe-	Selenol-
HSP	Heat shock protein
IAP	Inhibitor of apoptosis
IRI	Ischemia-reperfusion injury
IGF-II	Insulin-like growth factor type II
Ig	Immunoglobulin
JCRB	Japanese collection of research bio re-
JNK	Jun N-terminal kinase
KCL	Potassium chloride

kDa	Kilodalton
Lip-1	Lipoxystatin-1
LOH	Loss of heterozygosity
LOX	Lipoxygenase
mA	Milliampere
MAPK	Mitogen-activated protein kinase
mg	Milligram
ml	Millilitre
mM	Millimolar
µg	Microgram
µl	Microliter
µM	Micromolar
Mn	Manganese
mRNA	Messenger ribonucleic acid
MVA	Mevalonic acid
N/A	Not available
NAC	N-acetylcysteine
NaCl	Sodium chloride
NaOH	Sodium hydroxide
NADPH	Nicotinamide adenine dinucleotide
NDGA	Nordihydroguaiaretic acid
Nec-1s	Necrostatin-1s
NFκβ	Nuclear factor 'kappa-light-chain-en-
NOX	NADPH oxidase
NO	Nitric oxid
NRF2	Nuclear factor erythroid 2-related factor
ns	Not significant
OH-	Hydroxide
OH·	Hydroxyl radical
O ₂ ⁻	Superoxide radical
O ₂ ⁻	Superoxide anion
PAX3	Paired box 3
PBS	Phosphate buffered saline
PCD	Programmed cell death
PCR	Polymerase chain reaction

PDGFR	Platelet-derived growth factor receptor
PE	Phosphatidylethanolamine
PEBP1	Phosphatidylethanolamine
pH	Potential of hydrogen
PI	Propidium iodide
PI3K	Phosphatidylinositol-4,5-bisphosphate
PKC	Protein kinase C
PLA ₂	Phospholipase A ₂
PMA	Phorbol 12-myristate 13-acetate
PMSF	Phenylmethylsulphonyl fluoride
PRX	Peroxiredoxin
PS	Phosphatidylserine
PTEN	Phosphatase and tensin homolog
PUFA	Polyunsaturated fatty acid
RIRR	ROS-induced ROS release
RCC	Renal cell carcinoma
RT	Room temperature
qRT-PCR	Quantitative real-time polymerase chain
RIP	Receptor-interacting protein kinase
RMS	Rhabdomyosarcoma
RNA	Ribonucleic acid
ROO·	Peroxy radical
ROOH	Lipid peroxide
ROH	Lipid alcohol
ROS	Reactive oxygen species
rpm	Rounds per minute
RPMI	Roswell park memorial institute medium
RSL3	RAS selective lethal 3
SAS	Sulfasalazine
SD	Standard deviation
SDS	Sodium dodecyl sulphate
Smac	Second mitochondrial activator of
SMP	Skim milk powder
-SO ₂ -	Sulphinic acid
-SO ₃ -	Sulphonic acid

SOD	Superoxide dismutase
SSC	Sideward scatter
TEMED	Tetramethylethylenediamine
TNF α	Tumour necrosis factor α
TFR1	transferrin receptor 1
TRX	Thioredoxin
TrxR	Thioredoxin reductase
V	Volt
VAC	Vincristine,
VDAC	Voltage dependent anion channel
VEGFR	Vascular endothelial growth factor re-
WB	Western blot
WT	Wildtype
X _c -	Cystine/glutamate antiporter
XO	Xanthine oxidase
Zil	Zileuton
Zn	Zinc
zVAD.fmk	Carbobenzoxy-valyl-alanyl-aspartyl-[O-

List of figures

Figure 1: Ferroptotic cell death pathway induced by Erastin or RSL3.....	12
Figure 2: Cell death kinetic upon RSL3 stimulus.	35
Figure 3: RSL3 stimulates ferroptosis in ALL.....	36
Figure 4: Caspases and RIP1 are not involved in ferroptosis.	37
Figure 5: LOX are involved in RSL3-triggered ferroptotic cell death.	38
Figure 6: LOX inhibitors do not affect GPX4 protein level.....	38
Figure 7: 15-LOX and 12-LOX mRNA levels are not affected by RSL3 stimulation. .	39
Figure 8: BV6 potentiates RSL3- and Erastin-induced cell death.	41
Figure 9: RSL3/BV6- but not Era/BV6-induced cell death is iron-dependent.	42
Figure 10: Fer-1 rescues from RSL3/BV6- and Era/BV6-generated lipid peroxidation, but it only prevents RSL3/BV6-induced cell death.....	43
Figure 11: GPX4 overexpression reduces RSL3/BV6- and Era/BV6-generated lipid peroxidation, but it only prevents RSL3/BV6-induced cell death.....	44
Figure 12: RSL3/BV6- or Era/BV6-triggered cell death is independent of caspases.	45
Figure 13: Era/BV6 cotreatment does not trigger RIP1-and RIP3-dependent necroptosis.....	46
Figure 14: α -Tocopherol depletes RSL3/BV6- and Era/BV6-generated ROS production, whereby Fer-1 only blocks RSL3/BV6-triggered ROS production.	48
Figure 15: Erastin as single agent does not trigger ferroptosis.	49
Figure 16: RSL3 or Erastin cooperate with BV6 to induce ROS-dependent cell death in primary ALL blasts.....	50
Figure 17: Erastin induces dose-dependent cell death in several RMS cells.	51
Figure 18: RMS display heterogeneous basal mRNA levels of xCT.	52
Figure 19: RMS show no correlation between sensitivity to ferroptosis and xCT expression.	53
Figure 20: Erastin-induced cell death can be characterized as ferroptosis, which is blocked through the addition of NOX inhibitors.....	53
Figure 21: Erastin-induced cell death can be characterized as ferroptosis, which is blocked through the addition of NOX inhibitors.....	54
Figure 22: RSL3-induced ferroptosis is suppressed by NOX inhibitor GKT137831. ...	55
Figure 23: Cell death kinetic upon Erastin stimulus.	56

Figure 24: Erastin leads to GSH depletion, accompanied by ROS and lipid peroxide formation.	57
Figure 25: Erastin-induced ROS production and lipid peroxidation is decreased through ferroptosis and NOX inhibitors.	58
Figure 26: Genetic silencing of NOX4 rescues from Erastin-induced cell death.	59
Figure 27: Bim1, a broad PKC inhibitor, decreases Erastin-induced cell death, ROS accumulation and lipid peroxidation.	61
Figure 28: PKC α is more abundantly expressed in RMS.	62
Figure 29: PKC α and β selective inhibitor Gö6976 reduces Erastin-induced cell death and lipid peroxidation, whereas it has only minor effect on ROS production.	63
Figure 30: Genetic silencing of PKC α attenuates Erastin triggered cell death in RMS.	64
Figure 31: Hypothetical scheme of the involvement of Lipoxygenases in ferroptotic cell death in ALL.	66
Figure 32: Hypothetical model of cell death induction upon RSL3/BV6 and Era/BV6 treatment in ALL.	69
Figure 33: Hypothetical model of Erastin-induced ferroptosis in RMS.	77
Figure 34: Detailed cell death induction of RMS after 24 hours of Erastin treatment.	102
Figure 35: Detailed cell death induction of RMS after 48 hours of Erastin treatment.	102
Figure 36: Statins do not induce ferroptosis.	103
Figure 37: Whitaferin A does not trigger classical ferroptosis.	103
Figure 38: Sorafenib and BV6 in combination stimulate oxidative stress that is independent of ferroptosis.	104
Figure 39: Different LOX inhibitors rescue from Erastin- and RSL3-induced ferroptosis in RMS.	104
Figure 40: PKC inhibitors rescue from Erastin-induced cell death in RH36.	105

List of tables

Table 1: Cell lines	17
Table 2: Packaging cell lines.....	17
Table 3: Primary ALL samples	18
Table 4: Cell culture materials.....	18
Table 5: Cell death-inducing compounds	19
Table 6: Cell death inhibitors, antioxidants and ROS scavenger	19
Table 7: Fluorescent dyes used for FACS and microscope measurements.....	20
Table 8: Plasmids	20
Table 9: siRNA oligonucleotides.....	21
Table 10: Primary western blot antibodies.....	21
Table 11: Secondary western blot antibodies	21
Table 12: Oligonucleotides for qRT-PCR	22
Table 13: General reagents, chemicals, consumable material	22
Table 14: Kits	25
Table 15: Equipment.....	25
Table 16: Software	27

1 Abstract

Reactive oxygen species (ROS) are involved in various signalling mechanisms. Redox homeostasis is important in cancer cells, since they are dependent on upregulated antioxidant defence pathways to cope with elevated ROS levels. Therefore, targeting the antioxidant defence system and/ or increasing ROS to a lethal level may be a feasible strategy to counteract cancer cell progression.

Acute lymphoblastic leukaemia (ALL) is the most frequent malignant childhood cancer, displaying on one side resistance to cell death induction and on the other side elevated ROS levels. Therefore, inducing ferroptosis, a ROS- and iron-dependent cell death pathway might be useful to trigger cell death in ALL as a novel treatment strategy. In the first study of this thesis we observed that RSL3, a glutathione (GSH) peroxidase 4 (GPX4) inhibitor, triggered ROS accumulation and lipid peroxidation which contributed to ferroptotic cell death. These observations were based on suppression of RSL3-stimulated cell death using different ferroptosis inhibitors like Ferrostatin-1 (Fer-1), Lipoxstatin-1 (Lip-1), as well as iron chelator Deferoxamine (DFO) and the vitamin E derivate α -Tocopherol (α -Toc). RSL3-triggered ROS and lipid peroxide production were also inhibited through Fer-1 and α -Toc. Furthermore, lipoxygenases (LOX) were activated upon RSL3 stimulation and contributed to ferroptotic cell death in ALL as well. Selective inhibition of LOX with the 12/15-LOX inhibitor Baicalein and the pan-LOX inhibitor nordihydroguaiaretic acid (NDGA) abolished RSL3-induced ROS production, lipid peroxidation and cell death. In addition, RSL3 induced lipid peroxide-dependent ferroptotic cell death in FAS-associated Death Domain (FADD)-deficient, death receptor-induced apoptosis resistant cells, demonstrating that ferroptosis might circumvent apoptosis resistance.

The second part of the study revealed that RSL3 and Erastin (Era), a GSH-depleting agent, inhibiting the cystine/glutamate antiporter system x_c^- and ferroptosis inducer, cooperated with the Smac mimetic BV6 to trigger cell death in ALL cells. RSL3/BV6 and Era/BV6 combination-induced cell death was dependent on ROS accumulation, but independent of caspases and key modulators of necroptosis. RSL3/BV6-treated ALL cells exhibited classical features of ferroptotic cell death with iron-dependency, ROS accumulation and lipid peroxidation which was diminished through either pharmacological inhibition (Fer-1, DFO, α -Toc) or genetic inhibition by overexpressing GPX4. Interestingly, Era/BV6-induced cell death in ALL cells was independent of iron

but dependent on ROS accumulation, since α -Toc rescued from Era/BV6-triggered ROS production, lipid peroxidation and cell death. Moreover, inhibition of lipid peroxide formation through the addition of Fer-1 or by overexpressing GPX4 failed to rescue from Era/BV6-triggered cell death, even if Era/BV6-stimulated lipid peroxidation was diminished. Likewise, Fer-1 protected from RSL3/BV6-, but not from Era/BV6-generated ROS production, leading to the assumption that other ROS besides lipid-based ROS contributed to cell death in Era/BV6-treated cells. In summary, while RSL3/BV6 induced ferroptosis in ALL, Era/BV6 stimulated a ROS-dependent cell death, which was neither dependent on iron nor caspases or receptor-interacting protein (RIP) kinase 1 nor 3. Additionally, using Erastin alone did not trigger ferroptotic cell death in ALL. Finally, with these two studies we tried to unravel the molecular pathway of ferroptosis by using RSL3 and Erastin as well described ferroptosis stimulators. Here, we demonstrate the possibility of a novel treatment strategy to reactivate programmed cell death by impeding redox homeostasis in ALL.

Since ALL failed to induce ferroptosis upon Erastin treatment, we investigated in the third part of this thesis a new model system to induce ferroptosis upon Erastin and RSL3 exposure. Previous studies revealed that rhabdomyosarcoma (RMS) cells might be susceptible to oxidative stress-induced compounds. To this end, we used Erastin as a prototypic ferroptosis stimulus and GSH-depleting agent and demonstrated that GSH depletion, ROS and lipid ROS accumulation contributed to cell death. Additionally, Fer-1, Lip-1, DFO, lipophilic vitamin E derivate α -Toc and GSH, a cofactor of GPX4, protected from Erastin-stimulated ROS accumulation, lipid peroxidation and cell death. Also, the use of a broad spectrum protein kinase C (PKC) inhibitor Bisindolylmaleimide I (Bim1), a PKC α and β selective inhibitor Gö6976 and siRNA-mediated knockdown of PKC α suppressed Erastin-mediated cell death in RMS. Moreover broad spectrum nicotinamide-adenine dinucleotide phosphate (NADPH) oxidase (NOX) inhibitor Diphenyleneiodonium (DPI) and a more selective NOX1/4 isoform inhibitor GKT137831 abrogated Erastin-generated ROS formation, lipid peroxidation and cell death. With this, we demonstrate that RMS are vulnerable to ferroptotic cell death and investigated the molecular mechanism of ferroptosis by unravelling that PKC and NOX could have a pivotal role in ROS-mediated ferroptosis signalling in RMS. In this regard, ferroptosis inducers may act as a possible novel treatment strategy for RMS, especially those with poor clinical outcome.

2 Introduction

2.1 Paediatric cancer entities

Cancer can emerge when cellular homeostasis of proliferation and cell death is disturbed [1]. In almost every part of the body, cancer can arise with unique features and hallmarks [2]. Within these unique features, it is difficult to treat cancer cells. Most anti-cancer therapies work by inducing cell death or direct toxicity, which might also affect normal cells [1]. Therefore, more specific treatment options are needed.

2.1.1 Acute lymphoblastic leukaemia

Acute lymphoblastic leukaemia mostly occurs in children under the age of 15, with an incidence of 75-80% [3]. The development and cause are described to be dependent on genetic and environmental factors, whereas the precise mechanism has not been unravelled yet [4, 5]. It is considered that genetic alterations and mutations like leukaemia-specific fusion genes, hyper- and hypodiploidy, immunoglobulins (Ig) or rearrangements of clonal Ig, affect lymphoid progenitor cells, leading to a disruption of differentiation, proliferation and self-renewal [4-6].

ALL can be clustered into different subtypes that differ in pathogenic characteristics, treatment response, risk of relapse and putative clinical outcome, making this disease relative heterogeneous [4, 7]. Two major categories are identified based on cellular origin, the precursor B cell acute lymphoblastic leukaemia (B-ALL) and the precursor T cell acute lymphoblastic leukaemia (T-ALL) [8].

Treatment strategies include the administration of chemotherapeutics like doxorubicin, vincristine or L-asparaginase in combination with glucocorticoids or haematopoietic stem-cell transplantation [4].

In the last decades, the overall survival rate of paediatric ALL has increased in a way that 90% of patients with a good prognosis are cured over the long term [4, 9]. Despite improvements, there are still cases of relapsed ALL and very high risk groups with poor prognosis, demanding for new treatment options [6, 10].

2.1.2 Rhabdomyosarcoma

Rhabdomyosarcoma is a malignant tumour that is considered to arise from mesenchymal progenitor cells and displays the most common paediatric soft tissue sarcoma, whereas it is very uncommon in adults [11-13]. RMS was first described in 1946 by Stout et al., whereas it is considered that about 100 years ago Weber already described the occurrence of RMS [14, 15].

Because mesenchymal cells occur everywhere in the body, RMS can develop in almost every organ. The most common areas of RMS development are the head and neck region (about 40% of all cases), followed by the genitourinary tract (about 25%), the extremities (about 20%) and other sites like the chest wall and retroperitoneum [13, 16-18]. The majority of RMS occur sporadically, but some cases are characterized by genetic risk factors [19, 20] and/or by the overexpression of insulin-like growth factor II (IGFII) [21].

RMS can be divided into two subtypes, the most common embryonal (eRMS, approximately 75% of all cases) subtype and the less common, but more aggressive alveolar subtype (aRMS, about 20-25% of all cases) [22]. Some cases cannot be clustered to either subtype and are considered therefore as “undifferentiated” [13, 18, 23]. These subtypes exhibit distinct genetic alterations and characteristics as prognostic markers. Loss of heterozygosity (LOH) at chromosome locus 11p15 is a hallmark of eRMS, leading to an enhancement of the insulin-like growth factor type II gene (IGFII) that promotes eRMS progression [24, 25]. Additionally, mutations of p53 and the RAS pathway are also associated with eRMS and poorer prognosis [26, 27]. This type of tumour often occurs in younger children, mostly in the head and neck region and the genitourinary tract [16]. On the other side, aRMS subtype is most frequent in adolescents where tumours can be frequently found in the extremities [23]. Genetic characteristic of aRMS is the translocation between chromosome 2 and 13 and 1 and 14, referred as $t(2;13)(q35;q14)$ and $t(1;13)(p36;q14)$, resulting in a fusion gene of paired box 3 and 7 (*PAX3/7*) and *FKHR*, member of the forkhead family of transcription factors, also known as forkhead box protein O1 (FOXO1). This translocation promotes the expression of a constitutively activated *PAX3/PAX7-FOXO1* fusion gene [28, 29]. Besides, aRMS lacking this fusion gene, called “fusion-negative” aRMS, are considered to have a better prognosis as “fusion-positive” aRMS [29, 30].

Treatment and prognosis of RMS largely depend on the age and onset of diagnosis, tumour size and side, the histological subtype and the absence or presence of metastasis [31]. Treatment protocols include chemotherapy, radiation and surgery [32]. The intermediate-risk groups which contains the majority of newly diagnosed RMS patients, receive a standard chemotherapy of three drugs, namely vincristine, actinomycin-D and cyclophosphamide (VAC) in combination with radiation [33]. The overall survival of this group comprises approximately between 50% and 70% at 5 years after diagnosis [31, 34]. In contrast, high-risk patients, including metastatic alveolar and embryonal subtypes, show dismal prognosis. The overall cure rate is only 25%, even with aggressive chemotherapy, surgery and radiation [31]. Therefore, new treatment options are necessary to increase the overall survival rate of RMS, especially of those with poor prognosis.

2.2 Reactive oxygen species and oxidative stress

Oxidative stress is characterized as an imbalance of ROS production and removal [35]. Cancer cells show increased levels of oxidative stress because of elevated aerobic glycolysis (Warburg effect) [36, 37]. ROS are also involved in processes of aging, cardiovascular and neurodegenerative diseases [38, 39].

In general, ROS summarize a class of oxygen-containing radical species that are produced after metabolic exploitation of oxygen. This class encompasses various radical and non-radical species, whereas the most physiologically important ROS are hydroxyl radicals ($\text{OH}\cdot$), superoxide anions ($\text{O}_2^{\cdot-}$) as well as non-radical hydrogen peroxide (H_2O_2) [40]. The role of ROS in signalling is quite diverse and complex.

At low level, ROS function as signalling molecules for proliferation and differentiation [41, 42]. Also, low to moderate ROS levels can promote tumour formation by modulating downstream signalling cascades that include redox-sensitive phosphatases and kinases which are involved in cell survival and growth, like kinases from the mitogen-activated protein kinase (MAPK) family such as Jun N-terminal kinase (JNK), p38 kinase and extracellular signal-regulated kinase (ERK) [43-46]. Furthermore, phosphatases, such as the tumour suppressor phosphatase and tensin homolog (PTEN) and protein tyrosine phosphatases (PTPs), are oxidized, leading to an inhibition of apoptosis and cancer progression [47-49]. Activation or oncogenic mutation of K-RAS is associated with ROS-dependent cancer progression [50], whereby activation of RAS can

be due to oxidation of Cys 118 [51]. This results in the activation of ROS-generating enzymes, e.g. NOX, or mitochondria [50, 52]. In addition, cysteine residues of proteins are susceptible for redox modification, for example H_2O_2 can oxidize cysteine residues of proteins which exist in physiological pH ($pK_a < 6$) as a redox sensitive thiolate anion residue (Cys-S⁻) within proteins [42, 49]. This oxidation leads to a conformational and functional change of targeted proteins by oxidizing the thiolate anion (Cys-S⁻) to its sulfenic form (Cys-SOH). In addition, cysteine residues can be modified via nitrosylation (Cys-SNO), glutathionylation (Cys-SG) or via intramolecular disulphide bonds (Cys-SSR) [42, 53].

However, high level of ROS causes cell death through cellular DNA [54], lipid [55] and protein damage [56]. Therefore, ROS production and detoxification pathways has to be tightly balanced.

2.2.1 Sources of ROS

ROS can be generated through endogenous cellular sources or through exogenous sources. The endogenous sources comprise non-enzymatic ROS generators like the mitochondria, endoplasmic reticulum (ER) and peroxisomes. Furthermore, several enzymes are known to induce ROS like NADPH oxidases, lipoxygenases, xanthine oxidases (XO) and cytochrome p450 [57].

One major cellular ROS source is represented by the mitochondrial electron transport chain (ECT). Through one-electron reduction of molecular oxygen, $O_2^{\cdot-}$ is mainly produced at complex I and III and released into the mitochondrial matrix and the intermembrane space during oxidative phosphorylation [58, 59]. Because of its short half-life, $O_2^{\cdot-}$ can react with nitric oxide (NO) to peroxynitrite ($ONOO_2^{\cdot-}$) or is converted to H_2O_2 via mitochondrial superoxide dismutases [58]. Thereafter, $O_2^{\cdot-}$ and the more stable H_2O_2 can then be released into the cytosol by volt-dependent anion channels (VDACs) [57, 60].

In the ER, ROS can be generated through disulphide bond generation when proteins are folded [61, 62]. In this process, protein disulphide isomerase (PDI) plays a crucial role [63]. ROS can be either produced in the ER through cyclooxygenases (COX) [64] or via cytochrome P450 monooxygenase [65].

Apart from COX, LOX generate ROS through oxidation of polyunsaturated fatty acids (PUFA) and arachidonic acid (AA) which is released in a phospholipase A2-dependent manner from membrane phospholipids [66]. This oxidation process results in bioactive lipid hydroperoxide (ROOH) formation, leukotriene and lipoxin generation [66, 67]. Extensive lipid peroxidation results in further ROS production, but also in membrane integrity and stability loss [68-70].

Lipid peroxides can likewise be generated non-enzymatically via Fenton reaction [71]. In this redox reaction, labile iron pools react with hydrogen peroxide or superoxide anion to highly reactive hydroxyl radicals ($\text{H}_2\text{O}_2 + \text{Fe}^{2+} \rightarrow \text{OH}^\cdot + \text{HO}^\cdot + \text{Fe}^{3+}$) [72].

Besides the ER, oxidases located in peroxisomes such as xanthine oxidases generate ROS as an enzymatic by-product in the process of β -oxidation of fatty acids [73, 74].

The family of NADPH oxidase are relevant enzymes that produce ROS as a sole function by using NADPH as an electron donor [75]. This family comprises seven homologous transmembrane proteins termed NOX1 to NOX5 and Duox1 and 2 [76] with binding sites for NADPH, FAD and heme [75]. In general, these enzymes are inactive as monomers [77]. To become catalytically active, all isoforms interact with one or more membrane and/or cytosolic proteins to more complex enzymatic systems [76]. To name a few, NOX1 to NOX4 bind to p22^{phox}, whereas Duox 1 and 2 are dependent on Duoxa1 and 2 and NOX5 homo- or oligomerize for proper function. The latter also require calcium for their activation [77]. Furthermore, NOX1 and 3 require activator proteins such as NOXA1 (or its homologous p67^{phox} for NOX2) and NOXO1 (or its homologous p47^{phox} and p40^{phox} for NOX2) and a small GTPase Rac [75]. In addition, phosphorylation of cellular subunits is implicated in activation processes of some NOX isoforms [78]. NOX4 also binds to possible regulatory elements like PolDip2 (polymerase delta interacting protein 2), PDI and tyrosine kinase substrate 4/5 SH3 domain (Tsks4/5), but it is mainly regulated via mRNA level [77, 79]. However, NOX4 differs from the other isoforms, because it is constitutively active [80], though the exact mechanism of regulation is still unclear [77]. ROS production with regard to the generated species differs between NOX isoforms. NOX4 mainly generates H_2O_2 , whereas the other isoforms produce $\text{O}_2^{\cdot-}$ [79]. Respective NOX isoforms are heterogeneously expressed in various tissues and in different cellular compartments [76].

On the other hand, smoking, alcohol, certain drugs, air pollution, ionizing radiation account for exogenous ROS sources [81, 82].

2.2.2 ROS detoxification systems

To avoid cellular damages by ROS production, redox homeostasis is balanced by ROS scavenging systems. Detoxification can be divided into non-enzymatic molecules, for example GSH, flavonoids, vitamin A, C, E and enzymatic ROS scavenger, which are described in detail in the following paragraph.

Superoxide dismutases (SOD) are located in the cytosol (Cu/ZnSOD, SOD-1), in the mitochondria (MnSOD, SOD-2) and at the extracellular matrix (SOD-3) [83]. By using specific metal ions like copper, zinc, manganese and iron as cofactors, SOD can catalyse the dismutation of $O_2^{\cdot-}$ to H_2O_2 [84]. The generated H_2O_2 is decomposed by catalases, glutathione peroxidases (GPX) and peroxiredoxins (PRX) [84].

Catalases are present in the cytosol and in peroxisomes, degrading H_2O_2 enzymatically to water without cofactors [37, 85].

Peroxiredoxins (PRX) can eliminate H_2O_2 to water through oxidation of redox sensitive cysteines in their active centre [86, 87]. The oxidation of the thiol to sulphenic acid leads to an inactivation which can be converted by a reducing cycle in which thioredoxin (TRX), thioredoxin reductase (TXNRD) and NADPH are involved [88]. The family of PRX comprises six isoforms which are distributed in different cellular compartments [89].

Glutathione peroxidase family members (GPX1-8) can also decompose H_2O_2 to water. In this process, GSH is oxidized to glutathione disulphide (GSSG), whereby GSSG is normalized to GSH by GSH reductase (GR) by using NADPH [86, 90]. In addition, different isoforms can be located in the cytosol, mitochondria and also in the nucleus [91]. Besides the other GPXs, GPX4 differs because of its monomeric structure and the function to reduce lipid hydroperoxides within membranes [91, 92].

The most abundant thiol containing tripeptide (γ -L-glutamyl-L-cysteinylglycine) and non-enzymatic ROS scavenger is GSH. Among acting as a cofactor, this small molecule with its active sulphhydryl group counteract oxygen-free radicals, such as $O_2^{\cdot-}$ and OH^{\cdot} [81, 93]. The synthesis of GSH is ensued by glutamate-cysteine ligase (GCL) and GSH synthetase (GSS) [93]. Another detoxification enzyme is glutathione-S-transferase (GST) which catalyses the conjugation of GSH to electrophilic substrates [94].

Vitamin E, C, A and selenium are important cellular non-enzymatic antioxidants like GSH [95, 96]. There are lipophilic antioxidants (vitamin E and β -carotene) and water-

soluble antioxidants (vitamin C) that reduce oxygen-free radicals and also lipid peroxides [97]. Selenium is a necessary component of ROS scavenging enzymes like GPX4 and TRX [98].

2.2.3 ROS-inducing compounds

Targeting oxidative stress is a promising target for cancer therapy. There are several opportunities to affect redox balance, for example by targeting one of the three major antioxidant defence systems, namely the GSH, TRX or catalase pathway. In our study we focused on the GSH detoxification pathway. Therefore this pathway is described in more detail in the following paragraph.

Erastin (eradicator of RAS and ST-expressing cells) was first identified by Dolma and colleagues in 2003 after a synthetic lethal compound screening. It was described to affect tumour cells harbouring oncogenic RAS and small T oncoprotein whereas isogenic non-malignant cells remain unaffected [99, 100]. Furthermore, Erastin is classified as a small molecule compound which stimulates an iron-dependent, non-apoptotic cell death designated as ferroptosis, by inhibiting the cystine/glutamate antiporter x_c^- in a potent and selective manner [101, 102]. In addition, a recent study investigated that Erastin irreversibly binds to the substrate-specific subunit xCT (SLC7A11) and thereby promoting its inactivation [103]. Inhibition of this antiporter leads to a drop in intracellular cystine which is necessary for GSH *de novo* synthesis [101, 104]. Also, analysis revealed that Erastin can also bind to the subunit SLC7A5 of system x_L [101] and mitochondrial voltage anion channels 2 and 3 [105]. Inhibition of VDAC2/3 results in a decreased transport of NADH into the mitochondria [106]. Moreover, a more water stable analogue of Erastin (piperazine Erastin (PE)) exhibits tumour reducing effects in xenograft tumour mouse models through the induction of ferroptosis [104] and is being used in clinical trials (ClinicalTrials.gov Identifier: NCT01695590).

(1S, 3R)-RSL (RSL3) (RAS Selective Lethal 3) is a small molecule compound which also exhibited selectivity against tumours bearing oncogenic RAS [100]. The mode of action is distinct from Erastin [100, 101]. RSL3 directly binds to the catalytically active selenocysteine of GPX4, leading to its inhibition and subsequent accumulation of lipid peroxides which stimulates ferroptosis [104]. Furthermore, RSL3 also prevents tumour growth in xenograft mouse models by inducing ferroptosis [104].

Sorafenib is a FDA approved multikinase inhibitor that targets multiple serine/threonine and tyrosine kinases. Besides the family of Raf kinases, Sorafenib also inhibits proangiogenic vascular endothelial growth factor receptor (VEGFR), tyrosine kinases and platelet-derived growth factor receptor- β (PDGFR- β) [107, 108]. It is used for patients who suffer from advanced renal cell carcinoma (RCC), unresectable hepatocellular carcinoma (HCC) [109, 110] and osteosarcoma [111]. Additionally, Sorafenib decreases tumour growth *in vitro* and *in vivo* by triggering ROS-dependent cell death [112]. Besides, Sorafenib is in phase III clinical trials in HCC [113] and in phase II osteosarcoma [114].

BV6 is a small molecule compound which mimics the function of endogenous second mitochondria-derived activator of caspases (Smac). In the cell, Smac blocks inhibitor of apoptosis (IAP) proteins [115]. BV6 is a bivalent Smac mimetic that targets x-linked inhibitor of apoptosis (XIAP) and cellular inhibitor of apoptosis proteins (cIAP) [115]. Therefore, XIAP mediated caspase inhibition is abolished, whereas cIAP1 and 2 are autoubiquitinated and degraded through the proteasome [116]. Moreover, some studies indicate that BV6 induces ROS-mediated cell death through various mechanisms [117, 118].

2.2.4 ROS in cancer

ROS have dual functions in cancer. On one side, ROS lead to cancer initiation and progression, but on the other side increased oxidant generation can counteract tumour formation [119].

By inducing damage to lipids, proteins and DNA, ROS can activate oncogenes [120] or inactivate tumour suppressor genes [121], thereby promoting tumour development. Furthermore, ROS are implicated in modulation of proteins which are necessary for tumour proliferation, for example the PI3K/Akt and MAPK signalling [122, 123]. Moreover, ROS-mediated tumorigenesis also depends on the regulation of transcription factors like nuclear factor erythroid 2-related factor 2 (Nrf2), nuclear factor- κ B (NF- κ B) and hypoxia-inducible factor-1 α (HIF-1 α) for angiogenesis and further tumour progression [124]. Several studies revealed that administration of antioxidants like N-acetyl cysteine (NAC) reduces tumour growth in mice [125] as well as overexpression of antioxidant enzymes such as catalases [126] and SOD [127] counteracted tumour formation.

Thus, cancer cells exhibit higher ROS levels than their non-malignant counterparts [128]. To cope with this oxidative stress, cancer cells upregulate their antioxidant defence system to maintain redox homeostasis [35, 57]. Therefore, treatment strategies to suppress cancer progression comprises either an enhancement of ROS generation and/or the diminution of the antioxidant system to shift ROS from a beneficial to a toxic level [57]. This ROS-dependent lethality is often linked to various cell death mechanisms, since for example superoxide accumulation in HepG2 cells induces rapid cytochrome c release through VDAC permeabilization, triggering apoptosis [129]. Furthermore, necroptosis can also be triggered in a ROS-dependent manner. Ye and colleagues confirmed that fibrosarcoma cells underwent ROS-dependent necroptosis after administration of Tumour necrosis factor α (TNF α) [130]. Another newly identified cell death mechanism, called ferroptosis, is induced in an iron- and ROS-dependent manner through GPX4 and x_c^- inhibition [100, 101].

2.3 Ferroptosis

Programmed cell death is an important cellular mechanism for tissue homeostasis and proper function of multicellular organisms. However, one hallmark of cancer progression is cell death resistance [131]. To circumvent resistance, the induction of programmed cell death (PCD) is utilised as a possible treatment option. For the last two decades, apoptosis was described to be the most common programmed cell death type, whereas necrotic cell death was considered to be a spontaneous cell death form [132]. This point of view was changed later on, after multiple studies revealed that necrosis can be tightly regulated and distinguished into several, sometimes interconnecting pathways like necroptosis, ferroptosis, oxytosis, parthanatos, ETosis, NETosis, pyronecrosis and pyroptosis [133-135]. Our study addresses the molecular mechanism of ferroptosis (Figure 1), therefore this topic is explained in more detail in the following paragraph.

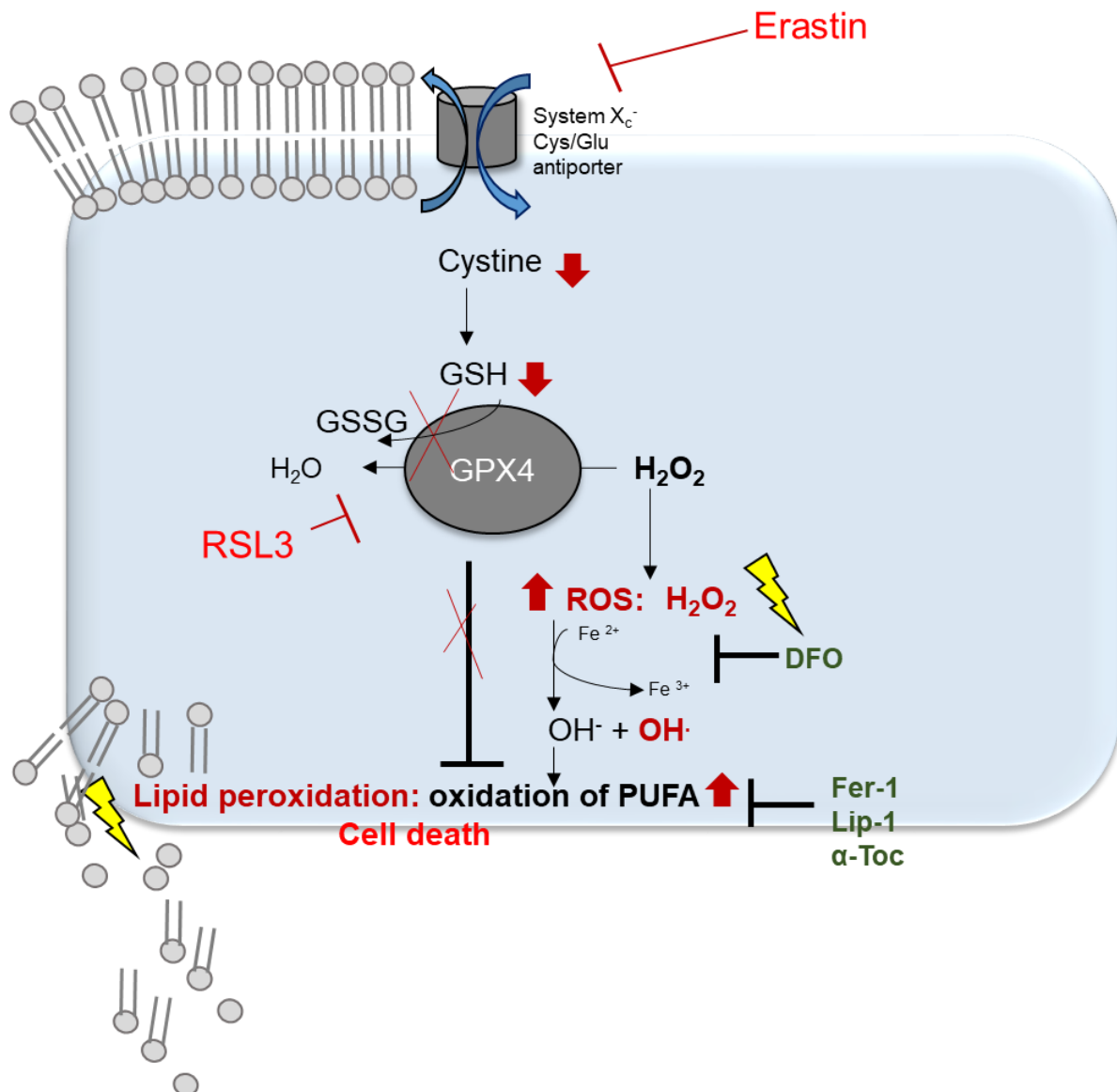


Figure 1: Ferroptotic cell death pathway induced by Erastin or RSL3.

Erastin indirectly inhibits GPX4 by depleting its cofactor GSH, leading to ROS accumulation and lipid peroxidation, whereas RSL3 directly suppresses GPX4 by binding to its active site. Cell death can be diminished through lipid peroxide scavenger (Fer-1 and Lip-1), iron chelation (DFO) and ROS scavenger (α -Toc). This figure is adapted from [136].

Ferroptosis was first described by Dixon and colleagues in 2012, elucidating a new form of cell death which differs from apoptosis, necroptosis and autophagy in morphology and signalling [101]. It is dependent on iron and lipid peroxide formation and is morphologically characterized through condensed mitochondrial morphology and cell volume shrinking [101]. Additionally, ROS accumulation plays a crucial role, whereby the involvement of mitochondrial ROS in ferroptosis is controversially discussed [101, 137]. Ferroptosis inducers can be distinguished by their mode of action. There are GSH depleting agents, leading to an antioxidant impairment and ferroptotic cell death induction by ROS accumulation. This includes Erastin [101], Sulfasalazine (SAS) [138]

and Sorafenib [139] which target system x_c^- as well as buthionine sulphoximine (BSO) [104] which inhibits γ -glutamate cysteine ligase (γ GCL) [140]. Moreover, there are several ferroptosis inducers that do not deplete GSH. RSL3 and DPIs directly inhibit GPX4 [104], an important selenocysteine-containing protein that reduces hydroperoxides and lipid hydroperoxides (ROOH) to their corresponding alcohols (ROH) by using GSH as a cofactor [141-143]. Pharmacological inhibition or genetic silencing of GPX4 induces ferroptosis through lethal lipid peroxide formation which is reversed by GPX4 overexpression [141, 144]. In addition, other drugs like Artesunate [145] and its derivate are also able to induce ferroptotic cell death [146], as well as excessive extracellular glutamate [147].

As the name of this specific cell death discloses, iron plays a crucial role in this cell death type. It is suggested that an increased iron uptake through enhanced expression level of transferrin receptor 1 (TFR1) and decreased iron storage through downregulated ferritin lead to iron accumulation and execution of ferroptosis by producing lipid peroxides via Fenton chemistry [100, 148]. Furthermore, iron chelation by lipophilic antioxidants like DFO rescues from ferroptosis [100, 101, 104]. Alternatively, lipoxygenase-mediated formation of lipid peroxidation can be abrogated through the addition of iron chelators [149]. This and various other ROS-producing enzymes like XO, P450 and NOX need iron or iron derivates for their proper function [102]. In contrast to iron, calcium is not sufficient for ferroptotic cell death induction in mammalian but in plant cells [101, 150].

Concerning iron, lipid ROS accumulation is an event downstream of x_c^- and GPX4 inhibition [101, 151]. Lipid peroxides are generated enzymatically [68] and non-enzymatically [152]. On the molecular level in a non-enzymatically manner, hydroxyl ($\text{OH}\cdot$) and peroxy radicals ($\text{ROO}\cdot$) which are generated by Fenton chemistry can react with adjacent PUFA, inducing a propagation of lipid peroxidation similar to a chain reaction [68]. Enzymatically and in a more controlled manner, LOX oxidize PUFA to lipid hydroperoxides. There are several LOX with different substrate specificity. 5-LOX oxidizes AA at carbon 5 to its corresponding lipid peroxide hydroperoxyeicosatetraenoic acid (5-HPETE), whereas 12/15-LOX generate 12-HPETE and 15-HPETE [68, 153]. Polyunsaturated fatty acids like arachidonic, linoleic and docosahexaenoic acids are susceptible for oxidation because of their pentadiene moiety [68]. Especially AA plays a crucial role in ferroptotic signalling. Acyl-CoA synthetase long-chain family member

4 (ACSL4) and lysophosphatidylcholine acyltransferase 3 (LPCAT3) modulate ferroptosis sensitivity, as suppression of these enzymes has anti-ferroptotic function [154, 155]. These enzymes are important for the production and insertion of AA into membranes [154, 155]. In addition, α -Tocopherol and α -Tocotrienol diminish ferroptotic cell death not only by scavenging hydroxyl radicals, but also through LOX inhibition by competing for their PUFA substrate binding site (corking mechanism) [141, 155]. Besides vitamin E, other ferroptosis inhibitors like Lip-1, Fer-1, ebselen and iron chelator DFO are described to effectively block ferroptotic cell death [101, 151, 156]. Sensitivity to ferroptosis is dependent on many different factors, e.g. genes, proteins and lipid metabolisms [157-159]. These modulators include RAS in certain cells [104], genes involved in iron metabolism [100, 101, 148], protein synthesis [160, 161], lipid metabolism [154, 155, 162] and p53, which has a pleiotropic function in regulating ferroptosis [163, 164]. Based on RAS and p53, observations on modulators can be cell- and context specific. For example diffuse large B-cell lymphoma (DLBCL) cells are RAS wildtype (WT) but highly sensitive to ferroptosis induction [104, 136]. In this context, DLBCL may display a defect in the transsulfuration pathway that render them dependent on cystine import via x_c^- [136, 138, 165]. In this pathway, methionine is utilized to generate cysteine under conditions of cysteine depletion [166]. Recent research revealed that upregulated transsulfuration pathway through the loss of cysteinyl-tRNA synthetase (CARS) blocked Erastin-induced ferroptosis [160]. Moreover, the mevalonate (MVA) pathway is also an important regulator, because this pathway provides selenocysteine for selenocysteine-containing enzymes like GPX4. The addition of statins, which inhibit this pathway can diminish GPX4 synthesis [167-169]. Other modulators are heat-shock proteins (HSP) [170]. Sun and colleagues showed that knock-down of HSPB1 sensitizes cells to Erastin-induced ferroptosis, whereas overexpression blocks this event. Activation of HSPB1 by PKC phosphorylation also prevent cells to undergo ferroptosis [161]. Also p62-Keap1 (Kelch ECH associating protein 1)-Nrf2 is a regulatory element in ferroptosis. Nrf2 is activated via oxidative stress and as a stress response it upregulates antioxidant target genes like xCT (SLC7A11), thereby counteracting ferroptosis onset [171, 172].

In a screen of 117 cancer cell lines, Yang and colleagues identified that Erastin sensitivity is not exclusively dependent on RAS mutations which was in contrast to first observations [101, 104]. Erastin also acts in concert with chemotherapeutic agents to

induce cell death in some cancer cell lines [103, 173, 174]. Also, FDA approved compounds like Sorafenib, Sulfasalazine and Artesunate are described to inhibit cancer growth by inducing ferroptosis in several cancer cell lines [101, 139, 145]. Additionally *in vivo*, ferroptosis can be induced through Erastin, Erastin analogues, RSL3 and ultra-small nanoparticles, whereby the rescuing effect of ferroptosis inhibitors or prostaglandin-endoperoxide synthase 2 (PTGS2) upregulation is used as biomarker for ferroptotic signalling [153, 175].

Ferroptosis also occur in neurodegenerative diseases, since glutamate-induced neurotoxicity in rat hippocampal brain slices is inhibited through the addition of Fer-1 [101]. Hambright and colleagues investigated that deletion of GPX4 in mice forebrain exhibited neurodegeneration which is inhibited through the addition of vitamin E and Fer-1 [176].

The involvement of ferroptosis in acute kidney and liver failure was demonstrated through the usage of ferroptosis inhibitors Fer-1 and Lip-1 to block lethality of iron-induced cell death of isolated mouse kidney tubules and mouse model of ischaemia/reperfusion injury (IRI) [144, 151].

To this end, ferroptosis induction is immunogenic. Therefore, further studies are necessary to unravel molecular biomarkers and possible immune responses.

3 Aim of the study

Evasion of programmed cell death like apoptosis contributes to tumour progression and is often linked to poor prognosis [131]. Elevated ROS levels and impaired redox homeostasis through upregulated antioxidant defence mechanisms are characterized as hallmarks of cancer progression and proper function of cancer cells as well [35, 57, 128]. ALL and RMS often exhibit upregulated antioxidant defence mechanisms which make them vulnerable for oxidative stress-induced compounds [177, 178].

In this study we explore a promising treatment strategy for ALL and RMS by depriving tumour cells of vital ROS signalling by targeting their cellular antioxidant defence systems, shifting intracellular ROS signalling to cell death induction. Furthermore, as a second aspect we reveal molecular insights into ferroptosis signalling stimulated by Erastin or RSL3 alone or in combination with Smac mimetic BV6 in two distinct cancer cell types.

4 Materials and methods

4.1 Materials

4.1.1 Paediatric cell lines

Table 1: Cell lines

Cell line	Subtype	Entity	Source
Jurkat	T-lymphoblast	Acute lymphoblastic leukaemia	DSMZ
Molt-4	T-lymphoblast	Acute lymphoblastic leukaemia	DSMZ
RD	Embryonal	Rhabdomyosarcoma	ATCC
RH30	Alveolar	Rhabdomyosarcoma	DSMZ
RH36	Embryonal	Rhabdomyosarcoma	ATCC
RH41	Alveolar	Rhabdomyosarcoma	DSMZ
Kym-1	Controversial	Rhabdomyosarcoma	JCRB
TE441.T	Embryonal	Rhabdomyosarcoma	ATCC
TE381.T	Embryonal	Rhabdomyosarcoma	ATCC
T174	Embryonal	Rhabdomyosarcoma	DSMZ
RH18	Alveolar	Rhabdomyosarcoma	DSMZ

4.1.2 Packaging cell lines

Table 2: Packaging cell lines

Cell line	Subtype	Source
Phoenix (AMPHO)	2 nd generation retrovirus producing	ATCC

4.1.3 Primary acute lymphoblastic leukaemia samples

Table 3: Primary ALL samples

Cell line	Source material	Subtype	Source
HA-10022016	Peripheral blood	Pro B ALL	Dep. paed. onc. Goethe University Frankfurt, Prof. Klingebiel
KM-15022016	Peripheral blood	Unknown/BL	Dep. paed. onc. Goethe University Frankfurt, Prof. Klingebiel

4.1.4 Cell culture materials

Table 4: Cell culture materials

Reagent	Supplier
Dulbecco's Modified Eagles Medium (DMEM) GlutaMAX-I	Life Technologies
RPMI 1640 medium, GlutaMAX-I	Life Technologies
Dulbecco's phosphate buffered saline (PBS)	Life Technologies
Trypsin/EDTA (0.05%), phenol red	Life Technologies
Foetal Calf Serum (FCS)	Life Technologies
Penicillin/Streptomycin (10,000 U/ml)	Life Technologies
Sodium pyruvate (100 mM)	Life Technologies
HEPES (1M)	Life Technologies
Trypan blue	Invitrogen
Puromycin	Clontech Laboratories
Ficoll	Clontech Laboratories
X-VIVO	Lonza

4.1.5 Cell death-inducing compounds

Table 5: Cell death-inducing compounds

Compound	Function	Supplier
Erastin	xc- system inhibitor	Sigma-Aldrich
RSL3	GPX4 inhibitor	InterBioscreen
BV6	Smac mimetic	Genentech
Sorafenib	Multi kinase inhibitor, xc- system inhibitor	Abcam
TNFα	Tumour necrosis factor α	Biochrom
Etoposide	Inhibitor of DNA synthesis	TEVA GmbH
ABT737	pan-Bcl-2 inhibitor	Selleckchem

4.1.6 Cell death inhibitors, antioxidants and ROS scavengers

Table 6: Cell death inhibitors, antioxidants and ROS scavenger

Compound	Function	Supplier
Ferrostatin-1	Ferroptosis inhibitor	Sigma-Aldrich
Liproxstatin-1	Ferroptosis inhibitor	Sigma-Aldrich
Deferoxamine	Iron chelator	Sigma-Aldrich
α-Tocopherol	Vitamin E derivate	Sigma-Aldrich
N-acetylcysteine	GSH precursor	Sigma-Aldrich
Glutathion	Thiol-containing antioxidant	Carl-Roth
Butylated hydroxyanisole	Lipophilic antioxidant	Sigma-Aldrich
MnTBAP	MnSOD mimetic	Santa Cruz
zVAD.fmk	Pan-caspase inhibitor	Bachem
Necrostatin-1s	RIP1 inhibitor	Calbiochem
Necrostatin-1	RIP1 inhibitor	Merck
GKT137831	NOX1/4 inhibitor	Selleckchem

Diphenyleneiodonium	Pan-NOX inhibitor	Sigma-Aldrich
Bisindolylmaleimide I	Pan-PKC inhibitor	Cayman Chemicals
Gö6976	PKC α and β inhibitor	Tocris Bioscience
Baicalein	Selective 12/15-LOX inhibitor	Sigma-Aldrich
NDGA	Pan-LOX inhibitor	Sigma-Aldrich
Zileuton	Selective 5-LOX inhibitor	Cayman Chemicals
PD146176	Selective 15-LOX inhibitor	Sigma-Aldrich

4.1.7 Fluorescent dyes used for FACS and microscope measurements

Table 7: Fluorescent dyes used for FACS and microscope measurements

Dye	Function	Supplier
BODIPY 581/591-C11	Lipid peroxide sensor	Life Technology
CMH₂DCF-DA	General oxidative stress sensor	Life Technology
CellROX	General oxidative stress sensor	Life Technology
CellEvent Caspase-3/7 Green Detection Reagent	Detection of activated caspase 3/7	ThermoFisher
Hoechst-33342	Staining of DNA and nucleus	Sigma-Aldrich
Propidium iodide (PI)	Indicator of dead cells in a population by visualising of DNA	Sigma-Aldrich

4.1.8 Plasmids

Table 8: Plasmids

Plasmid	Plasmid backbone	Gene	Supplier
Empty vector (EV)	pBabe-puro	none	Life Technology
GPX4	pBabe-puro	hGPX4	Life Technology

4.1.9 siRNA oligonucleotides

Table 9: siRNA oligonucleotides

siRNA	Target gene	Cat. No.	Supplier
siCtrl	none	s4390842	ThermoFisher
siRIP3#1	RIP3	s21741	ThermoFisher
siNOX4#2	NOX4	s27014	ThermoFisher
siPKC α #1	PKC α	s11092	ThermoFisher
siPKC α #2	PKC α	s11094	ThermoFisher

4.1.10 Primary western blot antibodies

Table 10: Primary western blot antibodies

Antibody	Working dilution	Species	Supplier
anti-GPX4	1:1000 in 2 % BSA	mouse	R&D Systems
anti- β -Actin	1:10 000 in 2 % BSA	mouse	Sigma-Aldrich
anti-GAPDH	1:5000 in 2 % BSA	mouse	HyTest
anti-Vinculin	1:5000 in 2 % BSA	mouse	Sigma-Aldrich/Merck

4.1.11 Secondary western blot antibodies

Table 11: Secondary western blot antibodies

Antibody	Working dilution	Species	Supplier
HRP-conjugated anti-mouse IgG	1:5000 in 5 % SMP in PBS-T	goat	Santa Cruz
IRDye680-conjugated anti-mouse IgG	1:5000 in 5 % SMP in PBS-T	donkey	LI-COR

4.1.12 Oligonucleotides for qRT-PCR

Table 12: Oligonucleotides for qRT-PCR

Primer	Sequence	Supplier
15-LOX for	TTGGTTATTTTCAGCCCCCATC	Eurofins Genomics
15-LOX rev	TGTGTTCACTGGGTGCAGAGA	Eurofins Genomics
12-LOX for	AGAATGGTTCCTGTTTGAAGCT	Eurofins Genomics
12-LOX rev	CCATTGGGCTCCATCTTCAG	Eurofins Genomics
NOX4-for	TCCTCGGTGGAAACTTTTGT	Eurofins Genomics
NOX4-rev	CCACAACAGAAAACACCAACT	Eurofins Genomics
PKC α for	TCGACTGGGAAAAACTGGAG	Eurofins Genomics
PKC α rev	CTCTGCTCCTTTGCCACAC	Eurofins Genomics
PKC β for	CTTCAAGCAGCCCACCTTCT	Eurofins Genomics
PKC β rev	TCCCCGAAGCCCCAGATG	Eurofins Genomics
PKC δ for	ATTATCCCCGCTGGATCAC	Eurofins Genomics
PKC δ rev	CTTGGTTGGTTCCTTTCAA	Eurofins Genomics
PKC ϵ for	AACACCCGTACCTTACCCAAC	Eurofins Genomics
PKC ϵ rev	CGAAAAAGAGGCGGTCCT	Eurofins Genomics
28S rRNA for	TTGAAAATCCGGGGGAGAG	Eurofins Genomics
28S rRNA rev	ACATTGTTCCAACATGCCAG	Eurofins Genomics
GAPDH for	CAAGGTCATCCATGACAACTTTG	Eurofins Genomics
GAPDH rev	GGGTCCAAGTTGTCCAGAATGC	Eurofins Genomics

4.1.13 General reagents, chemicals, consumable material

Table 13: General reagents, chemicals, consumable material

Reagent/Chemical	Supplier
Albumin fraction V (BSA)	Carl Roth

Ammonium persulphate (APS)	Carl Roth
CaCl₂ (Transduction)	Carl Roth
Cell scraper	BD Biosciences
Chloroquine (transduction)	Sigma-Aldrich
Combi tips (0.5 ml, 1 ml, 2.5 ml, 5 ml and 10 ml)	Eppendorf
Cryovials	Starlab
Dimethyl sulphoxide (DMSO)	Sigma-Aldrich
Disodium hydrogen phosphate dihydrate (Na₂HPO₄)	Carl Roth
Dithiothreitol (DTT)	Calbiochem
Ethanol	Carl Roth
Ethylene diamine tetra acetic acid (EDTA)	Carl Roth
FACS Clean / Rinse solution	BD Biosciences
FACS Flow sheath fluid	BD Biosciences
FACS Shutdown solution	BD Biosciences
FACS tubes	BD Bioscience
Falcon (15 ml, 50 ml) dark/transparent	Greiner Bio-One
Filter paper	Carl Roth
Gel blot paper	Carl Roth
Hybond enhanced chemiluminescence (ECL) 0.45 Amersham	Bioscience
Hyperfilm ECL Amersham	Bioscience
Hydrochloric acid (HCl)	Carl Roth
Lipofectamine RNAiMAX	Life Technologies
Methanol	Carl Roth
Milk powder (skimmed milk powder, SMP)	Carl Roth
Opti-MEM transfection medium	Life Technologies
Pasteur pipettes	Carl Roth

PageRuler plus prestained protein ladder	Fermentas
Phenylmethanesulphonyl fluoride (PMSF)	Carl Roth
Pierce ECL western blotting substrate	ThermoScientific
Pipette tips (10 µl, 200 µl, 1000 µl)	Starlab
Potassium chloride (KCl)	Carl Roth
Potassium dihydrogen phosphate (KH₂PO₄)	Carl Roth
Protaminsulphate (Transduction)	Sigma-Aldrich
Reaction tubes (0.5 ml, 1.5 ml, 2 ml)	Starlab
Roentertoll HC x-ray developer	TETENAL
Sodium chloride (NaCl)	Sigma-Aldrich
Sodium dodecyl sulphate (SDS)	Carl Roth
Sodium hydroxide (NaOH)	Carl Roth
Sodium-orthovanadate	Sigma-Aldrich
Starter for x-ray developer	TETENAL
Sterile pipettes (2 ml, 5 ml, 10 ml, 25 ml)	Greiner Bio-One
Sterile filter (0.22 µm, 0.45 µm)	Millipore
Superfix MRP x-ray fixing solution	TETENAL
Tetramethyl-ethylenediamine (TEMED)	Carl Roth
Tissue culture dishes (6cm, 10 cm)	Greiner Bio-One
Cell culture flasks (25 cm², 75 cm², 175 cm²)	Greiner Bio-One
Tissue culture plates (6-, 24-, 48-, 96-well)	Greiner Bio-One
Tris Base	Carl Roth
Tris HCl	Carl Roth
Tween 20	Carl Roth
β-Mercaptoethanol	Merck

4.1.14 Kits

Table 14: Kits

Kit	Supplier
GSH/GSSG-Glo™ assay	Promega
Neon transfection system	Invitrogen
pegGOLD total RNA kit	Peqlab Biotechnologie GmbH
Bicinchoninic acid (BCA) protein assay kit	Abcam
RevertAid H minus first strand cDNA synthesis kit	MBI Fermentas GmbH

4.1.15 Equipment

Table 15: Equipment

Equipment	Supplier
ARE heating magnetic stirrer	VELP Scientifica
Avanti J-26 XP ultracentrifuge	Beckman Coulter
Autoclave Systec V150	Systec
Blotting chamber	BioRad
Cell culture incubator, MCO-20AIC	Sanyo
Centrifuge 50RS	Hettich
Centrifuge ROTANTA 460 R	Hettich
Counting chamber	Marienfeld GmbH
Electronic analytical balance EW	Kern
Electronic precision balance 770	Kern
FACS Canto I	BD Biosciences
Heating block	Eppendorf
ImageXpress micro XLS system	Molecular Devices

Infinite M100 microplate reader	Tecan
Microcentrifuge	Benning
Microscope CKX41, cell culture	Olympus
Mini-PROTEAN Tetra Cell electrophoresis system	Bio-Rad
Multipette plus	Eppendorf
NanoDrop 1000 spectrophotometer	PEQLAB
Odyssey infrared imaging system	LI-COR
PCR-thermocycler	Eppendorf
PerfectBlue dual gel twin L electrophoresis system	PEQLAB
pH meter inoLab pH7310	WTW
Pipettes Research plus (2.5 µl; 10 µl; 20 µl; 100 µl; 200 µl; 1000 µl)	Eppendorf
Power pac HC high-current power supply	Bio-Rad
Quantstudio 7 flex real-time PCR system	Applied Biosystems
Rocking shaker	MS-L
Roller mixer	Ratek
Sunrise microplate reader	Tecan
Thermomixer comfort	Eppendorf
Trans-blot SD semi-dry transfer cell	Bio-Rad
Vacuum pump HLC	Ditabis
Vortex mixer (ZX classic; wizard X)	VELP Scientifica
Water bath SWB20	Medingen

4.1.16 Software

Table 16: Software

Software	Supplier
CalcuSyn version 2.0	Biosoft
FACSDiva version 6.1.3	BD Biosciences
FlowJo version 7.6.5	Tree Star
i-control version 1.10	Tecan
ImageJ version 1.48v	Open source
Image Studio version 2.1.10	LI-COR
ImageXpress 2015	Molecular Devices
Magellan data analysis version 7.2	Tecan
Microsoft-office 2013	Microsoft Deutschland GmbH
Paint.NET v4.0.5.	dotPDN LLC

4.2 Methods

4.2.1 Cell biology methods

4.2.1.1 Cell culture

Acute lymphoblastic leukaemia cells were cultured in RPMI medium, supplemented with 10% foetal calf serum (FCS), 1% penicillin/streptomycin (P/S), 1% pyruvate and 25 mM HEPES buffer (RPMI ++++).

Primary ALL blasts were isolated with Ficoll, cultured and directly stimulated in X-VIVO medium, containing 20% FCS and 0.5% P/S.

Rhabdomyosarcoma cells were cultivated in DMEM GlutaMAX™-I or respectively RPMI 1640 medium, supplemented with 10% FCS, 1% penicillin/streptomycin and 1% pyruvate, whereby RPMI 1640 was additionally supplemented with HEPES (25 mM) (DMEM +++, RPMI ++++).

Both, suspension and adherent cell lines were cultured in cell culture flasks in a humidified atmosphere at 37 °C with 5% CO₂. All cells were passaged twice a week, whereas suspension cells were passaged by directly adding the appropriate amount of cell culture into a new flask and adherent cells by trypsinization with trypsin/EDTA.

4.2.1.2 Freezing and thawing of cells

As a long time storage method, cells were frozen in FCS containing 10% DMSO. The suspension of cells was kept in cryovials over night at -80 °C, then transferred into a nitrogen tank.

Cells that had to be thawed were transferred from defrosted cryovials into a new flask, containing new growth medium (DMEM +++, RPMI ++++). After 24 hours medium was changed to remove residual DMSO.

4.2.1.3 Cell counting, seeding and treatment

ALL cells were centrifuged at 1000 rpm at RT for 5 minutes. Residual medium was removed and the generated pellet was resuspended in fresh growth medium. 60 µl of 0.4% (v/v) trypan blue dye was added to 20 µl of cell suspension and counted via a

Neubauer chamber. The appropriate number of cells was then diluted in growth medium in their required density (Jurkat, Molt-4, Jurkat FADD def.: 2×10^5 cells/ml), including treatment substances in definite concentrations.

RMS cells were seeded approximately 24 hours before treatment in the required density (0.2×10^5 cells/cm², except TE441.T: 0.6×10^5 cells/cm² and RH18: 0.5×10^5 cells/cm²). First, old medium was removed, cells were washed with sterile PBS and trypsinized, adding trypsin/EDTA for 5 minutes at 37 °C. Step of trypsinization was stopped by the addition of fresh growth medium (minimum of twofold in ratio to trypsin/EDTA). 60 µl of 0.4 % (v/v) trypan blue dye was added to 20 µl of cell suspension and counted via a Neubauer chamber. The appropriate number of cells was then diluted in growth medium and seeded in corresponding culture flask or plates. After cells were adhered (~ 24 hours), consumed medium was discarded and replaced by medium, accommodating the desired treatment substances in definite concentrations.

Afterwards, ALL and RMS cells were incubated for indicated time points at 37 °C and 5% CO₂.

4.2.1.4 Preparation of primary ALL cells

Primary ALL blasts from children were isolated using Ficoll. Therefore blood samples were washed with PBS (ratio 1:1 or 1:3) and carefully loaded into a conical 50 ml tube containing Ficoll solution. Centrifugation ensued 30 minutes without stopping at 1200 rpm and RT. Finally, erythrocytes were located at the bottom and the needed lymphocytes were located on top of the Ficoll solution as a grey film. These were collected gently, transferred to a second conical tube and washed with sterile PBS twice. Afterwards cells were seeded in a density of 2×10^6 cells/ml.

4.2.1.5 Retroviral transduction

The retroviral vector pBabe-puro was used to overexpress human GPX4 in Molt-4 cells (ALL). In detail, Phoenix AMPHO cells were seeded 24 hours prior to transfection (0.9×10^5 cells/cm²) and transfected with either 20 µg of empty vector (EV) or vector containing human GPX4 using calcium phosphate transfection. Over a period of 48 hours virus-containing supernatant was collected, sterile-filtered, supplemented with protamine sulphate (8 mg/ml) and centrifuged with 1300 rpm for 90 minutes without

breaks at RT. After 8 hours medium containing virus was removed and fresh growth medium was supplemented. Puromycin selection (10 µg/ml) started after 48 hours and was kept for two weeks. Transduction efficacy was verified using western blot analysis.

4.2.1.6 Transient siRNA transfection

In general, transient siRNA-mediated knockdown was performed using SilencerSelect. RMS cells were transfected using Lipofectamine RNAiMAX. Exemplarily, either 1.5 µl Lipofectamine or 10-20 nM siRNA were diluted in 25 µl Opti-MEM. The siRNA-Opti-MEM mixture was added to Lipofectamine-Opti-MEM mixture and incubated for 10 minutes. 50 µl of transfection-mix was transferred into a 24-well plate and 0.2×10^5 cells/cm² were seeded afterwards (450 µl per well). To verify knockdown efficacy via siRNA, additional 6 cm dishes were prepared with 500 µl transfection-mix and 3500 µl cell suspension.

In contrast, ALL cells were splitted one day prior to transfection in a ratio of 1 to 3. For electroporation, cells were washed with sterile PBS and 2×10^6 cells were mixed with 80 nM of corresponding siRNA in resuspension buffer. Neon® Transfection System (Life Technologies) was used for transient transfection. Electroporated cells were re-seeded in 6 well plates containing 3 ml growth medium without antibiotics. After 24 hours, cells were counted and used for subsequent experiments. Successful knock-down was verified using western blot analysis.

4.2.1.7 Determination of cell death using flow cytometry (forward/sideward scatter)

Cell death of ALL cells was assessed by forward/sideward scatter (FSC/SSC) analysis and flow cytometry (FACSCanto I, BD Biosciences). In general, suspension cells were transferred into FACS tubes and directly measured by FSC/SSC, whereby cells are sorted by morphology, distinguishing between smaller size (FSC) and granularity of the cell (SSC).

4.2.1.8 Determination of cell death using PI-staining

Cell death of RMS cells was measured by Hoechst/PI-staining, analysing the plasma membrane permeability using fluorescence microscopy (ImageXpress Mikro XLS). After cells had been incubated with desired substances, Hoechst (10 µg/µl) and PI (1 µg/µl) were supplemented and cells were incubated for 5-15 minutes at 37°C in the cell incubator. After incubation time, cells were analysed in DAPI and TRITC channel. Analysis was performed by automated analysis using MetaXpress software.

4.2.1.9 Determination of caspase 3/7 activity

Caspase activity was determined using the CellEvent caspase 3/7 green detection Reagent following the instructor's manual. After treatment incubation, cells were stained with 10 µg/µl Hoechst for 5-10 minutes at 37 °C. FITC and Hoechst fluorescence were analysed with microscopy (ImageXpress Mikro XLS) using corresponding channels DAPI and FITC. Analysis was made by automated analysis using MetaXpress software.

4.2.1.10 Determination of GSH depletion

Analysis of cellular GSH levels was performed using GSH/GSSG-GloTM assay, following the instructor's manual. Luciferase signal was measured with the Tecan plate reader and normalized to 10 000 cells. For cell quantification, a separated plate was used for Hoechst-staining (4.2.1.8).

4.2.1.11 Determination of cellular ROS production and lipid peroxidation

Detection of ROS ensued in ALL at early time points before cells succumbed to cell death. Cells were incubated with 1 µM CellROX Deep Red Reagent (Invitrogen) in phenol free RPMI medium for 30 minutes at 37 °C in the dark and immediately analysed by flow cytometry using the APC channel.

For ROS detection in RMS cells, 5 µM of CM-H₂DCF (5-(and-6)-chloromethyl 2', 7'-dichlorodihydrofluorescein diacetate, acetyl ester) (Invitrogen) in phenol free RPMI medium was used. Cells were incubated for 30 minutes at 37 °C in the dark and analysed through flow cytometry using FITC channel.

4.2.1.12 Determination of lipid peroxidation

Lipid peroxidation was analysed in ALL and RMS cells by using 5 μ M BODIPY C11 in phenol free RPMI and before cells succumbed to cell death. Cells were incubated for 30 minutes at 37 °C in the dark and analysed through flow cytometry using FITC channel.

4.2.2 Molecular biology methods

4.2.2.1 Cell lysis, SDS Page and western blot analysis

After indicated treatment periods, ALL cells were transferred into conic tubes, whereas RMS cells were collected by scraping tissue culture dishes and centrifuged at 1800 rpm for 5 minutes (4 °C). After centrifugation, the supernatant was discarded and the pellet was washed with cold PBS, centrifugation was repeated and after discarding the supernatant the pellet was resuspended in lysis buffer (containing 30 mM TrisHCl, 150 mM NaCl, 1 % Triton X-100, 10% Glycerol, 0.5 mM PMSF, 2 mM DTT, 1x protease inhibitor cocktail, 1 mM sodium orthovanadate, 1 mM β -glycerolphosphate, 5 mM sodium fluoride) and kept for 20 minutes on ice. After incubation, lysates were centrifuged at 14 000 rpm for 25 minutes at (4 °C). The supernatant was transferred in a new Eppendorf tube and protein concentration was determined using Pierce® BCA protein assay kit according to the instructor's manual.

After determination of protein concentration, 50-100 μ g of total protein lysate were supplemented with ddH₂O and 6x SDS loading buffer (60 mM Tris HCl pH 6.8, 1% (v/v) SDS, 5% (v/v) Glycerol, 0.01 mg/ml bromphenolblue) to a final volume of 18 μ l. Protein samples were denaturated for 5 minutes at 95 °C and then loaded on the gel. The polyacrylamide gels consisted of a 5% stacking gel (consisting of 5% polyacrylamide, 125 mM TrisHCl pH 6.8, 0.1 % SDS, 0.1 % APS, 0.1 % TEMED ad ddH₂O) and a 12% or 15% resolving gel (consisting of 12% or 15% polyacrylamide, 250 mM TrisHCl pH 8.8, 0.1 % SDS, 0.1% APS, 0.04 % TEMED ad ddH₂O). First, proteins were separated by 80 V until they passed through the stacking gel, thereafter voltage was increased up to 120 V for the resolving gel.

Using semi-dry blotting method, proteins were transferred to a nitrocellulose membrane (1 mA per cm² nitrocellulose membrane). Therefore, membrane and blotting paper were soaked in blotting buffer (125 mM Tris Base, 1.25 mM Glycine, 0.1% SDS, 20% Methanol), organized in a package that contained two blotting papers, membrane,

gel and two blotting paper again and finally piled on the anode plate. After blotting, membranes were blocked for 1 hour in PBS-T (PBS containing 0.1% Tween) containing milk (5%) and tween (0.1%) to avoid unspecific binding of antibodies. After blocking, the membranes were washed with PBS-T three times for at least 5 minutes before incubation with primary antibody (diluted in blocking solution or 2% BSA) overnight (4 °C) on an orbital shaker. After incubation, membrane was washed three times for at least 5 minutes with PBS-T and incubated with secondary antibody conjugated to horseradish peroxidase (HRP) or fluorescence dye diluted in blocking solution for at least 1 hour on an orbital shaker (RT). Detection was ensued by enhanced chemiluminescence to visualize HPR enzymatic activity or detection of fluorescent signal by Infrared Odyssey® imaging system.

4.2.2.2 Isolation of RNA, cDNA synthesis and qRT-PCR

After indicated treatment time points, ALL cells were pelleted at 1800 rpm and RT, whereas lysis buffer for RNA isolation was directly transferred to RMS cells, after discarding the supernatant. In detail, RNA was extracted using peqGOLD total RNA kit according to the manufacturer's instructions. 1 µg of total RNA was subjected to cDNA synthesis using RevertAid H minus first strand cDNA synthesis kit, following the instructor's manual. Gene expression analysis was performed by quantitative real-time PCR with SYBR-green using Quantstudio Flex 7 fast real time PCR system (Primers are listed in Tab. 4.1.12). Data sets were normalized using house-keeping genes 28S rRNA and GAPDH. Quantitative RT-PCR reaction was performed for 50 cycles (start heating phase: 95 °C 10 minutes, cycle phase: 95 °C 15 seconds; 60 °C 1 minutes). Specificity of primers was analysed regarding melt curves of amplified products and water control. The relative expression level of the desired gene transcript and reference gene transcript was calculated using $\Delta\Delta C_t$ method.

4.2.2.3 Statistical analysis

Statistical significance was assessed by using Microsoft Excel Student's t-Test (two-tailed distribution, two-sample, equal variance) and was defined as significant at $p < 0.05$ (*), very significant at $p < 0.01$ (**) and as highly significant at ≤ 0.001 (***).

5 Results

The main part of the following results is a summary of three papers, two of them are accepted by the peer-reviewed journal *Biochemical Pharmacology* (Probst et al. 2017; shared first authorship: “*Lipoxygenase inhibitors protect acute lymphoblastic leukaemia cells from ferroptotic cell death*”) and *Oncotarget* (Dächert et al. 2016; shared first authorship: “*RSL3 and Erastin differentially regulate redox signalling to promote Smac mimetic-induced cell death*”), whereby parts of the second topic are described in the dissertation of Hannah Schoeneberger as well, handed in 2014. Currently, one is under revision by the peer-reviewed journal *Oncotarget* (Dächert et al. 2018: “*Targeting ferroptosis in rhabdomyosarcoma cells*”).

5.1 Oxidative cell death in acute lymphoblastic leukaemia cells

5.1.1 Lipoxygenase inhibitors protect against ferroptotic cell death in acute lymphoblastic leukaemia cells

In 2012, RSL3 was first described to induce ferroptosis by inhibiting GPX4 [101]. For that reason, we investigated if RSL3 stimulates ferroptotic cell death in prototypic ALL cells (Molt-4, Jurkat) and in a cell line which is resistant to extrinsic-induced apoptosis (Jurkat FADD def.) [179]. Furthermore, we examined if ferroptosis occur with classical features like iron-dependency, ROS accumulation and lipid peroxidation and by that identify, if lipoxygenases are involved in RSL3-induced ferroptosis in ALL cells.

5.1.1.1 RSL3 induces cell death in ALL cells which can be classified as ferroptosis

To examine the onset of cell death, we performed a kinetic upon RSL3 treatment in Molt-4 and Jurkat cells. We revealed that the onset of cell death was after approximately 12 hours in both cell lines (Figure 2).

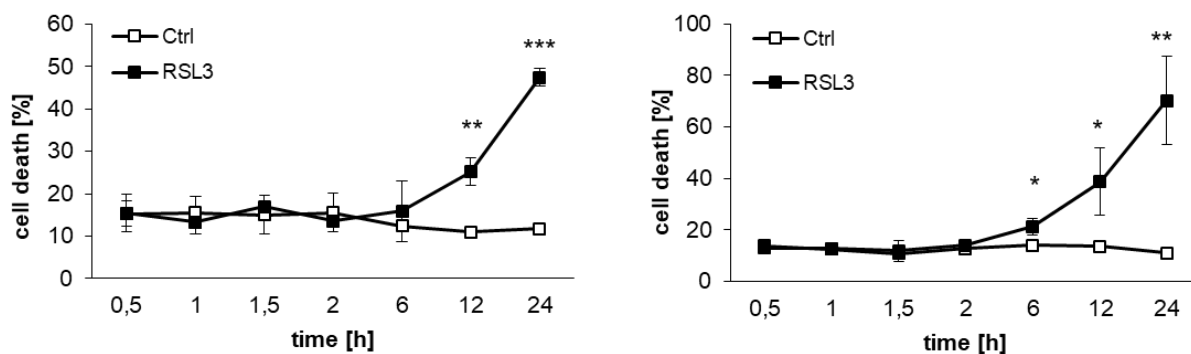


Figure 2: Cell death kinetic upon RSL3 stimulus.

Molt-4 (left) and Jurkat cells (right) were treated for indicated time points with RSL3 (Molt-4: 0.2 μ M, Jurkat: 0.3 μ M). Cell death was analysed by flow cytometry (FSC/SSC). Mean and SD of at least three experiments performed in duplicates are shown; *, $P < 0.05$; **, $P < 0.01$; ***, $P < 0.001$.

After 24 hours, RSL3-induced cell death and PI positivity in Molt-4 and Jurkat cells was significantly rescued through the addition of a lipid peroxide scavenger Lip-1 and DFO, a known iron chelator (Figure 3). Experiments on Fer-1, another well-known lipid peroxide scavenger and ferroptosis inhibitor besides Lip-1, as well as experiments with α -Toc, a vitamin E derivate, were performed by Lukas Probst, which showed that these inhibitors also blocked RSL3-induced cell death, ROS formation and lipid peroxidation [180].

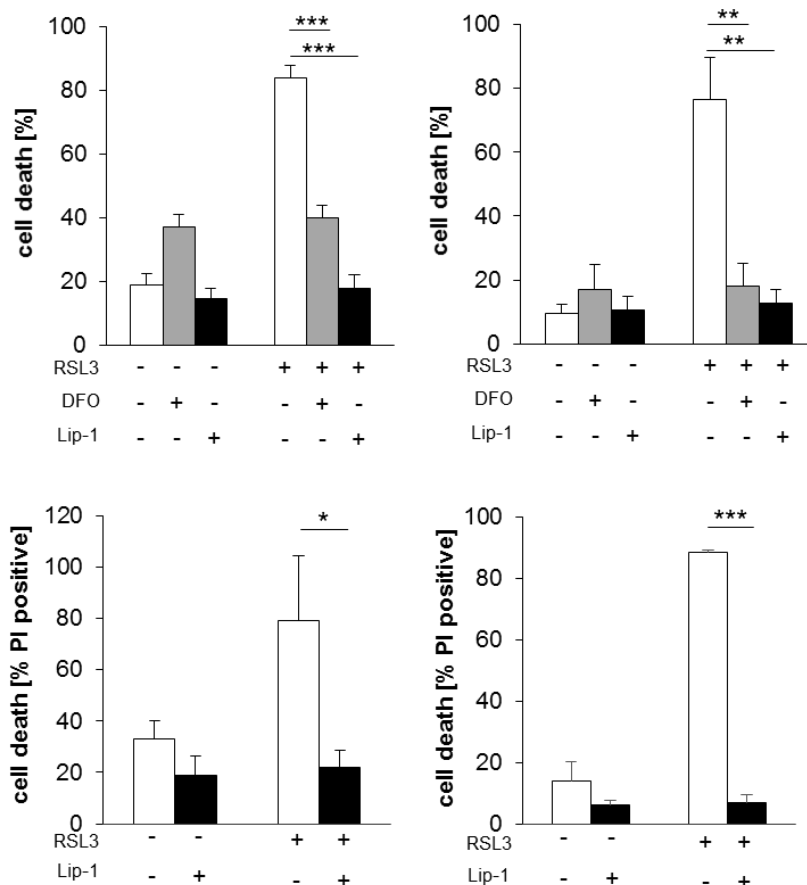


Figure 3: RSL3 stimulates ferroptosis in ALL.

Molt-4 (left) and Jurkat cells (right) were treated with RSL3 (Molt-4: 0.2 μ M, Jurkat 0.3 μ M) for 24 hours in the presence or absence of 5 μ M Fer-1, 25 μ M DFO, 25 nM Lip-1. Cell death was assessed by FSC/SSC analysis or PI staining using flow cytometry. Mean and SD of three experiments performed in triplicates are shown; *, P < 0.05; **, P < 0.01; ***, P < 0.001.

5.1.1.2 RSL3-induced ferroptosis is independent of caspases and RIP1

Inhibition of caspases using the pan-caspase inhibitor zVAD.fmk [181] and Nec-1s, a specific receptor-interacting protein kinase inhibitor [182], had no impact on RSL3-induced cell death (Figure 4). To ensure the efficiency of the employed inhibitors, control experiments for apoptosis (Etoposide/ABT737) and necroptosis (apoptosis resistant Jurkat FADD def. cells plus TNF α /BV6) were performed. These results suggest that RSL3-stimulated cell death is independent of caspases and RIP1.

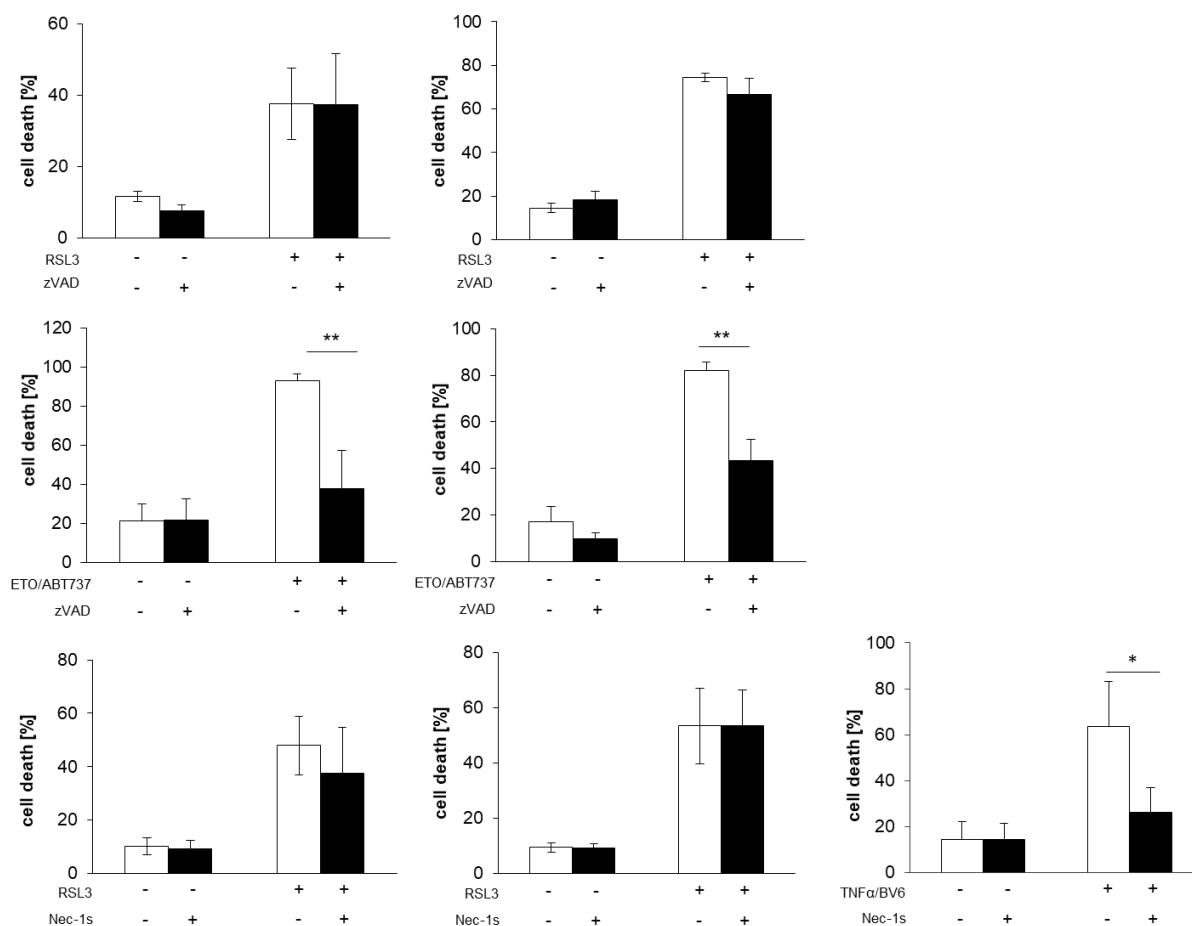


Figure 4: Caspases and RIP1 are not involved in ferroptosis.

Molt-4, Jurkat and Jurkat FADD def. cells (left to right) were treated for 24 hours with RSL3 (Molt-4: 0.2 μ M, Jurkat 0.3 μ M) Etoposide (100 μ M) and ABT737 (25 μ M), TNF α (Jurkat FADD def.: 1 ng/ml) and BV6 (4 μ M) in the presence or absence of 20 μ M zVAD.fmk or 30 μ M Nec-1s which were added two hours prior treatment. Cell death was defined by FSC/SSC analysis using flow cytometry. Mean and SD of three experiments performed in triplicates are shown; *, P < 0.05; **, P < 0.01 (experiments to RSL3 +/- zVAD.fmk and +/- Nec-1s were performed by Lukas Probst).

5.1.1.3 Lipoxygenases are involved in ferroptotic signalling

To verify the involvement of LOX in ferroptotic cell death in ALL cells, a variety of pharmacological LOX inhibitors were tested in different concentrations, namely Baicalein (selective 12/15-LOX inhibitor [183]), NDGA (pan-LOX inhibitor [184]), Zileuton (selective 5-LOX inhibitor [185]) and PD146176 (selective 15-LOX inhibitor [186]). All of the above mentioned LOX inhibitors significantly inhibited RSL3-induced cell death in a dose dependent manner (Figure 5). NDGA and Baicalein also blocked RSL3-induced ROS formation and lipid peroxidation in Molt-4, Jurkat and Jurkat FADD def. cells [180].

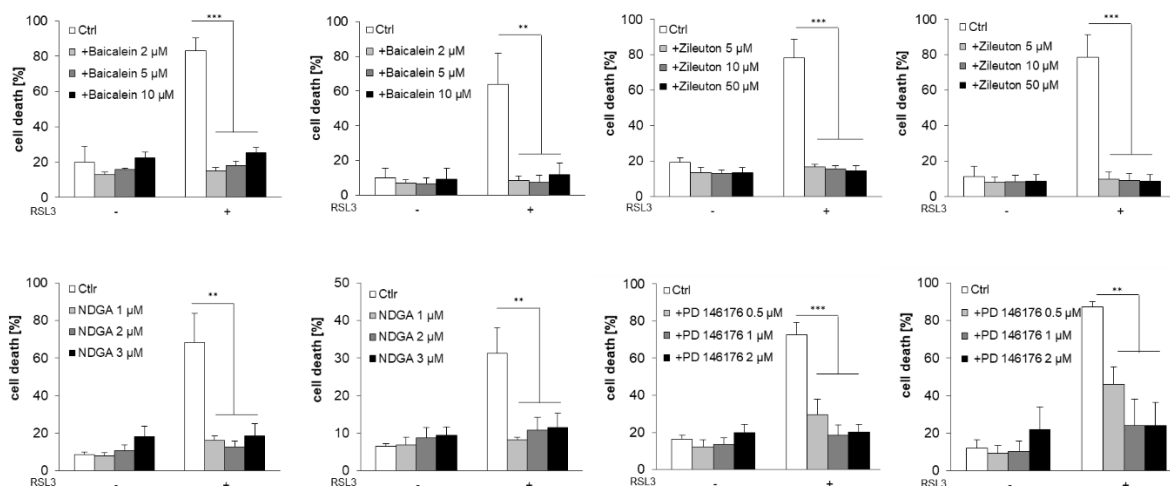


Figure 5: LOX are involved in RSL3-triggered ferroptotic cell death.

Molt-4 (first and third) and Jurkat cells (second and fourth) were treated for 24 hours with RSL3 (Molt-4: 0.2 μ M, Jurkat: 0.3 μ M) in the presence or absence of indicated concentrations of Baicalein, NDGA, Zileuton and PD146176, added two hours prior treatment. Cell death was analysed using flow cytometry (FSC/SSC). Mean and SD of at least three experiments performed in duplicates are shown; **, P < 0.01; ***, P < 0.001.

5.1.1.4 GPX4 protein levels are not affected by lipoxygenase inhibitors

GPX4 plays a crucial role in ferroptosis, since its inhibition leads to the accumulation of lipid peroxides [104]. To monitor if the rescuing effects of LOX inhibitors were due to changes in GPX4 protein levels, we performed western blot analysis. Here, LOX inhibitors had only minor effect on GPX4 protein levels (Figure 6).

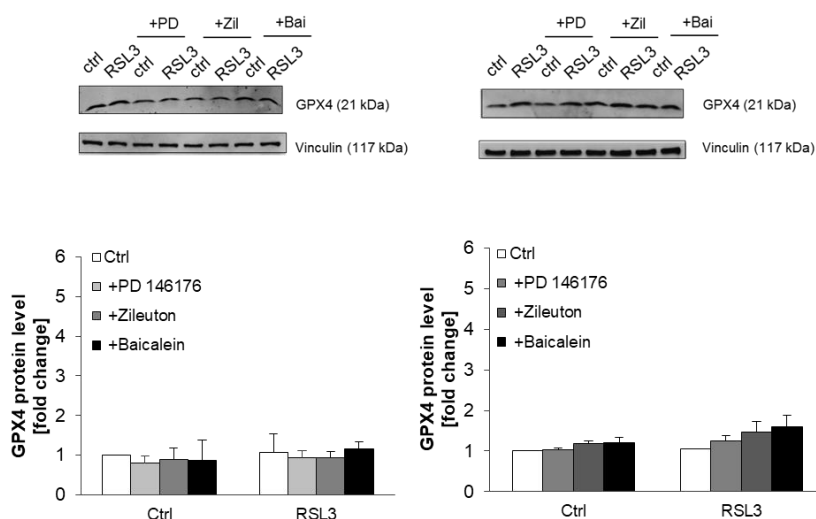


Figure 6: LOX inhibitors do not affect GPX4 protein level.

Molt-4 (left) and Jurkat cells (right) were treated for six hours with RSL3 (Molt-4: 0.2 μ M, Jurkat: 0.3 μ M) in the presence or absence of Baicalein (5 μ M), NDGA (2 μ M), Zileuton (5 μ M) and PD146176 (1 μ M), added two hours prior treatment. Protein expression level of GPX4 was analysed after six hours by western blot analysis and quantified using ImageJ, whereas GPX4 was normalized to loading control (Vinculin); shown as fold change. Mean and SD of at least three experiments performed in triplicates are shown.

5.1.1.5 Lipoxygenases are not regulated on mRNA level in ALL

To test the hypothesis, if lipoxygenases are genetically activated upon RSL3 treatment, mRNA expression levels of 15-LOX and 12-LOX were determined six hours after treatment. Neither 15-LOX, nor 12-LOX mRNA expression level were upregulated after RSL3 stimulation, indicating that other posttranscriptional mechanisms might be involved in the activation process of LOX (Figure 7).

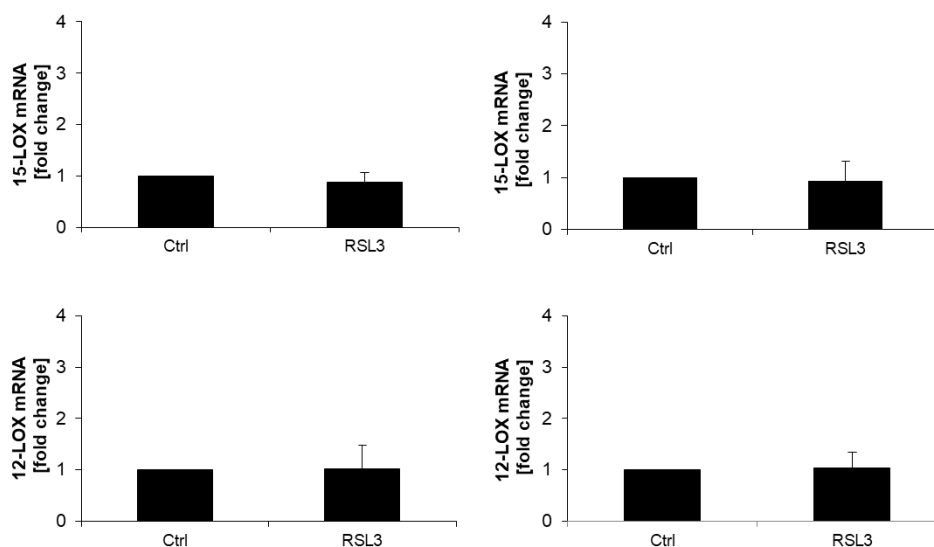


Figure 7: 15-LOX and 12-LOX mRNA levels are not affected by RSL3 stimulation.

Molt-4 (left) and Jurkat cells (right) were treated for six hours with RSL3 (Molt-4: 0.2 μ M, Jurkat: 0.3 μ M). 15-LOX and 12-LOX mRNA levels were determined after six hours by qRT-PCR and normalized to 28S rRNA expression, shown as fold change. Mean and SD of at least three experiments performed in duplicates and triplicates are depicted.

5.1.2 RSL3 and Erastin differentially promote redox-based Smac mimetic-induced cell death

In this study we investigated if minor concentrations of prototypic ferroptosis stimuli like RSL3 (inhibitor of GPX4) and Erastin (Era) (inhibitor of x_c^-) cooperated with Smac mimetic BV6, an antagonist of cellular inhibitor of apoptosis and x-linked inhibitor of apoptosis proteins, to induce cell death in prototypic ALL cells (Jurkat and Molt-4). Besides its function as an inhibitor of IAPs, BV6 is also described as a ROS producing compound [117]. By combining these ROS producing agents with different targets, we wanted to examine hallmarks of ferroptotic signalling, like ROS and lipid ROS accumulation as well as the involvement of iron after combination treatment (RSL3/BV6 and Era/BV6).

5.1.2.1 BV6 potentiates RSL3- and Erastin-induced cell death

RSL3 directly inhibits GPX4 by binding to its selenocysteine in the catalytic centre, whereas Erastin indirectly inhibits GPX4 by limiting its cofactor GSH. It has been reported that Erastin inhibits the membrane bound cystine/glutamate antiporter x_c^- , limiting cystine import and GSH synthesis. Of note, BV6 significantly potentiated RSL3- and Erastin-induced cell death (Figure 8).

Furthermore, GSH was depleted upon Erastin single treatment and in combination with BV6, whereas RSL3 treatment alone or in combination with BV6 did not affect GSH level [187]. This set of experiments was performed by Hannah Schoeneberger. The loss of GPX4 or the GSH antioxidant defence system accelerates the accumulation of ROS and lipid-based ROS, two important hallmarks of ferroptosis, contributing to cell death. To explore whether these hallmarks also occurred after combination treatment, cellular ROS and lipid-based ROS levels were quantified before cells succumbed to cell death. Importantly, ROS and lipid peroxide levels were significantly enhanced in combination treatment (RSL3/BV6 and Era/BV6) compared to single treatment [187].

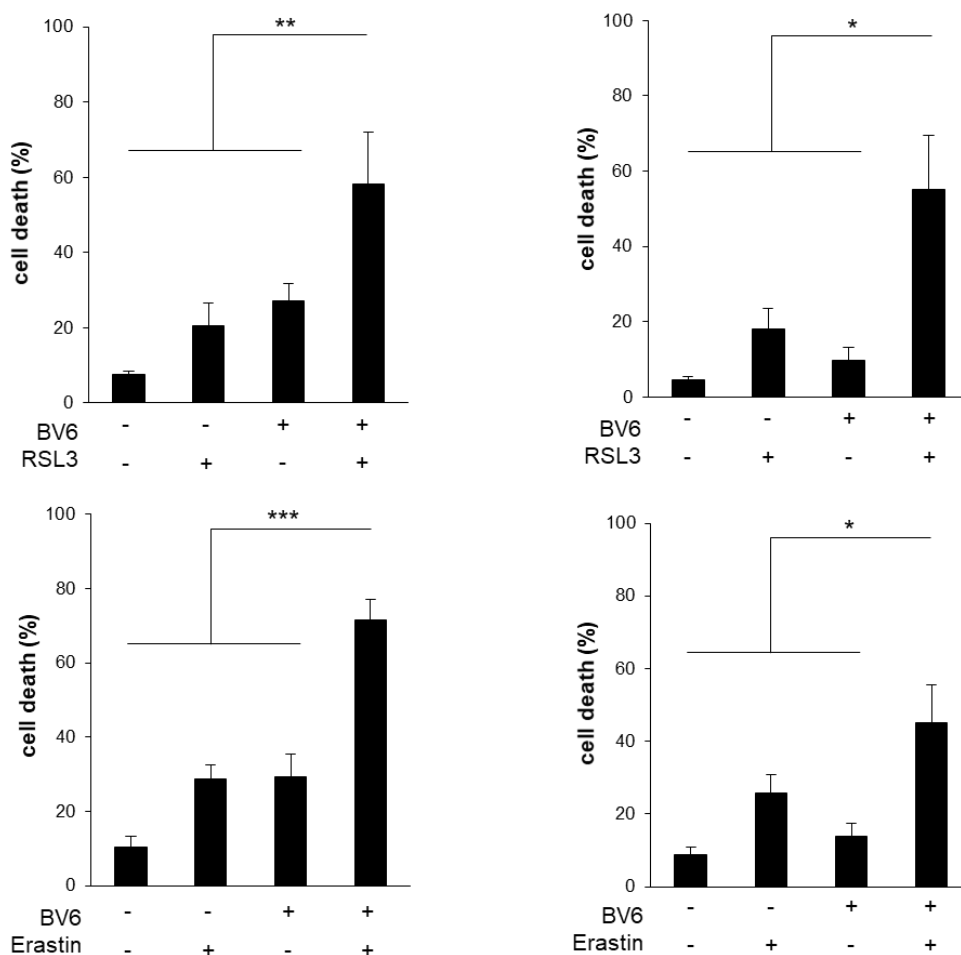


Figure 8: BV6 potentiates RSL3- and Erastin-induced cell death.

Jurkat (left) and Molt-4 cells (right) were treated for 24 hours (upper panel) and 48 hours (lower panel) with BV6 (Jurkat: 5 μ M, Molt-4: 4 μ M), RSL3 (Jurkat: 0.1 μ M; Molt-4: RSL3 0.075 μ M) and/or Erastin (Jurkat: 5 μ M; Molt-4: 7.5 μ M). Cell death was assessed by using FSC/SSC analysis and flow cytometry. Mean and SD of at least three experiments performed in triplicates are shown; *, P < 0.05; **, P < 0.01; ***, P < 0.001.

5.1.2.2 RSL3/BV6- but not Era/BV6-induced cell death is iron-dependent

To determine if ferroptosis plays a role in RSL3/BV6- or Era/BV6-induced cell death, we examined the dependency on iron. Therefore, we applied an iron chelator DFO, whereas high RSL3 concentrations served as positive control. Interestingly, DFO diminished RSL3/BV6-induced cell death, though no decreasing effect was observed in Era/BV6-induced cell death (Figure 9). These findings indicate that RSL3/BV6 and Erastin/BV6 differ in their mode of action in cell death induction.

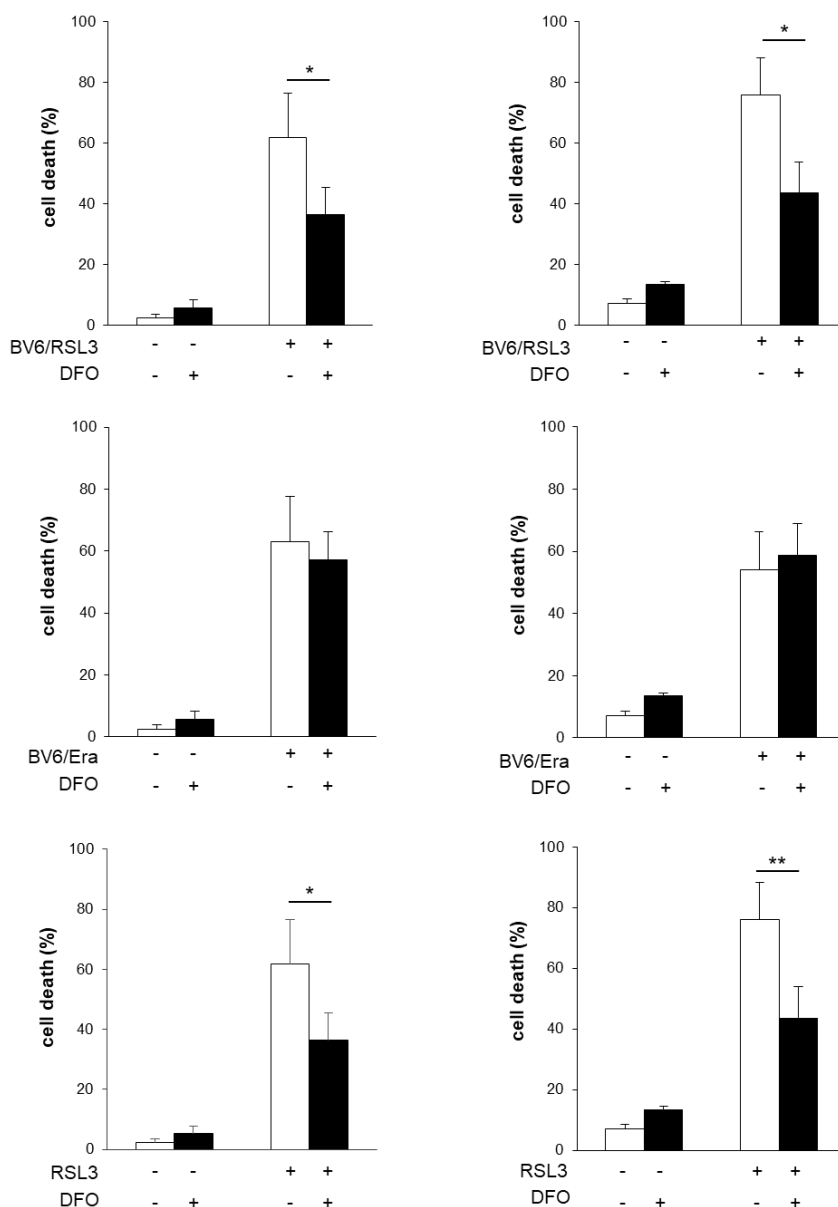


Figure 9: RSL3/BV6- but not Era/BV6-induced cell death is iron-dependent.

Jurkat (left) and Molt-4 cells (right) were treated for 24 hours with BV6 (Jurkat: 5 μ M, Molt-4: 4 μ M), RSL3 (Jurkat: 0.1 μ M; Molt-4: RSL3 0.075 μ M) and/or Erastin (Era) (Jurkat: 5 μ M; Molt-4: 7.5 μ M) and RSL3 alone (Jurkat: 10 μ M, Molt-4: 0.2 μ M) in the presence or absence of 25 μ M DFO, which was added two hours prior treatment. Cell death was defined by FSC/SSC analysis and flow cytometry. Mean and SD of at least three experiments performed in triplicates are shown; *, $P < 0.05$; **, $P < 0.01$.

5.1.2.3 Pharmacological and genetic inhibition of lipid peroxide formation rescue from RSL3/BV6- and Era/BV6-generated lipid peroxidation, whereby only RSL3/BV6-induced cell death is blocked

In addition, to the involvement of iron, lipid ROS formation is a central element of ferroptosis. Therefore, we evaluated the impact of Fer-1, an established pharmacological

inhibitor of lipid peroxides, on lipid peroxidation and cell death. Secondly, we performed a genetic approach to inhibit lipid peroxidation by overexpressing GPX4 to strengthen the results of pharmacological inhibition. Of note, Fer-1 decreased RSL3/BV6- and Era/BV6-generated lipid peroxidation significantly. However, it only reduced RSL3/BV6-stimulated cell death and failed to block Era/BV6-stimulated cell death (Figure 10).

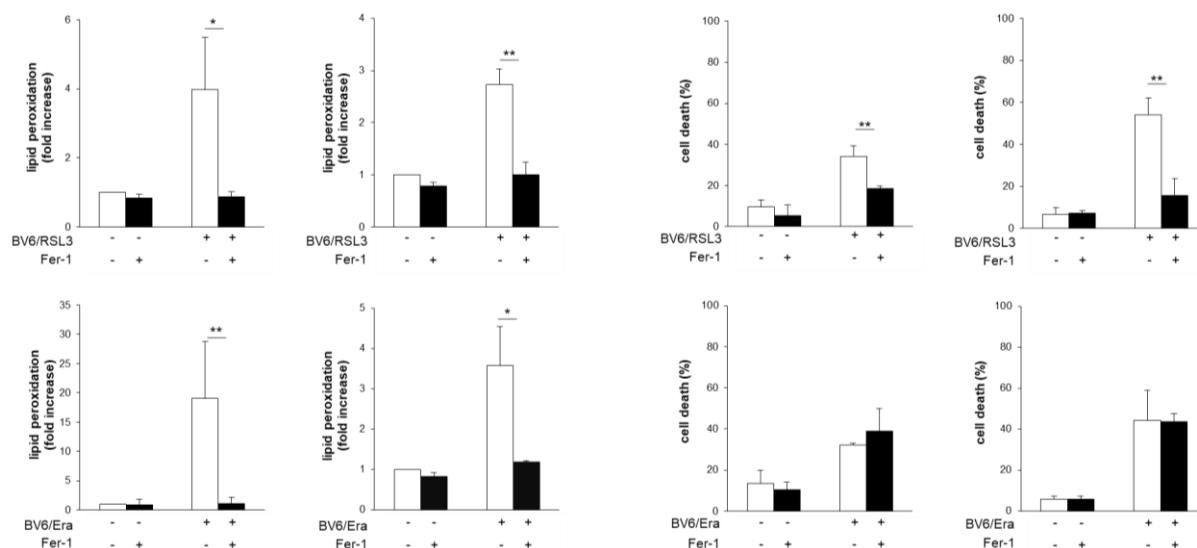


Figure 10: Fer-1 rescues from RSL3/BV6- and Era/BV6-generated lipid peroxidation, but it only prevents RSL3/BV6-induced cell death.

Jurkat (first and third) and Molt-4 cells (second and fourth) were treated with BV6 (Jurkat: 5 μ M, Molt-4: 4 μ M), RSL3 (Jurkat: 0.1 μ M; Molt-4: RSL3 0.075 μ M) and/or Erastin (Era) (Jurkat: 5 μ M; Molt-4: 7.5 μ M) in the presence or absence of 5 μ M Fer-1, which was supplemented two hours prior treatment. Lipid peroxidation was determined after 12 hours (Jurkat: Erastin/BV6), 18 hours (Molt-4: Erastin/BV6) or 24 hours (Jurkat: RSL3/BV6, Molt-4: RSL3/BV6) by flow cytometry in PI-negative cells using the fluorescent dye BODIPY-C11, shown as fold increase. Cell death was assessed by FSC/SSC analysis and flow cytometry. Mean and SD of three experiments performed in triplicates are shown; *, $P < 0.05$; **, $P < 0.01$.

These findings were consistent with results received by the genetic approach to inhibit lipid peroxide formation by GPX4 overexpression (Figure 11), suggesting that RSL3 in combination with BV6 triggers ferroptotic cell death. Nevertheless, cell death induced by Era/BV6 cannot be classified as classical ferroptosis, because cell death induction was independent of iron and lipid peroxidation.

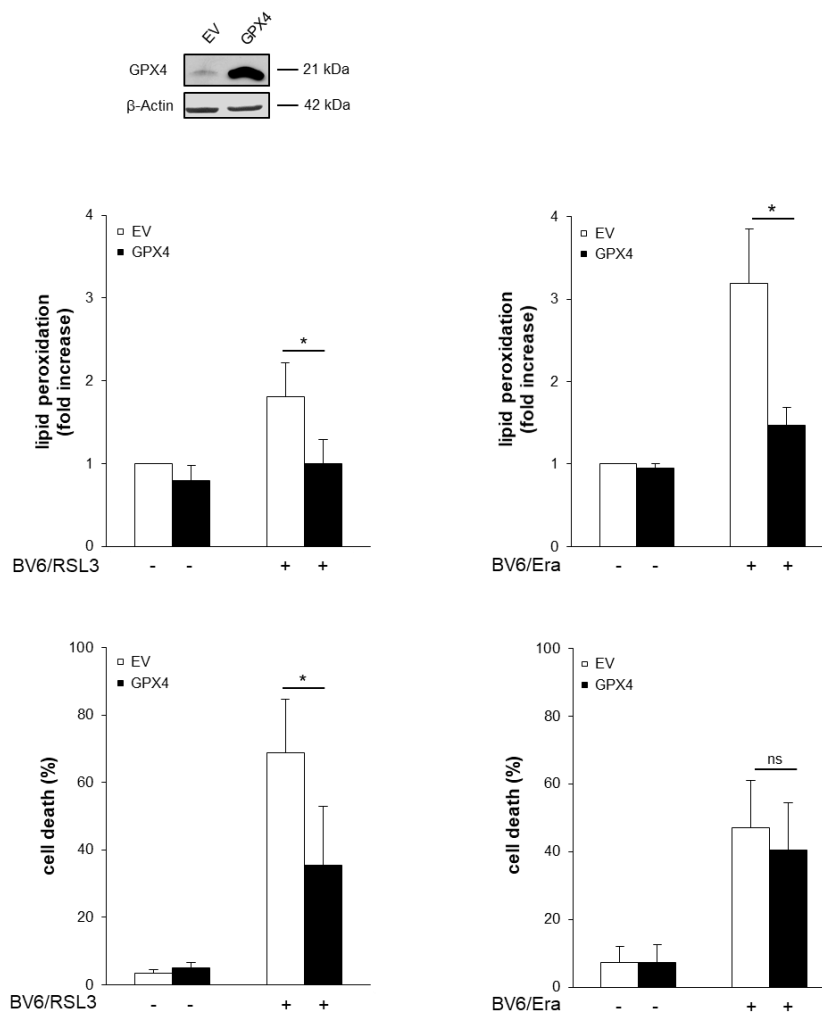


Figure 11: GPX4 overexpression reduces RSL3/BV6- and Era/BV6-generated lipid peroxidation, but it only prevents RSL3/BV6-induced cell death.

Stable transduction of the empty vector and a vector containing GPX4 was carried out in Molt-4 cells. GPX4 expression level was evaluated by western blot analysis. Cells were treated with 4 μ M BV6, 0.075 μ M RSL3 and/or 7.5 μ M Erastin (Era). Lipid peroxidation was defined after 18 hours (Erastin/BV6) or 24 hours (RSL3/BV6) by flow cytometry in PI-negative cells using the fluorescent dye BODIPY-C11, shown as fold increase. Cell death was assessed after 24 hours by FSC/SSC analysis and flow cytometry. Mean and SD of at least three experiments performed in triplicates are shown; *, $P < 0.05$; ns, not significant.

5.1.2.4 RSL3/BV6- or Era/BV6-induced cell death is independent of caspases, RIP1 and RIP3

Since BV6 can also trigger apoptosis in combination with GSH depleting agents [188], we examined if caspases were necessary for the induction of cell death, especially in Era/BV6-stimulated cell death. We monitored caspase-3/7 activity and found that only Era/BV6 cotreatment increased caspase activity significantly, while RSL3/BV6 treatment did not show alterations in comparison to control. To examine whether caspases are not only activated but also involved in the induction of cell death, we used

zVAD.fmk, a pan-caspase inhibitor to block cell death. Despite increased caspase activity in case of Era/BV6 cotreatment, the addition of zVAD.fmk failed to rescue cells from Era/BV6-induced cell death (Figure 12). Similar results were obtained after RSL3/BV6 treatment. Besides, the correct function of zVAD.fmk was confirmed through the inhibition of caspase-3/7 activity (Figure 12, upper panel). Also, increased lipid peroxidation upon treatment was not reduced through the addition of zVAD.fmk [187]. These results indicate that caspases may be activated. However, caspase activation is not relevant for cell death induction.

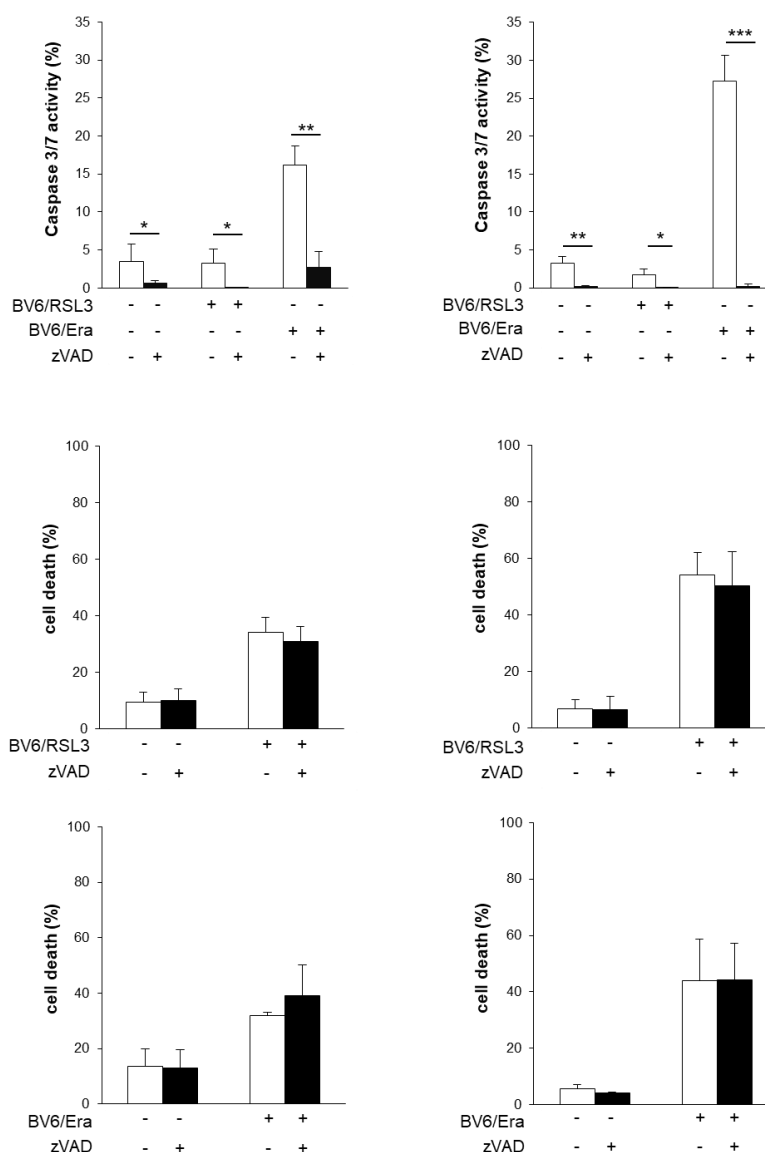


Figure 12: RSL3/BV6- or Era/BV6-triggered cell death is independent of caspases.

Jurkat (left) and Molt-4 cells (right) were treated with BV6 (Jurkat: 5 μ M; Molt-4: 4 μ M), RSL3 (Jurkat: 0.1 μ M; Molt-4: RSL3 0.075 μ M) and/or Erastin (Era) (Jurkat: 5 μ M; Molt-4: 7.5 μ M) in the presence or absence of 20 μ M zVAD.fmk, added two hours prior treatment. Activity of Caspase-3/7 was measured after 48 hours by Cell Event Caspase-3/7 Green Detection Reagent and ImageXpress Micro XLS system. Cell death was monitored after 12 hours (Jurkat cells: Erastin/BV6) or 24 hours (Jurkat cells: RSL3/BV6, Molt-4 cells: RSL3/BV6, Erastin/BV6) by FSC/SSC analysis and flow cytometry. Mean and SD of at least three experiments performed in triplicates are shown; *, $P < 0.05$; **, $P < 0.01$; ***, $P < 0.001$.

To examine whether Era/BV6 treatment induces necroptotic cell death when caspase activity is inhibited by zVAD.fmk, we used Nec-1, a pharmacological inhibitor of RIP1 and siRNA-mediated knockdown of RIP3 (Figure 13). Both failed to block Era/BV6-triggered cell death in the presence of zVAD.fmk. Positive controls to either experiment were performed to ensure the correct function of the inhibitor Nec-1s and siRNA-mediated knockdown of RIP3 [187]. This set of experiments shows that Era/BV6-mediated cell death is neither caspase-dependent, nor dependent on RIP1 or RIP3.

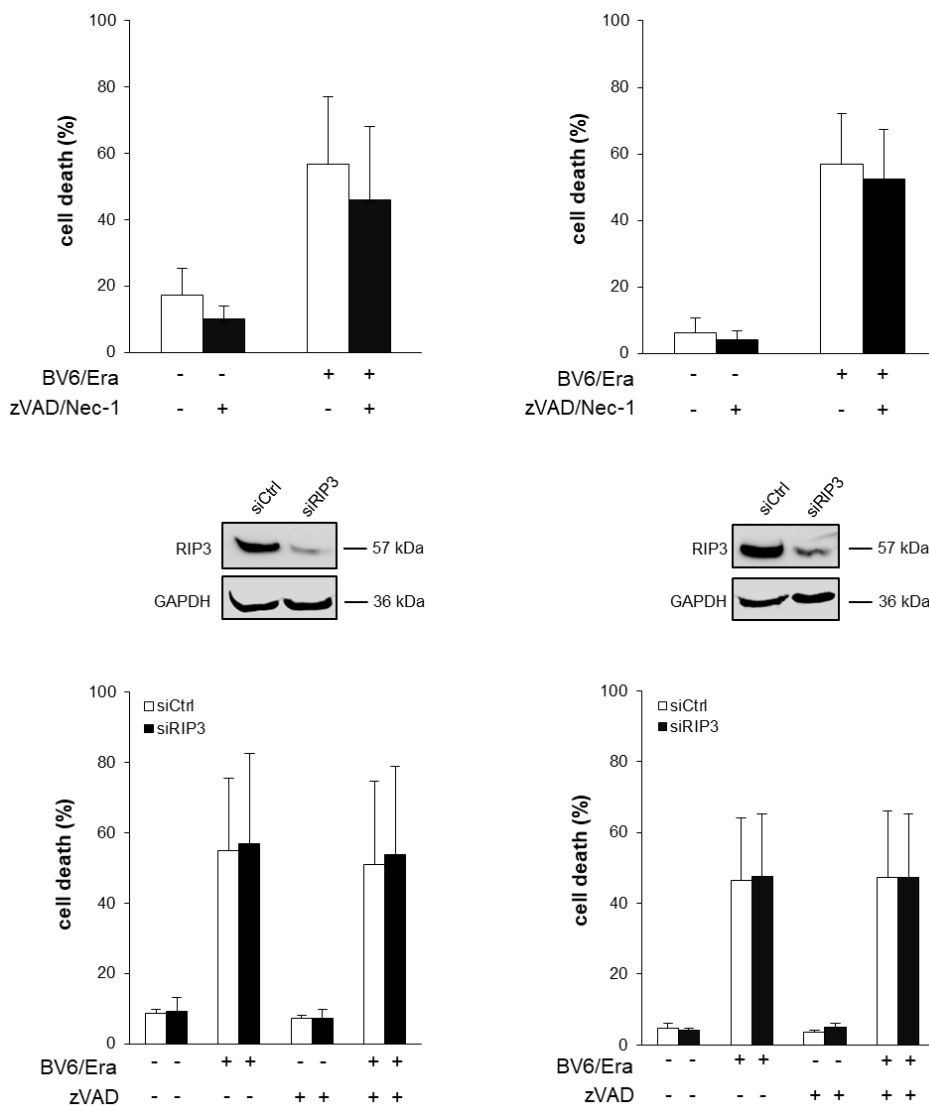


Figure 13: Era/BV6 cotreatment does not trigger RIP1- and RIP3-dependent necroptosis.

Jurkat (left) and Molt-4 cells (right) were treated for 24 hours with BV6 (Jurkat: 5 μ M, Molt-4: 4 μ M) and/or Erastin (Era) (Jurkat: 5 μ M; Molt-4: 7.5 μ M) in the presence or absence of 20 μ M zVAD.fmk and 15 μ M Nec-1, added two hours prior treatment. Additionally, transient siRNA-mediated knockdown against RIP3 was performed in ALL cells. RIP3 protein expression level was determined via western blot analysis (upper panel). Cell death was monitored by FSC/SSC analysis and flow cytometry. Mean and SD of at least three experiments performed in triplicates are shown.

5.1.2.5 α -Tocopherol depletes RSL3/BV6- and Era/BV6-generated ROS production, whereby Fer-1 only blocks RSL3/BV6-triggered ROS production

To determine the contribution of ROS to cell death in both combinations, we applied α -Toc, a lipophilic antioxidant. The application of α -Toc significantly attenuated lipid peroxidation and cell death in both combinations [187]. Simultaneously, ROS production by either RSL3/BV6 or Era/BV6 treatment was attenuated through α -Toc (Figure 14). By contrast, addition of Fer-1 only inhibited RSL3/BV6- but not Era/BV6-induced ROS production significantly, corresponding to cell death (Figure 10). Additionally, the presence of NAC, described as a thiol-containing antioxidant and precursor of GSH [189], suppressed Era/BV6-induced ROS production and cell death [187].

These results underscore that upon RSL3/BV6 treatment mainly lipid-based ROS contributes to cell death, since overall ROS production can be attenuated upon inhibition of lipid peroxidation. Though, other ROS sources besides lipid-based ROS are involved in Era/BV6-induced cell death.

In summary, the obtained results show that RSL3/BV6-stimulated cell death shares features of ferroptotic cell death, while Era/BV6-induced cell death largely depends on ROS accumulation but not on lipid peroxide formation or iron.

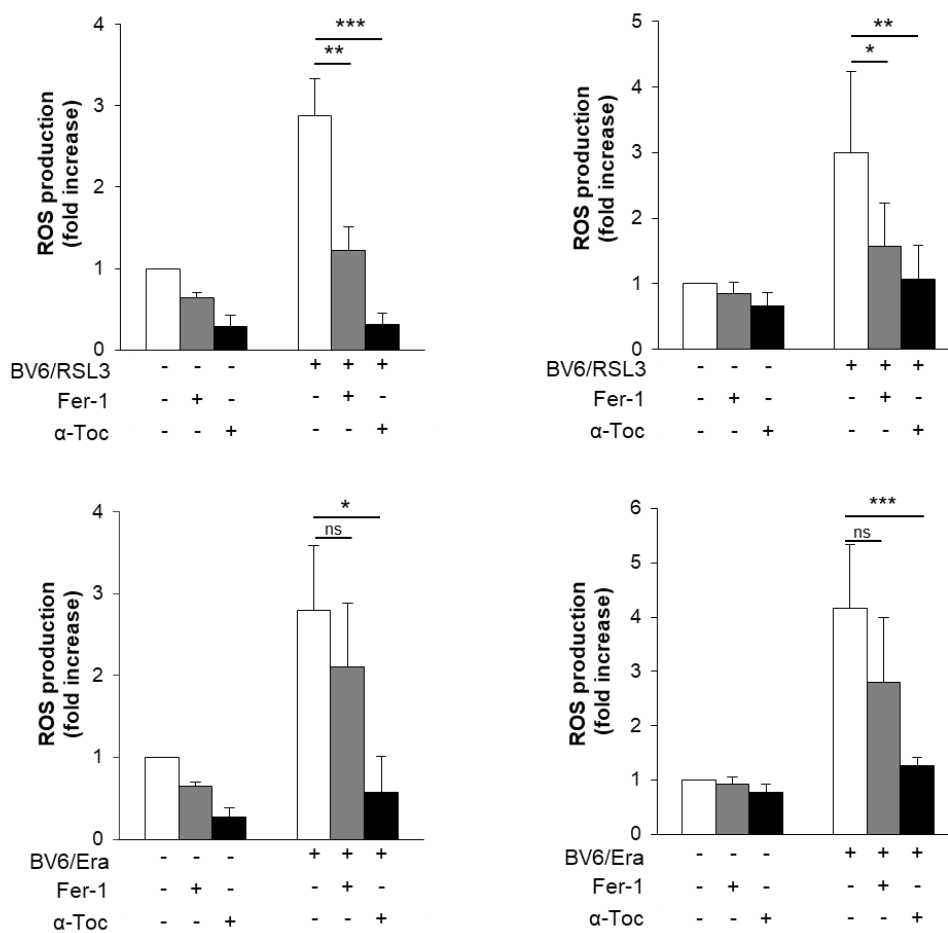


Figure 14: α -Tocopherol depletes RSL3/BV6- and Era/BV6-generated ROS production, whereby Fer-1 only blocks RSL3/BV6-triggered ROS production.

Jurkat (left) and Molt-4 cells (right) were treated with BV6 (Jurkat: 5 μ M, Molt-4: 4 μ M), RSL3 (Jurkat: 0.1 μ M; Molt-4: RSL3 0.075 μ M) and/or Erastin (Era) (Jurkat: 5 μ M; Molt-4: 7.5 μ M) in the presence or absence of 100 μ M α -Toc or 5 μ M Fer-1, added two hours prior treatment. ROS production was analysed after 15 hours by flow cytometry in PI-negative cells using the fluorescent dye CellROX, shown as fold increase with mean and SD of three experiments performed in triplicates; *, $P < 0.05$; **, $P < 0.01$; ***, $P < 0.001$; ns, not significant.

5.1.2.6 Erastin as single agent does not induce ferroptosis in ALL cells

These implications were further strengthened by experiments with the usage of RSL3 and Erastin as single agents. In comparison, RSL3 is much more potent than Erastin in inducing cell death in Jurkat and Molt-4 cells. The addition of Lip-1 and DFO attenuated RSL3-stimulated cell death, whereby the inhibitors failed to inhibit Erastin-induced cell death (Figure 15).

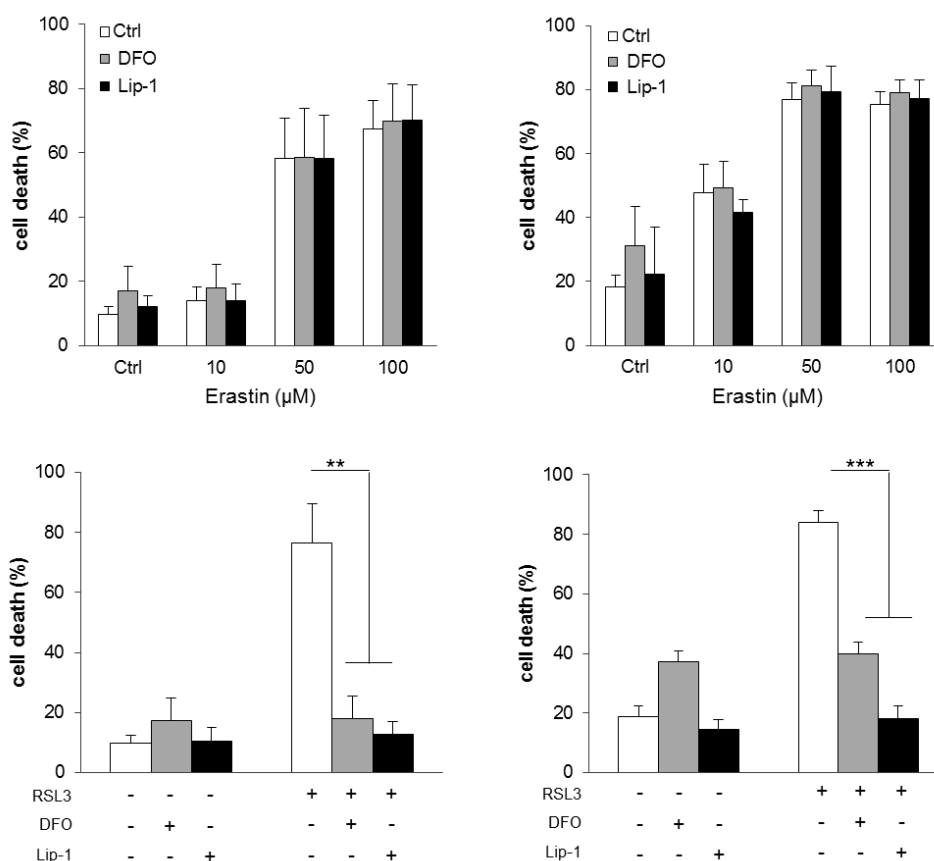


Figure 15: Erastin as single agent does not trigger ferroptosis.

Jurkat (left) and Molt-4 cells (right) were treated with RSL3 or Erastin for 24 hours, in the presence or absence of 25 μM DFO or 25 nM Lip-1, added two hours prior treatment. Cell death was determined by FSC/SSC using flow cytometry. Mean and SD of three experiments performed in triplicates are shown; **, $P < 0.01$; ***, $P < 0.001$.

5.1.2.7 RSL3 or Erastin cooperate with BV6 to generate ROS-dependent cell death in primary ALL blasts

Furthermore, we studied the physiological relevance of combination-induced cell death in a primary model. We investigated if RSL3/BV6 and/or Era/BV6 induce cell death in freshly isolated primary samples from children diagnosed with ALL before chemotherapy started. In addition, Fer-1 and α -Toc were used again to observe if RSL3/BV6 and Era/BV6 trigger ferroptosis in primary ALL blasts. In general, ROS production was increased upon treatment with both combinations (Figure 16). The addition of Fer-1 and α -Toc reduced ROS production, whereas cell death was just slightly affected. In Era/BV6 treated blasts, α -Toc diminished ROS production, whereby Fer-1 had only minor effects. Era/BV6-induced cell death was reduced upon α -Toc, particularly in sample #2 (Figure 16). These varying observations might be due to differences in samples and differences in basal cell death level at the onset of experiments. In summary, both combinations may stimulate ROS-dependent cell death in primary ALL blast.

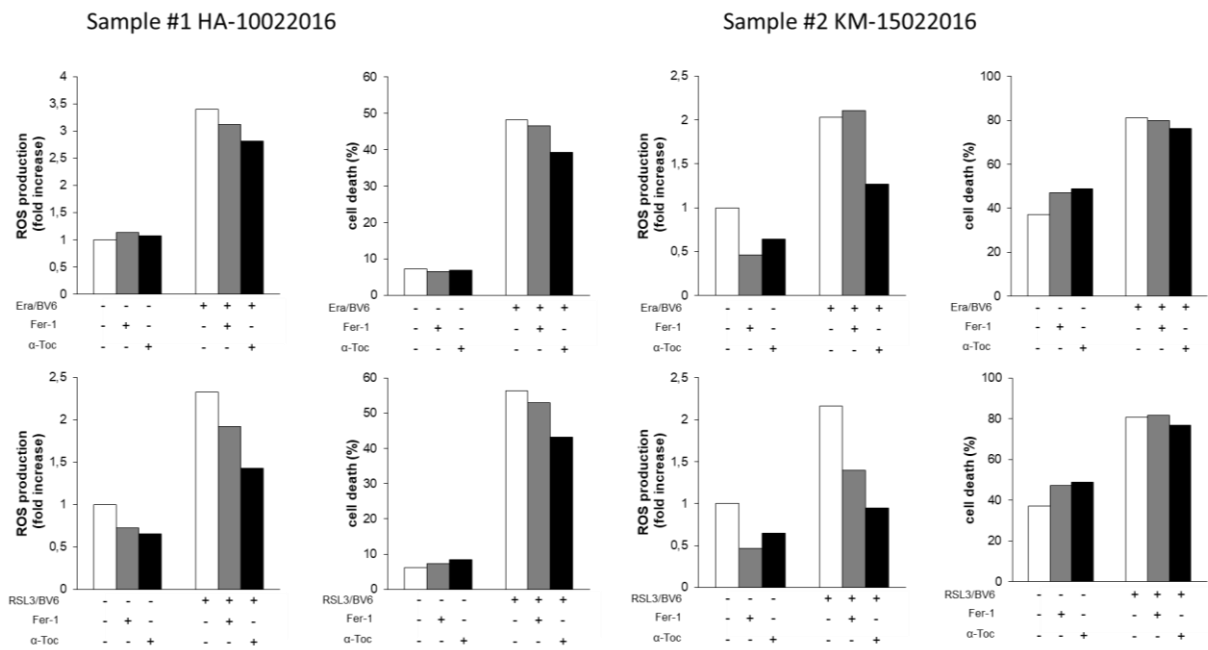


Figure 16: RSL3 or Erastin cooperate with BV6 to induce ROS-dependent cell death in primary ALL blasts. ALL blasts were treated for 24 hours with 5 μ M BV6, 0.1 μ M RSL3 and/or 5 μ M Erastin (Era) in the presence or absence of 100 μ M α -Toc or 5 μ M Fer-1, which were added two hours before treatment. Cell death was assessed by FSC/SSC using flow cytometry. ROS production was analysed after 15 hours by flow cytometry in PI-negative cells using the fluorescent dye CellROX, shown as fold increase and mean of either one experiment, performed in triplicates.

5.2 Oxidative cell death in rhabdomyosarcoma cells

Since Erastin did not induce ferroptosis in ALL cells, we considered another cellular system as a model for ferroptotic cell death. Recent studies suggested that RMS cells are vulnerable to oxidative stress-inducing compounds [178, 190].

5.2.1 Erastin induces cell death in several RMS cell lines

As previously described, Erastin is known to induce ferroptosis in various pathological entities, like cancer cells, kidney injury and neurodegenerative diseases [144, 158, 191]. Initially, we used Erastin as a prototypical stimulus to induce ferroptosis in our model of RMS cells.

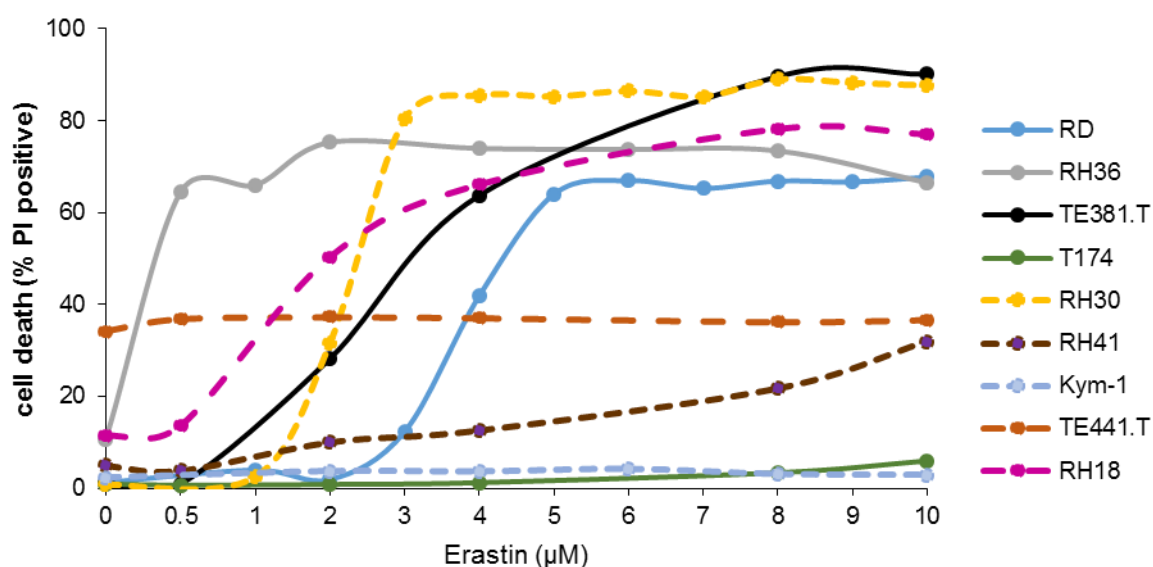


Figure 17: Erastin induces dose-dependent cell death in several RMS cells.

RMS cells (RAS mutated: solid line; RAS WT: dotted line) were treated with indicated Erastin concentrations for 24 hours. PI-positive cells were determined using PI/Hoechst-staining and the fluorescence microscope. Mean of at least three experiments performed in triplicates are shown (detailed cell death induction with SD is provided in the Appendix, Figure 34).

In a dose-dependent manner Erastin triggered cell in almost every RMS cells after 24 hours, whereby cell death induction was RAS-independent (Figure 17). In detail, RAS mutated RMS cells [192] (RD, RH36, TE381.T) respond more sensitive to Erastin treatment after 24 hours (Figure 17), whereas T174 responded only to Erastin after 48 hours at high concentrations in cell death induction (Appendix, Figure 34 and 35). Furthermore, Erastin stimulated cell death dose-dependently also in RAS WT RMS [192] after 24 and 48 hours (RH30, RH41, RH18) (Figure 17, Appendix Figure 34 and 35),

whereas Kym-1 and TE441.T cells showed resistance to Erastin treatment (Figure 17, Appendix Figure 34 and 35).

Since RAS mutated and RAS WT RMS responded to Erastin, we examined if differences in sensitivity to Erastin could be explained through differences in expression level of xCT, the light subunit of x_c^- and target of Erastin.

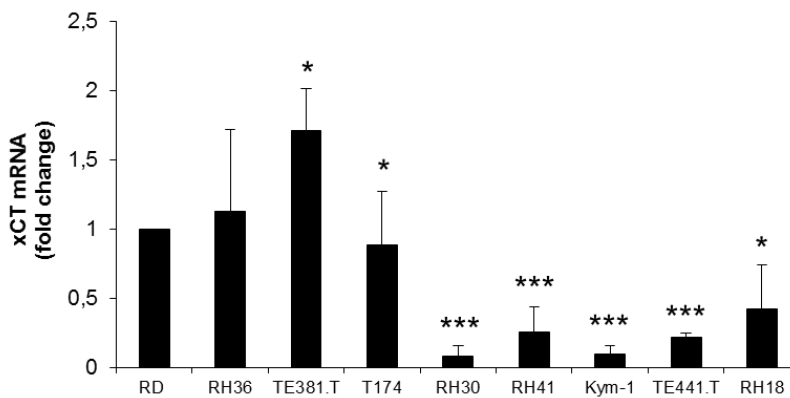


Figure 18: RMS display heterogeneous basal mRNA levels of xCT.

Basal mRNA expression level of xCT was analysed in RAS mutated (RD, RH36, TE381.T, T174) and RAS WT (RH30, RH41, Kym-1, TE441.T, RH18) RMS cells, applying qRT-PCR and shown as fold change. Mean and SD of at least three experiments performed in triplicates are shown; *, $P < 0.05$; **, $P < 0.01$. ***, $P < 0.001$.

Interestingly, RAS mutated RMS cells showed a higher basal level of xCT than RAS WT cells, when RD was used as reference. A very minor basal level of xCT was displayed in RH30 and Kym-1 (Figure 18). Plotting of cell death induction after treatment of 4 μM Erastin against the basal level of xCT revealed no clear correlation between vulnerability to Erastin treatment and xCT expression level which was indicated by $R^2 < 1$ (Figure 19).

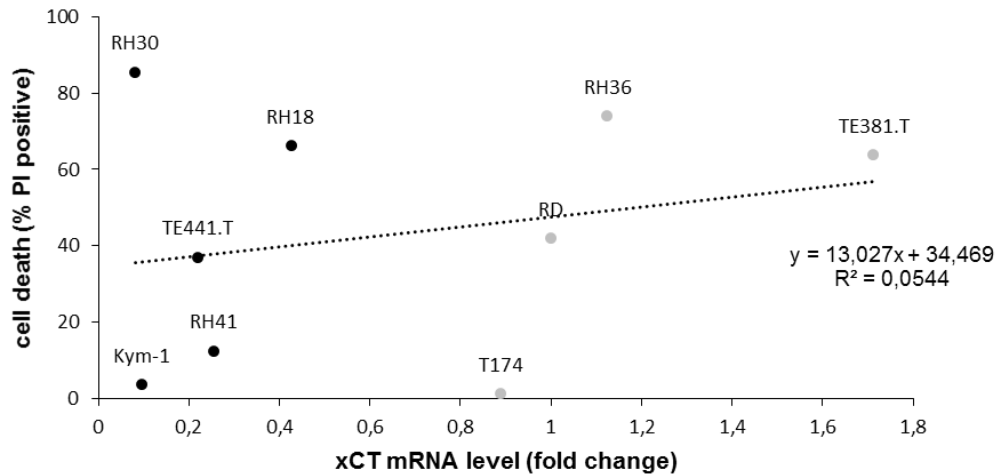


Figure 19: RMS show no correlation between sensitivity to ferroptosis and xCT expression.

Cell death (PI/Hoechst-staining at 4 μ M of Erastin) of RMS cells (RAS mutated: grey, RAS WT: black) was plotted against xCT mRNA expression level (qRT-PCR). Correlation between sensitivity to Erastin and expression level of xCT was assessed by using Excel.

5.2.2 Erastin-induced cell death shows characteristic features of ferroptosis, which is blocked through the addition of NOX inhibitors

To authenticate whether Erastin-induced cell death can be classified as ferroptosis, we used established ferroptosis inhibitors like Lip-1, Fer-1, ROS scavenger like α -Toc and GSH as well as iron chelator DFO to block Erastin-induced cell death (Figure 20).

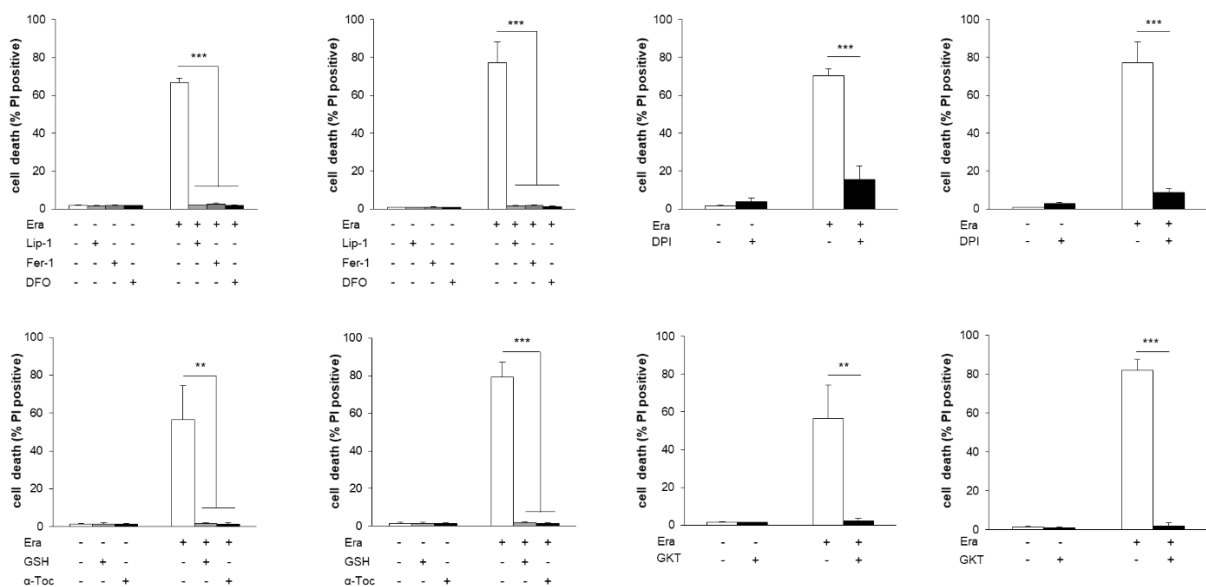


Figure 20: Erastin-induced cell death can be characterized as ferroptosis, which is blocked through the addition of NOX inhibitors.

RD (first and third) and RH30 cells (second and fourth) were treated with Erastin (Era) (RD: 5 μ M; RH30: 3 μ M) for 24 hours in the presence or absence of Liproxstatin-1 (50 nM), Ferrostatin-1 (5 μ M), Deferoxamine (25 μ M), GSH (2.5 mM), α -Tocopherol (100 μ M), Diphenyleiiodonium (1 μ M) and GKT137831 (20 μ M), which were added two hours prior treatment. PI-positive cells were determined using PI/Hoechst-staining and the fluorescence microscope. Mean and SD of at least three experiments performed in triplicates are shown; **, $P < 0.01$; ***, $P < 0.001$.

Importantly, the addition of all these inhibitors significantly decreased Erastin-induced cell death in RMS cells (Figure 20). Also the addition of GSH, which is an important ROS scavenging thiol and cofactor of GPX4 [142], inhibited cell death. Intriguingly, the addition of a broad spectrum NOX inhibitor DPI [193] impeded Erastin-induced cell death. Simultaneously, the widely used more selective NOX inhibitor GKT137831 that targets preferentially NOX1 and NOX4 [194] significantly reduced Erastin-triggered cell death in RD and RH30 (Figure 20) and additionally in RH36 cells (Figure 21).

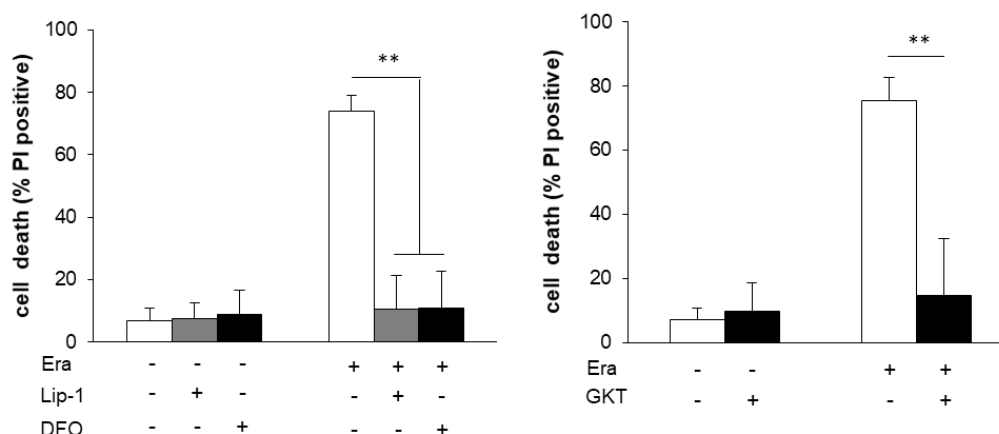


Figure 21: Erastin-induced cell death can be characterized as ferroptosis, which is blocked through the addition of NOX inhibitors.

RH36 cells were treated with 2 μ M Erastin (Era) for 24 hours in the presence or absence of Liproxstatin-1 (50 nM), Deferoxamine (25 μ M) and GKT137831 (20 μ M), which were added two hours before treatment. PI-positive cells were assessed using PI/Hoechst-staining and the fluorescence microscope. Mean and SD of at least three experiments performed in triplicates are shown; **, $P < 0.01$; ***, $P < 0.001$.

To examine if NOX plays a general role in ferroptosis, we used RSL3, another ferroptosis-inducing compound that directly targets GPX4. We observed that RSL3 also induced ferroptosis in RMS cells that was confirmed by using DFO and Fer-1 which effectively blocked RSL3-induced cell death (Figure 22). Further, RSL3-induced ferroptosis was also inhibited through the addition of the selective NOX1/4 inhibitor GKT137831 (Figure 22).

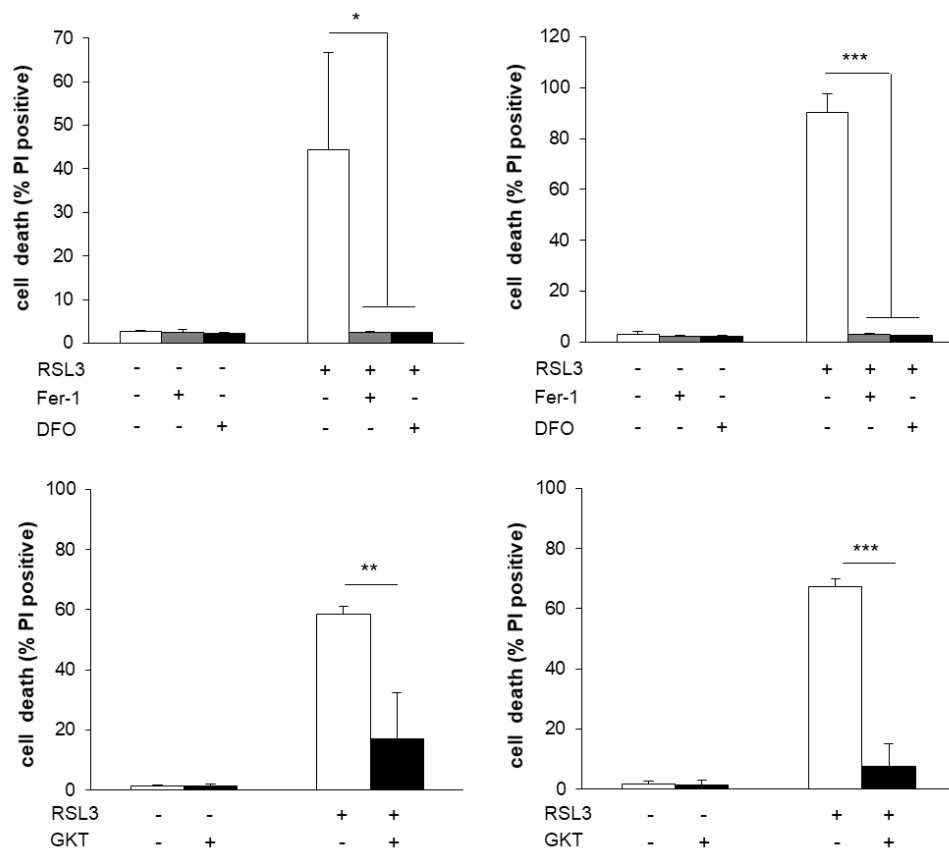


Figure 22: RSL3-induced ferroptosis is suppressed by NOX inhibitor GKT137831.

RD (left) and RH30 cells (right) were treated with RSL3 (RD: 1 μ M; RH30: 0.4 μ M) for 24 hours in the presence or absence of Ferrostatin-1 (5 μ M), Deferoxamine (25 μ M) and GKT137831 (20 μ M), added two hours before treatment. PI-positive cells were determined using PI/Hoechst-staining and the fluorescence microscope. Mean and SD of at least three experiments performed in triplicates are shown; *, $P < 0.05$; **, $P < 0.01$; ***, $P < 0.001$.

These results suggest a general involvement of NOX as a ROS-generating enzyme in ferroptosis in RMS, since Erastin- and RSL3-induced cell death was significantly suppressed upon the addition of GKT137831.

For further experiments we confined ourselves to a representative eRMS (RD) and representative aRMS (RH30) cell line.

5.2.3 Erastin leads to GSH depletion, accompanied by ROS and lipid peroxide formation

As Erastin induces ferroptosis through inhibition of the cystine/glutamate antiporter system x_c^- , we determined GSH levels, ROS production and lipid peroxidation after treatment of Erastin. First, we examined the kinetics of cell death upon exposure to Erastin to identify the onset of lethality in RMS cells after 15 to 18 hours (Figure 23).

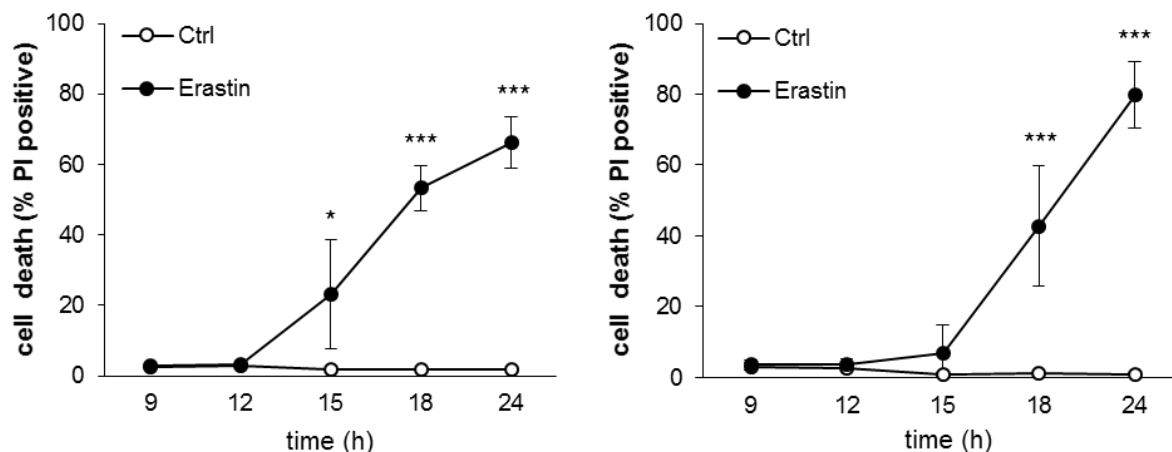


Figure 23: Cell death kinetic upon Erastin stimulus.

RD (left) and RH30 cells (right) were treated with Erastin for indicated time points (RD: 5 μ M, RH30: 3 μ M). PI-positive cells were determined using PI/Hoechst-staining and the fluorescence microscope. Mean and SD of at least three experiments performed in triplicates are shown; *, $P < 0.05$; ***, $P < 0.001$.

Of note, GSH levels were reduced after six hours treatment of Erastin in RMS cells (Figure 24). This GSH depletion was accompanied by a significant increase in ROS production and lipid peroxide formation after 12 hours (Figure 24). These findings strengthen the results that Erastin-induced GSH depletion, ROS and lipid ROS production contribute to ferroptotic cell death.

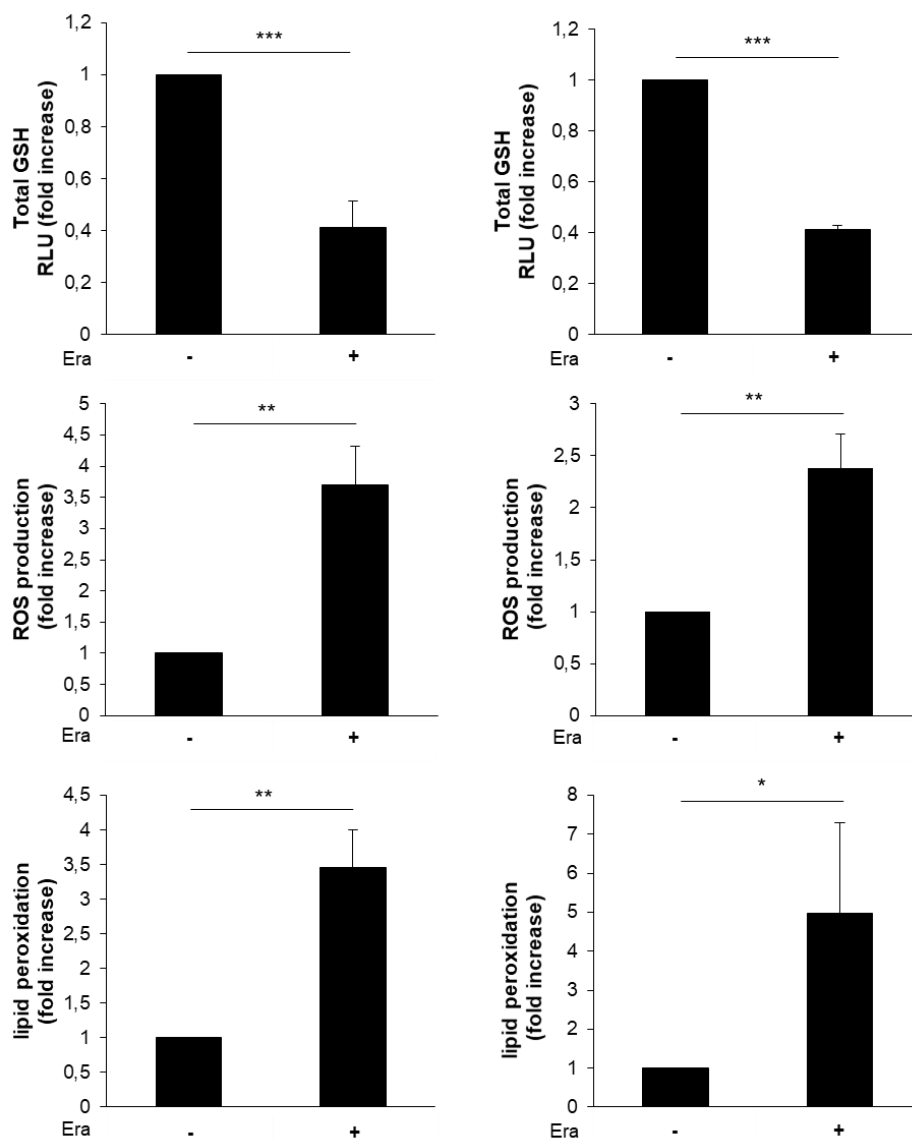


Figure 24: Erastin leads to GSH depletion, accompanied by ROS and lipid peroxide formation.

RD (left) and RH30 cells (right) were treated with Erastin (Era) (RD: 5 μ M, RH30: 3 μ M). GSH levels were defined in PI-negative cells after six hours Erastin treatment, using the chemiluminescent GSH/GSSG-Glo Assay. ROS production and lipid peroxidation were determined after 12 hours upon Erastin treatment in PI-negative cells using flow cytometry and the fluorescent dye H₂DCF (ROS) and BODIPY-C11 (lipid peroxidation), shown as fold increase. Mean and SD of at least three experiments performed in triplicates are shown; *, P < 0.05; **, P < 0.01; ***, P < 0.001.

5.2.4 Erastin-induced ROS production and lipid peroxidation is decreased through ferroptosis and NOX inhibitors

Since we observed hallmarks of ferroptosis like ROS production and lipid peroxidation in Erastin-treated RMS cells, we considered whether ferroptosis inhibitors and NOX inhibitors which inhibited cell death also suppress ROS formation and lipid peroxidation. Thus, Erastin-induced ROS production was significantly blocked through the addition of Fer-1, Lip-1, DFO, α -Toc, GSH and NOX inhibitors, whereas GSH and α -Toc

were the most potent inhibitors (Figure 25, upper panel). Likewise, lipid peroxide formation was significantly decreased through the addition of these inhibitors (Figure 25, lower panel).

These results indicate that ROS formation and lipid peroxidation indeed contribute to ferroptosis and that NOX might be a possible ROS source in ferroptotic signalling in RMS.

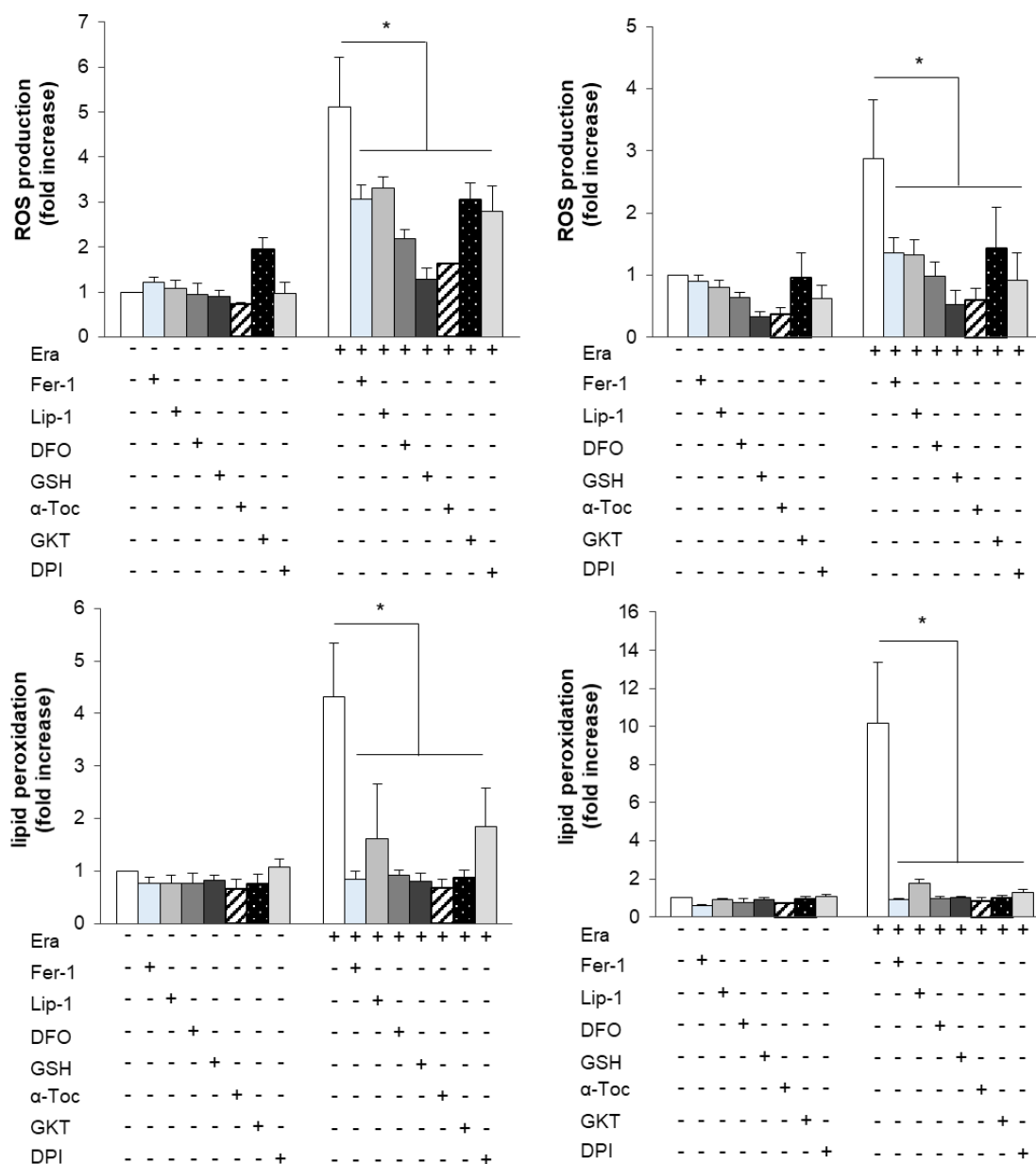


Figure 25: Erastin-induced ROS production and lipid peroxidation is decreased through ferroptosis and NOX inhibitors.

RD (left) and RH30 cells (right) were treated with Erastin (Era) (RD: 5 μ M; RH30: 3 μ M) for 12 hours in the presence or absence of Ferrostatin-1 (5 μ M), Liproxstatin-1 (50 nM), Deferoxamine (25 μ M), GSH (2.5 mM), α -Tocopherol (100 μ M) GKT137831 (20 μ M) and Diphenyleneiodonium (1 μ M), added two hours prior treatment. ROS production and lipid peroxidation were determined in PI-negative cells using flow cytometry and the fluorescent dye H₂DCF (ROS) and BODIYP-C11 (lipid peroxidation), shown as fold increase. Mean and SD of at least three experiments performed in triplicates are shown; *, P<0.05.

5.2.5 Genetic silencing of NOX4 rescues from Erastin-induced cell death

As GKT137831 targets NOX1 and NOX4 preferentially, we confirmed which isoform is most abundantly expressed in RMS cells. On mRNA level, RMS cells show higher expression level of NOX4 than NOX1 (Figure 26, upper panel). To validate if NOX4 is a possible ROS-generating enzyme in the displayed ferroptotic system, siRNA-mediated knockdown of NOX4 was performed. Of Note, NOX4 knockdown constricted Erastin-induced cell death (Figure 26, lower panel).

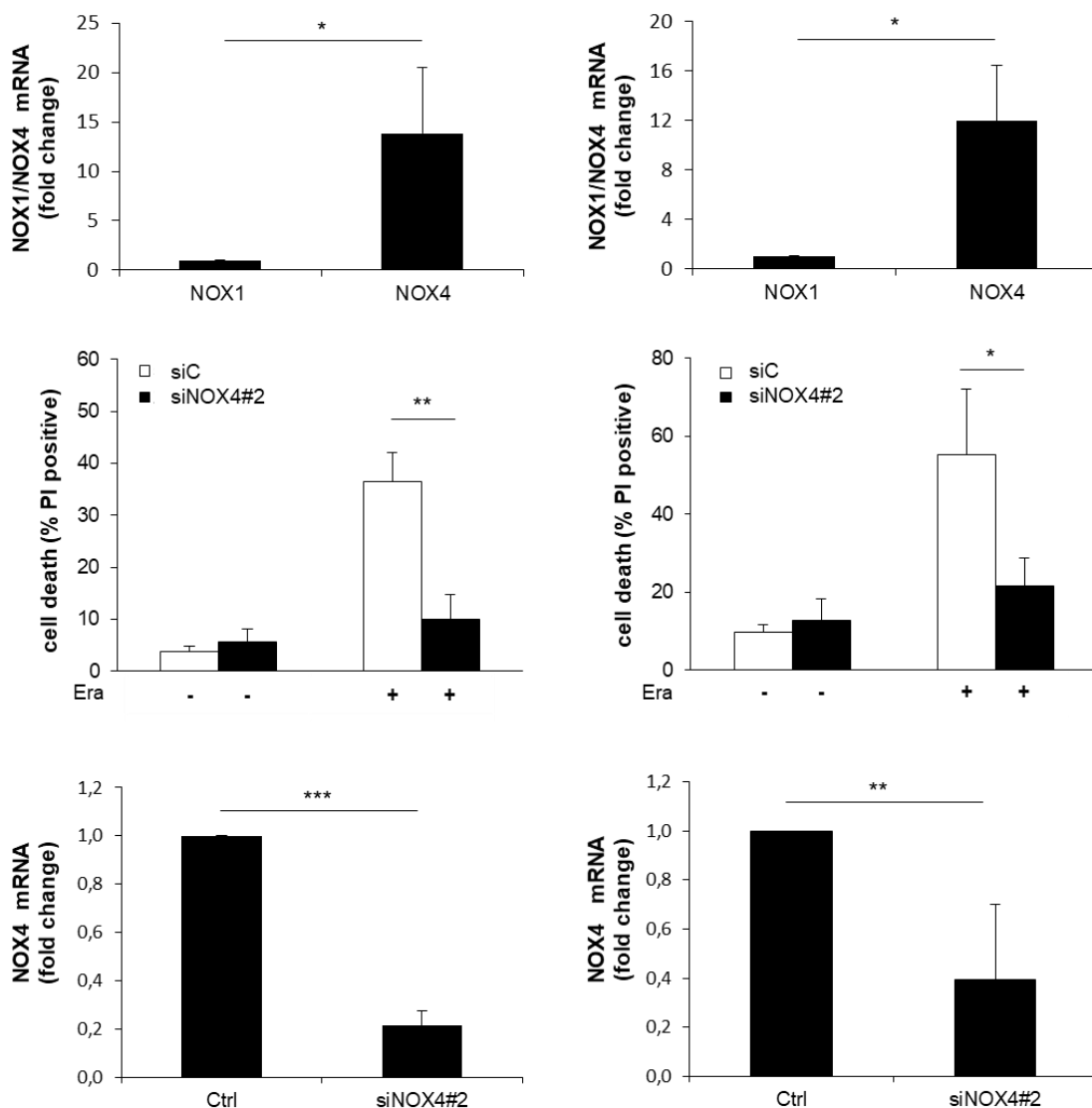


Figure 26: Genetic silencing of NOX4 rescues from Erastin-induced cell death.

NOX1 and NOX4 mRNA expression level in RD (left) and RH30 cells (right) were analysed after six hours applying qRT-PCR. RD and RH30 cells were treated with Erastin (Era) (RD: 5 μ M; RH30: 3 μ M) for 15 and 10 hours after transiently transfected knockdown of NOX4 (20 nM, 72 h). PI-positive cells were determined using PI/Hoechst-staining and the fluorescence microscope. NOX4 mRNA expression level was analysed as control of knockdown efficiency, applying qRT-PCR and shown as fold change. Mean and SD of at least three experiments performed in triplicates are shown; *, $P < 0.05$; **, $P < 0.01$; ***, $P < 0.001$.

These findings strengthen the suggestion that NOX4 might play a role in ferroptosis as a ROS-generating enzyme in RMS.

5.2.6 Bim1, a broad PKC inhibitor, decreases Erastin-induced cell death, ROS accumulation and lipid peroxidation

Different protein kinases C are characterized as upstream regulators of NOX isoforms, also of constitutively active forms like NOX4 [76, 195]. Since PKC have recently been implicated in ferroptosis [191], we screened for a potential involvement of PKC by using a broad PKC inhibitor Bim1 that targets different PKC isoforms [196]. The addition of Bim1 attenuated Erastin-induced cell death in a dose-dependent manner (Figure 27, Appendix Figure 40). Likewise, Erastin-induced ROS production and lipid peroxidation was significantly attenuated through the addition of Bim1 (Figure 27).

These results indicate that different PKC isoforms might be involved in ferroptotic cell death in Erastin-treated RMS cells.

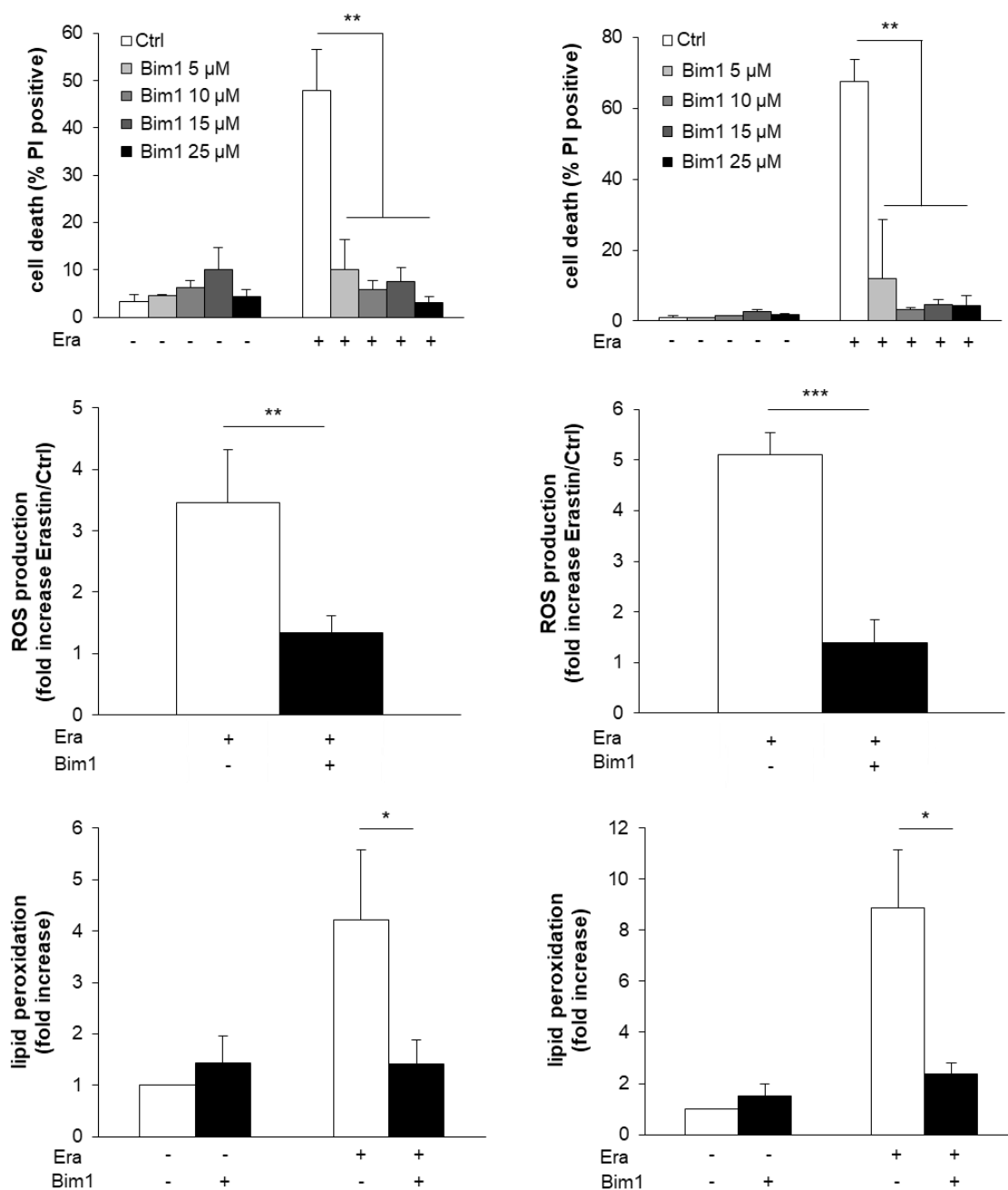


Figure 27: Bim1, a broad PKC inhibitor, decreases Erastin-induced cell death, ROS accumulation and lipid peroxidation.

RD (left) and RH30 cells (right) were treated with Erastin (Era) (RD: 5 μ M; RH30: 3 μ M) for 24 hours in the presence or absence of broad spectrum PKC inhibitor Bim1 with indicated concentrations. PI-positive cells were determined using PI/Hoechst-staining and the fluorescence microscope. ROS production and lipid peroxidation were determined after 12 hours upon Erastin treatment in PI-negative cells using flow cytometry and the fluorescent dye H₂DCF (ROS) (Depicted as Erastin/Ctrl fold increase because of own-fluorescence of Bim1) and BODIYP-C11 (lipid peroxidation), shown as fold increase. Bim1 (10 μ M) was added two hours before treatment. Mean and SD of at least three experiments performed in triplicates are shown; *, $P < 0.05$; **, $P < 0.01$; ***, $P < 0.001$.

5.2.7 The α and β selective PKC inhibitor Gö6976 reduces Erastin-induced cell death and lipid peroxidation

Furthermore, we analysed in detail which PKC isoforms might be involved in ferroptosis in RMS cells. Basal mRNA levels measured by quantitative real-time PCR revealed that PKC α was more abundantly expressed than δ , ϵ and β in RMS (Figure 28).

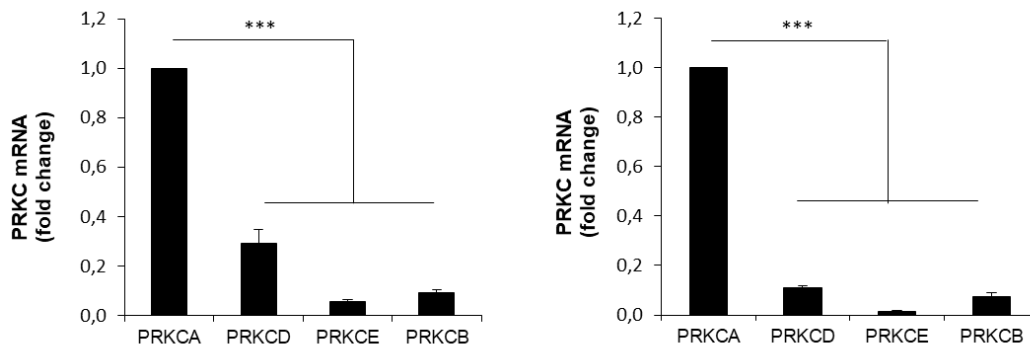


Figure 28: PKC α is more abundantly expressed in RMS.

Basal mRNA expression levels of indicated PKC isoforms were analysed, using qRT-PCR in RMS cells (RD left, RH30 right), shown as fold change. Mean and SD of three experiments performed in triplicates are shown; ***, $P < 0.001$.

To test the involvement of PKC α , we used a PKC inhibitor Gö6976, which is described to be more selective against PKC α and β isoforms [197]. Notably, the addition of Gö6976 reduced Erastin-induced cell death in a dose dependent manner (Figure 29, Appendix Figure 40). However, ROS production was not inhibited through the addition of Gö6976, whereas lipid peroxidation was significantly decreased (Figure 29).

These findings strengthen that PKC α and β are involved in Erastin-induced ferroptosis in RMS cells. Particularly, ROS production might be differently regulated by different PKC isoforms.

5.2.8 Genetic silencing of PKC α attenuates Erastin-triggered cell death

Since PKC α was most abundantly expressed as the other isoforms in RMS and recent study revealed an involvement of especially PKC α in ferroptosis in Parkinson's disease [191], a genetic silencing of PKC α was performed to confirm the involvement of this isoform in ferroptosis in RMS. In detail, siRNA-mediated knockdown of PKC α reduced Erastin-stimulated cell death in RMS cells significantly (Figure 30).

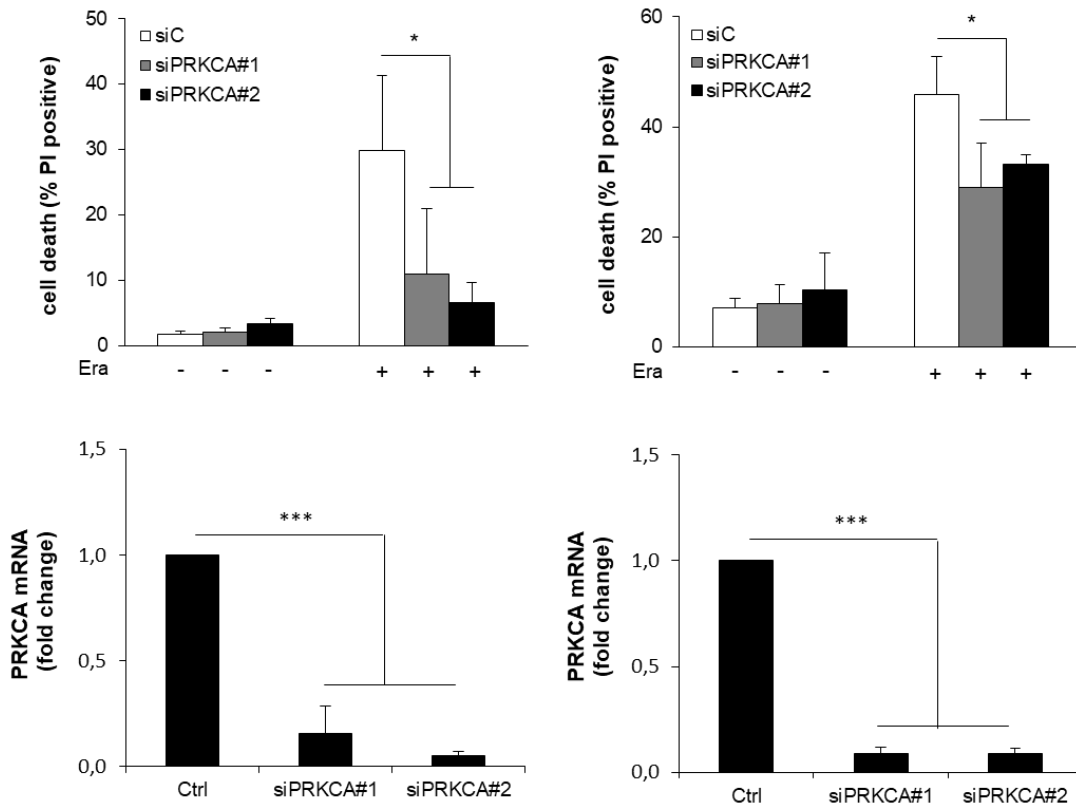


Figure 30: Genetic silencing of PKC α attenuates Erastin triggered cell death in RMS.

RD (left) and RH30 cells (right) were treated with Erastin (Era) (RD: 5 μ M; RH36: 2 μ M) for 15 hours (RD) and 22 hours (RH36) after transiently transfected knockdown of PKC α (10 nM, 72 hours). PI-positive cells were determined using PI/Hoechst-staining and the fluorescence microscope. Basal mRNA expression level of PKC α was assessed by applying qRT-PCR. Mean and SD of at least three experiments performed in triplicates are shown; *, $P < 0.05$; ***, $P < 0.001$.

This set of experiments suggests a regulatory involvement of particular PKC α in Erastin-induced ferroptosis in RMS.

6 Discussion

6.1 Oxidative cell death mechanisms in ALL cells

ALL is the most frequent malignant childhood disease. Despite improvements in therapy, there are still relapsed patients because of treatment failure [198]. In this respect, new treatment strategies to trigger programmed cell death are necessary, since cell death resistance is one hallmark of leukaemia cells [199]. Of note, ALL display upregulated antioxidant levels to cope with elevated ROS levels which is needed for cancer metabolism, function and progression [177]. Therefore, we considered if ALL cells might be sensitive to ferroptosis, an oxidative cell death which largely depends on the accumulation of ROS and iron.

This part of the study revealed that ferroptosis-inducing compound RSL3 (GPX4 inhibitor) alone or in combination with Smac mimetic BV6 induces ferroptotic cell death, whereas cells die distinct from ferroptosis by treatment with Erastin (x_c^- inhibitor) alone or in combination with BV6. Additionally, we confirmed that lipoxygenases play a crucial role in ferroptotic signalling in ALL cells after RSL3 treatment.

6.1.1 Lipoxygenases are involved in ROS-mediated ferroptotic signalling upon RSL3 stimulation in ALL cells

Ferroptosis was recently described as programmed cell death that depends on cellular iron accumulation, ROS and lipid-based ROS formation [101]. The present study investigated that LOX are crucial for RSL3-induced ferroptosis in ALL cells. This hypothesis was based on results, demonstrating that various LOX inhibitors with different target specificity rescued from RSL3-mediated ferroptosis. Particularly, RSL3-generated ROS and lipid peroxidation, two important execution mechanisms leading to ferroptotic cell death, were diminished through the addition of pan-LOX inhibitor NGDA [184] and Baicalein, a selective 12/15-LOX inhibitor [183], assuming that lipoxygenases contribute to ROS formation and lipid peroxidation (Figure 31).

6.1.1.1 Specific activation of LOX remains unclear in ALL

LOX inhibitors had no impact on GPX4 level, therefore the rescuing mechanisms might be due to inhibition of LOX, and is not dependent on upregulated GPX4 protein levels. It is still unclear, how LOX are activated. We could show that LOX mRNA expression levels are not altered upon RSL3 stimulation, leading to the hypothesis that other post-transcriptional regulatory elements are responsible for the activation of LOX. For 5-

LOX activation, an activating protein called FLAP is needed [200] and 5-LOX activation is triggered by p38 MAPK-mediated oxidative stress [201]. Thus, phosphorylation by serine/threonine kinases like MAPK and also activation via AA are described to play a crucial role in the activation of LOX [202]. Moreover, hydroperoxides also mediates the activation of some LOX isoforms [203]. Importantly, Schnurr and colleagues demonstrated that 15-LOX is in general inactivated in the presence of GPX4 and GSH [204].

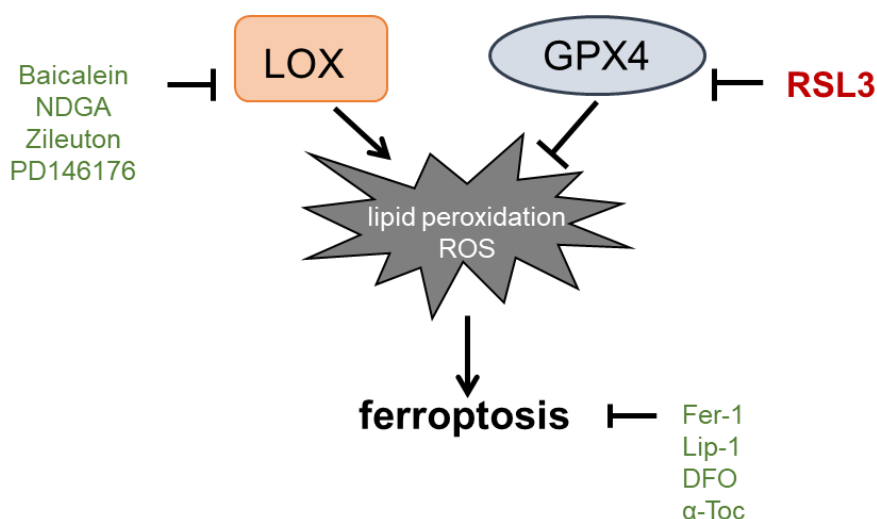


Figure 31: Hypothetical scheme of the involvement of Lipoxygenases in ferroptotic cell death in ALL.

Through the inhibition of GPX4 by RSL3, ROS and lipid peroxide formation contributed to ferroptotic cell death. The addition of various LOX inhibitors and ferroptosis inhibitors protected ALL cells from ROS, lipid peroxidation and cell death.

Furthermore, it is known that iron plays an important role in ferroptosis [101, 205]. ROS-generating enzymes like NOX, xanthine oxidases, cytochrome P450 and also LOX, require iron or iron derivatives for their proper function [206]. In addition, lipid-based ROS, a central executioner of ferroptosis, can be generated non-enzymatically by Fenton chemistry or enzymatically by lipoxygenases [68, 72].

6.1.1.2 LOX play a central role in cell death mechanisms, especially in ferroptosis. Previous studies revealed an involvement of LOX in models of oxidative stress-induced cell death and ferroptosis. Seiler and colleagues showed that GPX4 inactivation triggered lipid cell death in which apoptosis-inducing factor (AIF) and 12/15-lipoxygenase-dependent lipid peroxidation were identified as important cell death mediators [141]. Cell death was rescued by siRNA-mediated knockdown of AIF and through the supplementation of either lipophilic antioxidant α -Tocopherol or specific 12/15-lipoxygenase inhibitors like Baicalein and PD146176 [141]. Furthermore, RSL3 was identified as

ferroptosis-inducing compound which inhibits GPX4 in its enzymatic function by covalently binding to its selenocysteine, leading to the accumulation of PUFA, hydroperoxides and ferroptotic cell death [153]. In this study, Yang and colleagues identified two key enzymes which play an important role in lipid peroxide formation, namely phosphorylase kinase G2 (PHKG2) and lipoxygenases. In HT-1080 sarcomas, PHKG2 regulates ferroptosis by modulating iron homeostasis in labile iron pools and inhibition of lipoxygenases restricted Erastin-, but not RSL3-induced cell death [153]. These results were in line with observations in neuronal HT22 cells, in which the cystine/glutamate antiporter x_c^- was inhibited by excessive extracellular glutamate that led to cystine deprivation and impaired GSH synthesis which activated neuronal 12-LOX [207]. Recent publications discovered that only one class of phospholipids (phosphatidylethanolamines (PEs)), were oxidized in extra mitochondrial ER-associated compartments upon RSL3-induced ferroptosis. Oxidation was specific towards arachidonyl and adrenoly (AdA) fatty acyls-containing PEs and dependent on 15-LOX activation [154, 155]. Another interesting finding was that ferroptosis inhibitor Lip-1 inhibited 15-LOX enzymatic activity and therefore suppressed lipid peroxidation. Furthermore, they identified that vitamin E and derivatives (Tocopherols and Tocotrienols) which are often used to suppress ROS signalling in ferroptosis [208], efficiently suppressed 15-LOX activity, by competing for PUFA substrate binding site (corking mechanism) [155]. Further observations have strengthened the role of LOX activation, contributing to ferroptotic cell death by demonstrating that knockdown of lipoxygenases resulted in ferroptosis resistance [153, 209]. In addition, the mechanisms how lipoxygenase-mediated lipid peroxidation occurring during ferroptosis has not been fully understood. It was supposed that lipoxygenases oxidize free PUFA and do not affect PUFAs tightly anchored into membrane. Nevertheless, novel insights were revealed by Wenzel and colleagues, who demonstrated that a small scaffold protein phosphatidylethanolamine-binding protein 1 (PEBP1), known as RAF1 kinase inhibitory protein (RKIP1), builds a complex with 15-LOX [210]. Thereby, the LOX substrate specificity is altered so that they can directly oxygenate PUFA tails of phospholipids which are incorporated into cellular membranes. Moreover, they identified that this PEBP1-15-LOX complex plays a crucial role in lipid peroxidation-dependent ferroptosis in airway epithelial cells, kidney epithelial cells and neuronal cells [210]. These results strengthen recent observations that ferroptosis is implicated in several diseases like acute kidney injury [144] and neurodegenerative diseases [104, 147, 176].

Especially in cancer, ferroptosis may be a new treatment strategy for cancer which show resistance to other forms of programmed cell death. In our study we observed that ferroptosis is also triggered in FADD def. Jurkat cells, which show resistance to extrinsic apoptosis stimulation [179]. In addition, it is essential to unravel the molecular mechanism of ferroptosis in every disease model to identify new key mediators, like LOX, for the development of new therapeutic strategies.

6.1.2 RSL3 and Erastin in combination with BV6 differentially modulate ROS-induced cell death in ALL cells

In this study we showed that subtoxic concentrations of ferroptosis-inducing compounds RSL3 and Erastin cooperated with Smac mimetic BV6 to induce ROS-dependent cell death, since BV6 has been described to stimulate ROS production and ROS-induced cell death in several cancer cell lines [117, 188]. As a mechanism of treatment resistance, leukaemia cells exhibit high levels of cellular IAP proteins as well as elevated ROS levels for cancer progression [177, 211, 212]. Therefore, the investigated combination treatment, targeting redox homeostasis and IAP proteins could be a promising treatment strategy in ALL cells.

Our results confirmed that RSL3 also in combination with BV6 triggers ferroptotic cell death, whereas Erastin/BV6-induced cell death cannot be classified as classical ferroptosis, necroptosis or apoptosis. This hypothesis was strengthened by several experimental pieces of evidence. In summary, cell death induction upon both treatments was independent of caspases, RIP3 and RIP1. Moreover, RSL3/BV6- but not Era/BV6-induced cell death was diminished upon the addition of ferroptosis inhibitors like the lipid peroxide scavenger Fer-1 or iron chelator DFO. Also the genetic inhibition of lipid peroxide formation by overexpressing GPX4 failed to protect from Era/BV6-induced cell death, whereas overexpression of GPX4 impeded RSL3/BV6-stimulated cell death. Though, ROS is a mediator of cell death in both treatments, since inhibition of ROS accumulation by α -Tocopherol diminished cell death induction by RSL3/BV6 and Era/BV6. Nevertheless, ROS accumulation and lipid peroxidation are closely related events, triggering one and another in RSL3/BV6-stimulated cell death, enhanced by the results that Fer-1 and α -Tocopherol significantly inhibited ROS production. In contrast, Fer-1 had minor impact on ROS production upon Era/BV6 treatment, while α -Tocopherol declined ROS accumulation and lipid peroxidation, pointing to that lipid

peroxidation is not the executing mechanism in this type of cell death (Figure 32). Also in Era/BV6-stimulated cell death other forms of ROS besides lipid-based ROS, e.g. mitochondrial ROS [137] might be a ROS source in Era/BV6-treated cells, since Erastin targets additional VDAC at the mitochondria [105, 213]. In addition, Erastin used as single agent failed to induce ferroptosis in ALL cells as well.

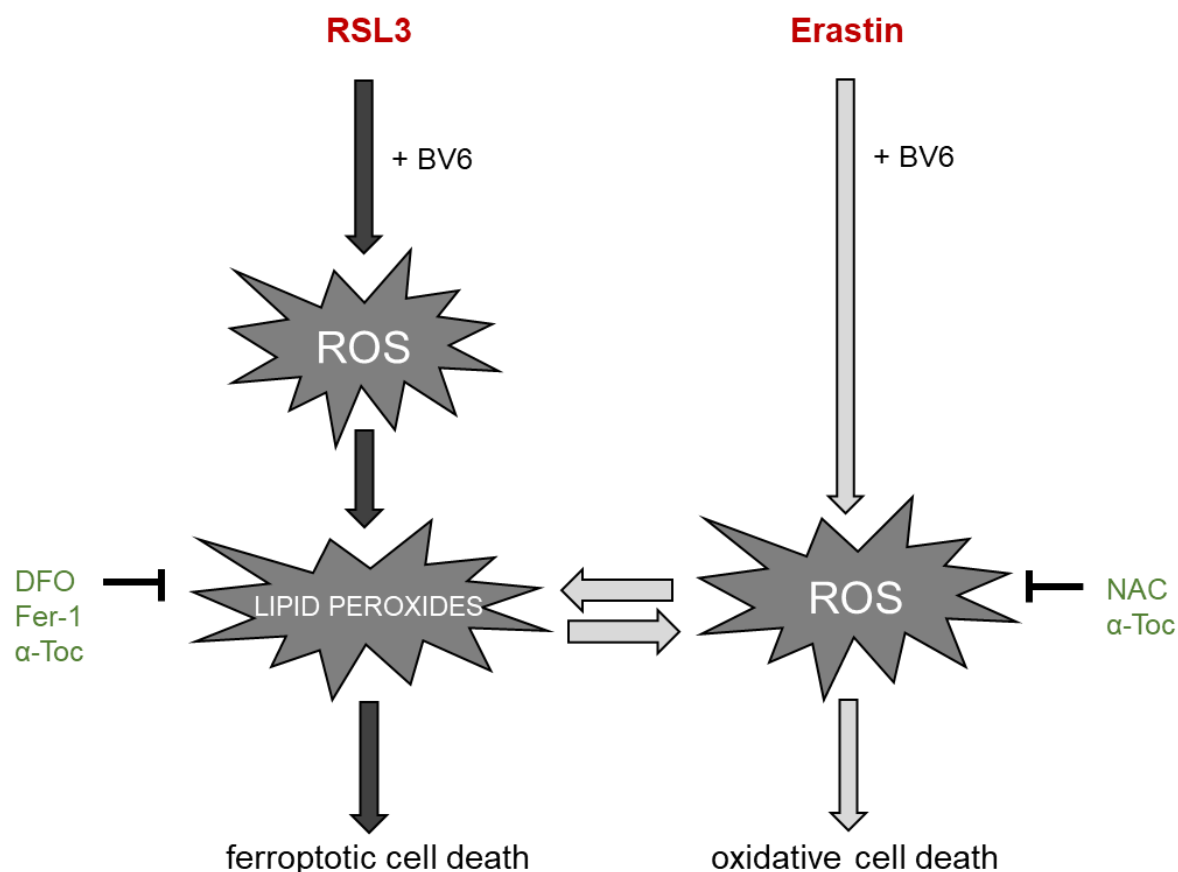


Figure 32: Hypothetical model of cell death induction upon RSL3/BV6 and Era/BV6 treatment in ALL. RSL3/BV6 triggers ferroptosis whereas Erastin/BV6-induced cell death cannot be classified as classical ferroptosis, necroptosis or apoptosis, but rather as ROS-dependent oxidative cell death.

6.1.2.1 Erastin and RSL3 differ in their mode of action

Our findings point to the fact that RSL3 and Erastin, described as prototypical ferroptosis-inducing compounds [100, 101] differ in their signalling pathway, while Erastin failed to induce ferroptosis in general in ALL cells. These observations can be explained by the distinct mechanism of action of RSL3 and Erastin. Previous study revealed that RSL3 directly binds to the active site of GPX4 at its selenocysteine [104]. In contrast, Erastin targets the cystine/glutamate antiporter x_c^- , resulting in impaired cystine import and impeded GSH synthesis [100, 101], an important thiol-containing

antioxidant. Therefore, Erastin indirectly inhibits GPX4 by depleting its essential cofactor GSH [91, 99, 104]. First, Yagoda and colleagues reported that in the mode of action of Erastin, RAS-RAF-MEK signalling is involved, whereby sensitivity of Erastin was displayed in tumour cells harbouring mutations in HRAS, KRAS and BRAF [105]. At last, this topic is still discussed controversially, since some cancer cells harbouring wildtype RAS also respond to Erastin [104]. Another discovery was that Erastin binds to mitochondrial outer membrane localised voltage-dependent anion channels 2 and 3, resulting in ferroptosis [105]. Erastin thereby interacts with VDAC2 and 3 by antagonizing the tubulin-associated blockage, leading to an opening of VDACs, an increase in mitochondrial metabolism that resulted in diminished for cancer cell progression important glycolysis (Warburg effect) and enhanced oxidative stress-induced cell death [137, 214, 215]. As VDACs are described to also be involved in apoptotic signalling by releasing cytochrome c or mitochondrial ROS into the cytosol [216], we tested if caspases are involved. However, caspase inhibitor zVAD.fmk failed to protect from lipid peroxidation-dependent cell death upon Era/BV6- and also RSL3/BV6-triggered cell death.

6.1.2.2 Era/BV6 does not trigger ferroptosis, neither apoptosis nor necroptosis

It has been reported that in case of caspase inhibition, cells can switch from apoptosis to necroptosis [217], therefore we investigated if Era/BV6 cotreatment induces necroptosis when caspase activation is suppressed by zVAD.fmk. In addition, Canli and colleagues ascertained that in absence of GPX4, erythroid precursor cells undergo RIP3-dependent necroptotic cell death [218]. Nonetheless, our results demonstrated that neither inhibition of RIP1 nor siRNA-mediated knockdown of RIP3, two major key regulators of necroptotic signalling [219, 220], had impact on Era/BV6-stimulated cell death, when caspases were inhibited. Therefore, Era/BV6- induced cell death cannot be classified as ferroptosis, nor as necroptosis or apoptosis.

6.1.2.3 Possible modulators of Erastin-induced cell death in ALL cells which negatively regulate ferroptosis onset

Recent study investigated that ALL cells are vulnerable to ROS-inducing compounds [188]. BSO was used as a GSH depleting agent, which is also reported as ferroptosis-inducing compound [104]. However, in combination with Smac mimetic BV6, ALL cells displayed apoptotic cell death upon treatment with BSO/BV6, hypothesizing that the mechanism of GSH synthesis could play a role in regulating ferroptosis induction in

our system of Era/BV6-triggered cell death. Research in the field of oxidative stress response reported that Burkitt's lymphoma cells overexpressing xCT, one of the subgroups of x_c^- , showed resistance to GSH depleting agents. This overexpression also protected cells against lipid peroxide formation and therefore cell death [221]. The protection was independent of GSH itself, but rather dependent on an elevated redox balance of cystine and cysteine, whereby the redox-cycle itself was the major antioxidant defense mechanism [221]. Moreover, xCT is transcriptionally activated upon oxidative stress, like cystine depletion, electrophilic agents and oxygen, similar to x_c^- activity [222, 223]. However, mice lacking xCT are viable and fertile, meaning that the x_c^- system is not the only cellular system that provides cysteine, since other mechanisms could compensate for the loss, e.g. the transsulfuration pathway [166, 222]. Also, oxidative stress like GSH or cystine depletion can activate Nrf2, an oxidative stress sensor, which is described as negative regulator of ferroptosis [171]. Pre-existing reports indicated that xCT expression is tightly controlled by Nrf2 in various models of oxidative stress, hypothesising that Nrf2 activation might compensate for the loss of GSH [35, 171].

Though, an interesting and important finding was mentioned 2012 by the group of Dixon. This previous study suggested that Erastin inhibits besides system x_c^- also system x_L , a phenylalanine antiporter, assembled by subunits SLC3A2 and SLC7A5 in Jurkat cells [224] which did not contribute to ferroptosis directly [101]. However, in HT-1080 and Calu-1 cells affinity purification assay identified that Erastin binds to x_c^- (SLC3A2 and SLC7A11), inhibiting cystine uptake [101]. Interestingly, Jurkat cells are described to not express x_c^- [225], hypothesizing that Erastin can bind to other transporter systems non-specifically when x_c^- is missing. Another suggesting could be that Erastin binds to other targets in Jurkat cells, by indirect inhibition of system x_L [101]. In general, this topic needs further investigations which type of cell death is induced after Erastin and Era/BV6 treatment in ALL cells and which key mediators play a functional role in this system. Besides apoptosis, necroptosis and ferroptosis, there are many more cell death pathways which could be induced [226].

In summary, within this study we could give more insights into ferroptotic signalling in ALL cells, whereby RSL3 can be used as ferroptosis-inducing agent in these cells. Erastin and its mode of action remained unclear and needs further investigations to

clarify the molecular mechanism of Erastin-induced cell death in ALL cells. These findings could unravel redox signalling upon ROS-mediated cell death induction in ALL, highlighting possible new treatment strategy for high risk and relapsed patients.

6.2 RMS cells display classical features of ferroptosis

Since ALL failed to display ferroptotic signalling upon Erastin stimulus, we investigated a new model for ferroptotic signalling to identify new key players. Previous studies reported that RMS are vulnerable to ROS inducing agents [178] and that GSH biosynthesis is crucial for proliferation, ROS detoxification and could also play a role in multi-drug resistance in extremity soft tissue sarcoma [227]. In this context, elevated GSH and GSH-S-transferase level were described as a mechanism of resistance in doxorubicin, topotecan and vincristine treated eRMS tumours [228]. Therefore, targeting GSH could have implications in RMS survival, which has been exhibited in a study where RMS were treated with Sorafenib, an inhibitor of x_c^- . This study revealed an anti-proliferative effect of Sorafenib *in vitro* and *in vivo*, but consistent effects were lacking in phase II clinical trial investigations [229, 230]. Lately oxidative stress-induced cell death in RMS cells by targeting two major antioxidant defence mechanisms, namely GSH and thioredoxin, has been described by our laboratory [231].

To this end, we tested in our study whether RMS cells respond to Erastin, a well-established GSH depleting agent, in inducing oxidative stress-induced ferroptosis. Indeed, we found that ferroptosis is induced in RMS upon prototypical stimuli of ferroptosis via Erastin or RSL3. We could observe classical features of iron-dependency, ROS accumulation and lipid-based ROS formation upon Erastin treatment and that different antioxidants, ferroptosis inhibitors and an iron chelator blocked these events. Interestingly, we explored that not only vitamin E and known ferroptosis inhibitors like Fer-1, Lip-1 and iron chelator DFO, but rather NOX and PKC inhibitors had an influence on ROS-mediated ferroptotic cell death mechanism upon Erastin treatment.

6.2.1 Ferroptosis sensitivity is independent on RAS and xCT expression level

Recent studies revealed that RAS mutations increase oxidative stress-driven oncogenesis [50]. In this context, it was observed that eRMS, often associated with high rate of RAS mutation, displayed an increased oxidative stress level [178]. Corresponding to that, drugs that modify oxidative stress had impact on patient derived xenograft

models [178]. As RAS is commonly mutated in cancer cells, the two small molecule compounds, namely Erastin and RSL3, were described to be lethal to cells expressing mutant RAS proteins [99, 100]. Additionally, RAS/RAF/MEK/ERK signalling seems to be an important pathway for Erastin, although this remains controversially discussed and needs further investigations, because also RAS WT cells like Fibroblasts and T cells respond to Erastin treatment sensitively [99, 104, 105, 158].

Here, we report that the majority of RMS, irregardless of their RAS status responded dose- and time-dependent to Erastin in inducing cell death. So neither RAS, nor expression level of xCT, the binding target of Erastin and regulatory subunit of x_c^- , correlated with susceptibility to Erastin treatment. Thus, sensitivity to ferroptosis is regulated through various mechanisms and proteins [158] besides x_c^- [101], which can be linked to lipid metabolism (e.g. ACSL4) [154], iron storage and import (e.g. TRF1) [148], as well as protein synthesis (e.g. HSPB1) [161]. Many more regulators of ferroptosis are described like Nrf2 [171], p53 [163, 164], VDACS [105] and GPX4 [104] that determine sensitivity to ferroptosis-inducing compounds.

6.2.2 NOX are involved in ferroptosis as a ROS-generating enzyme

Because ferroptosis is an iron-dependent cell death, excessive iron accumulation leads to formation of hydroxyl radicals via Fenton reaction, resulting in formation of lipid peroxidation and membrane rupture, causing cell death [232]. ROS-producing enzymes like NOX require iron for their proper function and can be modulated through additional heme [233, 234].

In line with Dixon *et al.* 2012, our study revealed that NOX are involved in ROS signalling and ferroptotic cell death in our model of RMS, since pharmacological and genetic silencing of NOX4 rescued from Erastin-stimulated cell death. In general, NADPH oxidases are the known enzyme family to produce ROS as a sole and primary function [76, 101]. The NOX family consists of seven members NOX1-5 and two dual oxidases (Duox1 and Duox2) [235]. The different isoforms are differentially localized at different compartments. Also expression pattern of different NOX isoforms is tissue specific and even ROS production differs, for example NOX4 produces mainly H_2O_2 , whereas NOX1, NOX2 and NOX5 mainly produce superoxide [77, 236]. NOX4 is most consistent located at the ER, but also in the mitochondria, nucleus, focal adhesion and cytoskeleton [237, 238]. A connection between ER and ferroptosis has been shown by Dixon and colleagues by figuring out that genes clustered in ER-stress response, like

CHAC1, were upregulated upon inhibition of x_c^- system [102]. Furthermore, new insights into the involvement of ER in ferroptosis was revealed by Kagan *et al.* 2016, identifying that accumulation of lipid hydroperoxides mostly occurred in compartments of the ER [155]. In addition, NOX2 and NOX4 driven H_2O_2 production is associated with glutamate induced-oxidative stress in neuronal cells, in which MEK/ERK inhibitors blocked the accumulating ROS [75]. In addition, NOX activation is often described in age-related diseases like arteriosclerosis, cardiovascular diseases and neurodegenerative diseases like stroke, Alzheimer and Parkinson's disease as well as cancer [239]. Hence, insights into ferroptosis in neurodegenerative diseases were depicted earlier, reporting that mice lacking GPX4 in the forebrain displayed hallmarks of ferroptosis in neuronal degeneration [176].

Our study showed that frequently used NOX inhibitors like DPI and GKT137831 rescued RMS cells from Erastin-mediated ROS and lipid ROS production and also from RSL3-induced cell death significantly. DPI is a general flavoprotein inhibitor which targets other ROS-producing enzymes like xanthine oxidases [193]. In contrast, GKT137831 is a more selective NOX1/NOX4 inhibitor, which has been used in *in vivo* models [240, 241]. Moreover, siRNA-mediated knockdown of NOX4 significantly reduced Erastin-induced cell death in RMS. The validation of NOX4 knockdown was observed via qRT-PCR, because specific antibodies for NOX4 are lacking in general [76]. As only one construct was used, these data are not significantly reliable and need further investigations. Besides, NOX4 is constitutively active, but it is bound to its subunit $p22^{phox}$, catalysing together the transfer of an electron to molecular oxygen to generate ROS [242]. Therefore, after silencing NOX4 genetically, $p22^{phox}$ remains undisturbed [243], thus free $p22^{phox}$ could then possibly interact with other NOX isoforms, compensating for NOX4 loss. At last, this suggesting has to be further investigated, for example knockdown of either NOX1 or NOX4 to mimic the inhibitory effect of GKT137831 or by genetic silencing of $p22^{phox}$.

6.2.3 The activation of NOX in RMS remains unclear

The regulation of NOX activity differs between the isoforms and catalytic subunits. Most are described to be regulated through either regulatory subunits, mostly $p22^{phox}$ [244], through calcium [245], mRNA level [76] or via phosphorylation, even in constitutively active forms [246, 247]. There are also indications that the RAS, ERK and NOX pathway acting together in a crosstalk, in which RAS transcriptionally upregulates NOX1

through MEK/ERK phosphorylation, promoting cell proliferation, DNA damage and oxidation, resulting in carcinogenesis [52, 248]. Other publications demonstrated that NOX activation can be regulated via lipid metabolism such as phospholipase A2 (PLA₂), AA and AA metabolites that can be produced by LOX [249], events which are further linked to ferroptotic signalling [155].

6.2.4 PKC, an upstream regulator of NOX, are involved in ferroptotic signalling in RMS

Activation of NOX subunits by phosphorylation can be induced through distinct kinases like PKC, mitogen-activated protein kinases and cAMP dependent kinases [250]. Several studies suggest PKC isoforms as dominant kinases, regulating NOX activity [246, 251]. Further explorations depicted that PKC α and β isoforms phosphorylate the p22^{phox} subunit at its Thr147 position to further promote interaction with p47^{phox} [75, 252], which strengthens the hypothesis that PKC activation is an upstream regulator of NOX. Interestingly, Do Van and colleagues showed that PKC α is activated in Erastin-induced ferroptosis in Parkinson's disease [191]. Similarly, we suggest that PKC α plays a crucial role in ferroptosis in RMS cells, since broad and selective inhibition of PKC as well as PKC α knockdown significantly attenuated Erastin-induced cell death in RMS. Furthermore, lipid peroxidation, an executing mechanism of ferroptosis was impaired when PKC were inhibited.

6.2.5 Different PKC might be differently activated through Erastin-induced ROS in RMS

In general, PKC are maintained in an inactive form, by binding the pseudosubstrate (PS) to the substrate-binding cavity [253], whereas PKC are activated through phosphorylation [254], changing of subcellular localization [255], diacylglycerol (DAG), calcium and phorbol-12-myristate-13-acetate (PMA) [195] or through oxidation upon ROS accumulation [256]. Regarding ROS, some studies investigated that especially GSH depletion leads to activation of specific PKC isoforms [257, 258]. Thus, ROS-dependent PKC activation is isoform, cell type and ROS generation specific and is involved in cell survival or death [195]. High levels of redox-sensitive cysteine residues in the zinc finger domain of PKC render these serine/threonine kinases receptive for redox regulation. ROS thereby destroy the zinc- finger domain and regulatory compartment, resulting in a catalytically active form of PKC without calcium, DAG or PMA [259]. However, it is reported that PKC can also promote the production of endogenous ROS,

resulting in a positive feedback loop by affecting mitochondrial and NADPH oxidase function which leads to ROS generation [239, 256, 260]. Linked to our results, experiments using the more selective PKC α and β inhibitor Gö6976 revealed that the activation of these PKC isoforms might be downstream of ROS formation, since Gö6976 failed to inhibit Erastin-induced ROS production. In contrast, ROS accumulation was diminished using the broad spectrum inhibitor Bim1, assuming that several PKC isoforms promote the accumulation of ROS (Figure 33). Therefore, it is important not to see the function of ROS production as an isolated system, it should be considered as an interplay and crosstalk between different ROS generators and mediators [239, 261]. This hypothesis involves two different mechanisms, a primary ROS source like mitochondria and a secondary which is stimulated by the primary source, called ROS-induced ROS release (RIRR) [262]. So, an initial ROS source is formed through impaired mitochondrial respiratory electron chain transport, promoting ROS accumulation into the cytosol through opening of mitochondrial pores or through impaired antioxidant defence mechanisms. In the cytosol, ROS activates redox-sensitive targets like PKC or tyrosine kinases (e.g. cSrc) which lead to the activation of NOX [262]. This leads to an increase in a secondary oxidative stress response, which could affect again redox-sensitive proteins like PKC in a feedback loop [260]. As a consequence, cellular redox balance is impaired [263].

Concerning our results, it needs further investigations if NOX is activated through PKC (feedback loop) and how PKC are activated in RMS cells upon ferroptotic stimulation such as Erastin or RSL3. A possible mechanism could be that Erastin-induced GSH depletion leads to an accumulation of cytosolic ROS that affects PKC activation. Through PKC activation NOX is stimulated which triggers a secondary ROS formation. Due to an increase in overall ROS, Fenton reaction via iron accumulation or lipoxygenase activation (Appendix Figure 39) participates in lipid peroxide formation, leading to ferroptotic cell death (Figure 33).

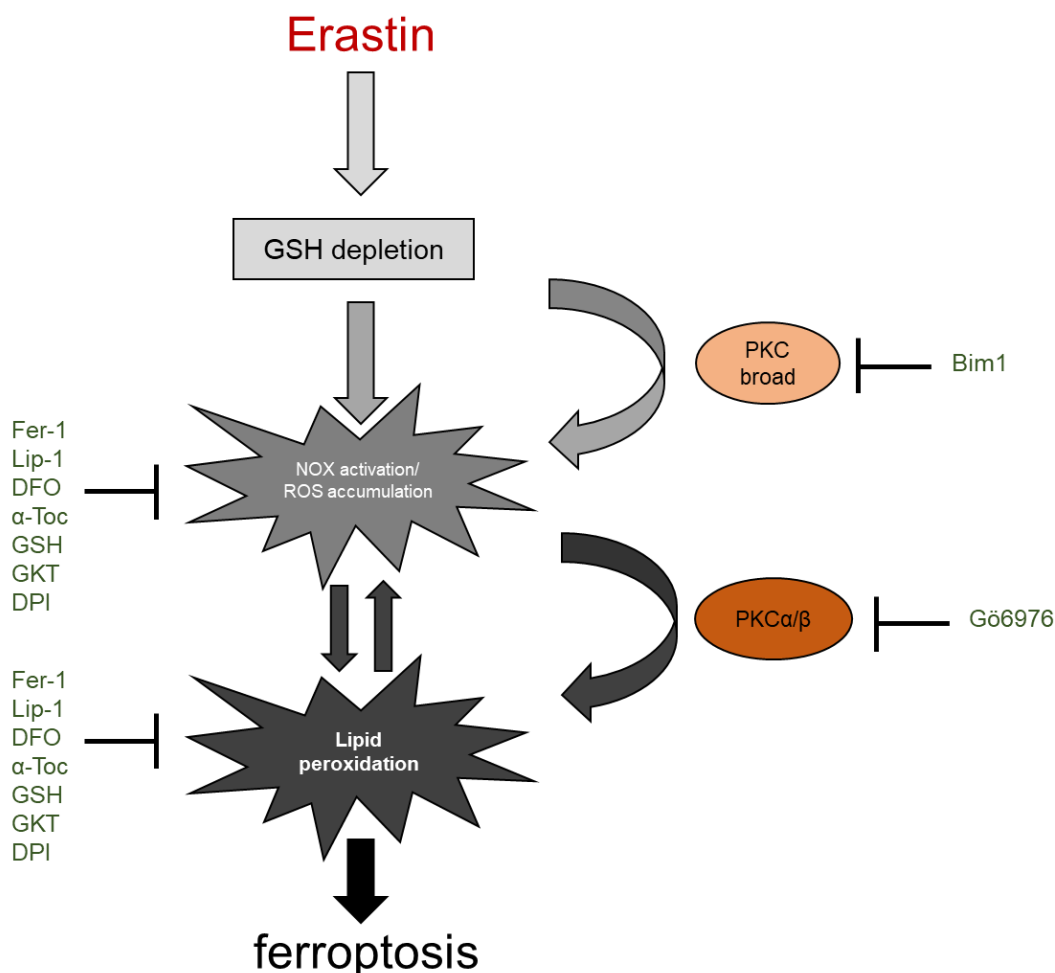


Figure 33: Hypothetical model of Erastin-induced ferroptosis in RMS.

Erastin triggers classical ferroptotic cell death with iron-dependency, ROS accumulation and lipid peroxidation which was also suppressed by PKC and NOX inhibitors.

Indeed, we could observe that Erastin was efficient in inducing ferroptosis in RMS cells in comparison to ALL cells. Other newly identified possible ferroptosis inducers were tested, but neither Whitafenin A (unpublished data, Van den Berghe, group of P. Vandenamee) nor statins [168, 169] triggered ferroptosis in RMS cells. Also, Sorafenib in combination with Smac mimetic BV6 stimulated oxidative cell death admittedly, but this type of cell death could not be classified as ferroptosis (Appendix Figures 36-38).

This study could have novel implications for treatment options, especially for refractory or relapsed RMS, where therapeutic options are limited. Within our study we can confirm that the majority of tested RMS respond sensitive to ferroptosis stimulation through Erastin. By that, we identified two enzymes, PKC and NOX which might possess a

crucial role in ROS production and signal transduction in ferroptosis. We could not clarify the whole crosstalk, but we could give further insights into new key players besides GPX4 in ferroptosis, which is important for new cancer treatment and treatment options for other diseases like Alzheimer, stroke and Parkinson [176].

7 Outlook

By this study of the molecular ferroptotic pathway in different cancer cells, we revealed novel insights into this relatively unknown pathway. Surprisingly, we exhibited that Erastin acted different in our two models, whereas RSL3 was able to induce ferroptosis in both, ALL and RMS cells. In the following paragraph, ideas of further experiments to strengthen the conclusions, drawn in this thesis, are listed.

Concerning ALL and the involvement of Lipoxygenases, it is worth to investigate a genetic approach to consolidate which LOX are activated upon RSL3 treatment. Furthermore, it would also be of interest through which mechanism LOX are activated, because no changes on mRNA level after RSL3 treatment was observed. Possible mechanisms are mentioned in 6.1.1.1. Moreover, Erastin does not induce ferroptotic cell death neither as a single agent nor in combination with BV6, whereas this combination triggered an oxidative stress-induced cell death that was independent of iron, caspases and RIP1 or RIP3. Furthermore, it is necessary to unravel which type of cell death is induced upon Erastin single and combination treatment. Finally, additional *in vivo* models could enhance the *in vitro* approach made in this study.

In contrast, RMS cells displayed a feasible model for ferroptotic cell death. Here it has to be clarified if PKC α is activated through ROS signalling and in which way this activation is dependent for NOX activation. In addition, to strengthen the involvement of NOX, it has to be confirmed which isoforms are activated. Furthermore, the use of additional NOX inhibitors like apocynin and VAS2870 could give more insights into NOX activation. As well, a genetic approach, e.g. siRNA-mediated knockdown of NOX or regulatory subunits or a specific NOX activity assay could be a method to intensify the hypothesis if NOX are involved as a possible ROS source in ferroptotic signalling in RMS. Though, an *in vivo* model would also strengthen the observations made in this study, concerning RSL3 and Erastin as a prototypical ferroptosis stimulus to counteract cancer progression in RMS.

8 Deutsche Zusammenfassung

Reaktive Sauerstoffspezies (ROS) stellen eine Gruppe von Molekülen dar, die Sauerstoff beinhalten und als freie Radikale oder nicht-radikalisch vorliegen können. ROS werden entweder als Nebenprodukt von enzymatischen Reaktionen gebildet, wie z.B. durch Oxydasen, Lipoxygenasen (LOX) oder nicht-enzymatisch, unter anderem durch die in den Mitochondrien stattfindende Atmungskette. In hohen Konzentrationen können sie durch ihre enorme Toxizität Proteine, Lipid und DNA zerstören, jedoch spielen sie in gewissen, niedrigeren Konzentrationen eine wichtige Rolle in verschiedensten Signalwegen. Zu den bekanntesten Signalmolekülen gehören Wasserstoffperoxid (H_2O_2), das Superoxid-Anion ($\text{O}_2^{\cdot-}$) und das toxischste Hydroxylradikal (OH^{\cdot}). In einer gesunden Zelle liegen ROS Produktion und ROS Detoxifikation in einem Gleichgewicht vor, der Redox-Homöostase. Wird diese Homöostase in Hinblick auf einen der beiden Faktoren gestört, führt dies unter Umständen zur Entstehung von Krankheiten wie Krebs, Alzheimer und Parkinson. Insbesondere Krebszellen machen sich die Funktion der Signalweiterleitung von ROS zunutze, denn in moderaten Konzentrationen kann ROS zur Proliferation und zum Überleben der Krebszelle beitragen. Damit die moderate Konzentration an ROS nicht in eine toxische umschlägt und um das für ihre Weiterentwicklung profitable ROS beizubehalten, werden antioxidative Mechanismen in Krebszellen erhöht. Als Therapieansatz zur Bekämpfung von Krebszellen im Allgemeinen dienen demnach Reagenzien, die ROS generieren aber auch Reagenzien, die ein erhöhtes antioxidatives Netzwerk zerstören bzw. verringern. Zu diesen ROS-abhängigen Mechanismen gehören meist Zelltod Signalwege, die aber auch am Transformationsprozess der Tumorzelle beteiligt sein können. Hierzu ist am häufigsten ein Defekt im apoptotischen Signalweg beschrieben, der mit einer Therapieresistenz in malignen Tumoren einhergeht.

Die oben beschriebenen Merkmale konnten beispielsweise in Zellen der akuten lymphatischen Leukämie (ALL) gezeigt werden. Diese Erkrankung gehört zu der am häufigsten diagnostizierten Leukämie, die im hohen Maße im Kindesalter und eher selten im Erwachsenenalter aufzufinden ist. ALL wird immunologisch in verschiedene Untergruppen unterteilt. Hierzu zählen B-ALL (B-lymphozytäre Differenzierung) und T-ALL (T-lymphozytäre Differenzierung). Zu den Standardtherapieansätzen gehören Chemotherapeutika (L-Asparaginase, Etoposide, Doxorubicin, Vincristin) mit Kortikosteroiden, sowie Bestrahlung. Trotz dieser Behandlungsmethode gibt es Patienten,

die nicht erfolgsversprechend auf diese Therapieform ansprechen oder der Tumor rezidiert. Aus diesen Gründen sind neue Therapieansätze unabdingbar, beispielsweise durch Redox-basierte Wirkmechanismen.

Um ROS auf ein toxisches Level zu erhöhen und damit Resistenzmechanismen entgegenzuwirken, wurden Reagenzien benutzt, die an einem erst kürzlich identifizierten und relativ unbekanntem eisen- und ROS-abhängigen Zelltod, genannt Ferroptose, beteiligt sind. Nicht nur die Akkumulation von Eisen, sondern auch die Akkumulation von ROS und oxidierten Fettmolekülen in der Zellmembran charakterisieren diesen Zelltod. Ferroptose kann zum einen durch die direkte und zum anderen durch die indirekte Inhibition von Glutathion Peroxidase 4 (GPX4) erfolgen. Zu den direkten Inhibitoren gehören RSL3 (RAS-selective lethal 3) und andere Moleküle. Diese hemmen durch direkte Bindung an GPX4 dieses in seiner enzymatischen Funktion, nämlich das Beseitigen von H₂O₂ oder Fettsäurehydroperoxiden, oder tragen zu dessen Degradation bei. Zum anderen können Reagenzien wie Erastin (eradicator of RAS and ST-expressing cells) eine Verminderung des für GPX4 wichtigen Cofaktors und Antioxidans Glutathion (GSH) bewirken und GPX4 somit indirekt hemmen. Erastin wirkt dabei inhibierend auf ein zellmembranständiges Cystine/Glutamat-Antiporter System x_c⁻, welches Cystine für die *de novo* Synthese von GSH in der Zelle bereitstellt.

In dem ersten Teil dieser Studie wurde gezeigt, dass die Zugabe von RSL3, einem synthetisch hergestellten Ferroptose-Stimulus, Zelltod in drei ALL Modellsystemen (Jurkat, Molt-4 und FADD defizienten Jurkat Zellen) induzierte. Dieser Zelltod wurde in Jurkat und Molt-4 Zellen mit den Ferroptose Inhibitoren Ferrostatin-1 (Fer-1), Liproxstatin-1 (Lip-1), einem Eisenchelator Deferoxamine (DFO) und mit Hilfe eines lipophilen Antioxidans, α-Tocopherol auch bekannt als Vitamin E, verringert und als Ferroptose charakterisiert. Dieser Zelltod war zudem unabhängig von Caspasen und Rezeptor-interagierender Proteinkinase 1 (RIP1), da weder ein Caspasen Inhibitor (zVAD.fmk) noch ein spezifischer RIP1 Inhibitor (Necrostatin-1s) den Zelltod hemmten. Nicht nur Zelltod, auch ROS Produktion und Lipidperoxidation, die wesentlich zum ferroptotischen Zelltod beitragen, wurden durch die Zugabe von Fer-1 und α-Tocopherol vermindert.

Des Weiteren wurde gezeigt, dass RSL3 induzierte Ferroptose durch selektive Lipoygenase Inhibitoren, die gegen bestimmte LOX Isoformen gerichtet sind und nicht

selektive LOX Inhibitoren, die viele Isoformen gleichzeitig inhibieren, gehemmt wurden. Zu den selektiven LOX Inhibitoren gehören Baicalein (12/15-LOX Inhibitor), Zileuton (5-LOX Inhibitor) und PD146176 (15-LOX Inhibitor). NDGA hingegen wurde als genereller LOX Inhibitor verwendet. Sowohl RSL3 vermittelte ROS Produktion als auch Lipidperoxidation wurden durch NDGA und Baicalein verringert. Die inhibierende Wirkung der LOX Inhibitoren konnte nicht auf eine erhöhte Expression von GPX4 zurückgeführt. Darüber hinaus wurde gezeigt, dass RSL3 in FADD defizienten Jurkat Zellen, die resistent gegenüber extrinsischer Apoptose sind, Ferroptose stimulierte. Ebenfalls waren in diesen Zellen LOX an der ROS Produktion und Lipidperoxidation beteiligt.

Zusammenfassend wurde in ALL durch die Inhibition von GPX4 Ferroptose ausgelöst und dabei bestätigt, dass LOX im ferroptotischen Wirkmechanismus eine zentrale Rolle spielen. Diese Ergebnisse bestärken vorangegangene Publikationen in diesem Feld. Im Allgemeinen könnte die Induktion von Ferroptose in Leukämiezellen dazu beitragen, Apoptose Resistenzen zu umgehen, indem ein mechanistisch unterschiedlicher, auf ROS-basierender, programmierter Zelltod aktiviert wird.

Im zweiten Teil dieser Studie wurden sowohl RSL3 als auch Erastin in kleinen Dosen mit BV6, einem Smac nachahmendem Reagenz, in ALL Zellen (Jurkat, Molt-4) kombiniert, um den zuvor beschriebenen ROS-abhängigen ferroptotischen Zelltod einzuleiten. BV6 ist ebenfalls als ROS-induzierendes Reagenz beschrieben, jedoch wirkt es hemmend auf endogene Apoptose Inhibitor Proteine (IAP), welche auch an Resistenzmechanismen gegenüber Apoptose stimulierenden Agenzien beteiligt sind. Es wurde gezeigt, dass RSL3 und Erastin in kleinen Dosen zwar minimal Zelltod auslösten, dieser aber durch die Addition von BV6 noch potenziert wurde. Auch die Produktion von ROS und die Oxidation von Lipiden waren in Kombination von RSL3 und Erastin mit BV6 höher als in der jeweiligen Einzelstimulation. Die Kombination RSL3/BV6 hatte keine Auswirkung auf basale GSH Level. Die Kombination Erastin/BV6 führte hingegen zu einer Verminderung von GSH, welches die vorher publizierten Daten zu den Wirkmechanismen von RSL3 und Erastin bekräftigt.

Um zu prüfen, ob es sich bei dem ausgelösten Zelltod um eisenabhängige Ferroptose handelte, wurden die Zellen zusätzlich mit einem Eisenchelator DFO behandelt. Interessanterweise wurde der RSL3/BV6 stimulierte Zelltod durch DFO gehemmt, jedoch hatte DFO auf den Erastin/BV6 induzierten Zelltod keine Auswirkung. Außerdem wur-

den Fer-1 und die genetische Überexpression von GPX4 genutzt, um zu testen, inwieweit Lipidperoxidation, ein zentrales Element der Ferroptose, in beiden Kombinationen eine Rolle spielt. Sowohl RSL3/BV6 induzierte Lipidperoxidation als auch der induzierte Zelltod wurden zum einen durch die pharmakologische Inhibition von Lipidperoxidation (Fer-1) und zum anderen durch die genetische Inhibition (GPX4 Überexpression) verringert. In Erastin/BV6 behandelten Zellen wurde zwar die ausgelöste Lipidperoxidation signifikant durch die Zugabe von Fer-1 oder aber auch durch die Überexpression von GPX4 gehemmt, allerdings wurde der durch Erastin/BV6 stimulierte Zelltod weder durch Fer-1 noch durch die Überexpression von GPX4 signifikant reduziert. Anhand dieser Resultate wurde angenommen, dass die Oxidation von Lipiden unabdinglich und maßgebend für den RSL3/BV6 induzierten Zelltod war, während in Erastin/BV6 behandelten Zellen zwar Lipidperoxidation stattfand, diese aber nicht an der Induktion des Zelltods beteiligt war.

Um die Beteiligung von ROS am RSL3/BV6 und Erastin/BV6 ausgelösten Zelltod zu charakterisieren, wurde das Antioxidans α -Tocopherol verwendet. Die Zugabe von α -Tocopherol verhinderte zum einen die durch RSL3 und Erastin in Kombination mit BV6 hervorgerufene Oxidation von Lipiden und zum anderen den jeweilig induzierten Zelltod. Zudem wurde die durch RSL3/BV6 und Erastin/BV6 bewirkte ROS Akkumulation durch α -Tocopherol signifikant verhindert. Die Zugabe von Fer-1 hatte einen reduzierenden Effekt auf die durch RSL3/BV6 ausgelöste ROS Produktion, nicht aber auf die, die durch Erastin/BV6 ausgelöst wurde. Somit wurde gezeigt, dass in dem durch RSL3/BV6 hervorgerufenen Zelltod überwiegend Lipid-basierte ROS eine Rolle spielen, da die Inhibition von oxidativen Lipiden durch Fer-1 die gesamte ROS Produktion hemmte. Im Gegensatz dazu spielten neben Lipid-basierten ROS weitere ROS Arten, die durch α -Tocopherol gehemmt wurden, eine wichtige Rolle in dem Erastin/BV6 induzierten Zelltod. Dies führte zu der Annahme, dass RSL3 und Erastin in Kombination mit BV6 unterschiedliche Zelltodmechanismen in ALL auslösten.

Um den durch Erastin/BV6 ausgelösten Zelltod noch weiter zu charakterisieren, wurden nekroptotische sowie apoptotische Schlüsselemente untersucht. Ob Caspasen in RSL3/BV6 und Erastin/BV6 generiertem Zelltod involviert waren, wurde mithilfe des Caspasen Inhibitors zVAD.fmk überprüft. Der Inhibitor zVAD.fmk zeigte zwar die Inhibition von Caspase 3 und 7 in RSL3/BV6 und Erastin/BV6 behandelten Zellen, den-

noch konnte zVAD.fmk weder die Oxidation von Lipiden noch die Induktion des Zelltods beeinträchtigen. Um Nekroptose nachzuweisen, wurde RIP1 pharmakologisch durch Necrostatin-1 und RIP3 genetisch durch einen siRNA-basierten Knockdown inhibiert. Weder die pharmakologische Inhibition von RIP1 noch die genetische Inhibition von RIP3 hatten einen Einfluss auf den RSL3/BV6 oder Erastin/BV6 erzeugten Zelltod. Zusammenfassend zeigen die Ergebnisse des zweiten Teils der Studie, dass RSL3 auch in Kombination mit dem Smac imitierenden Reagenz BV6 ferroptotischen Zelltod mit charakteristischen Schlüsselementen wie Eisenabhängigkeit, ROS Akkumulation sowie Lipidperoxidation auslöste. Hingegen löste die BV6 Kombination mit Erastin, welches nicht wie RSL3 GPX4 direkt hemmt, sondern über einen indirekten Weg durch die Reduktion von GSH, nur einen ROS-abhängigen Zelltod aus. Dieser Zelltod war unabhängig von der Oxidation von Lipiden. Auch in Verwendung als Einzelstimulus induzierte Erastin keinen ferroptotischen Zelltod in ALL. Dies könnte sowohl auf die unterschiedliche Signaltransduktion der Reagenzien als auch darauf zurückzuführen sein, dass ALL den für Ferroptose wichtigen Cystine/Glutamat-Antiporter x_c^- kaum bis nicht exprimieren. Dafür exprimieren sie einen anderen Phenylalanin-Antiporter, der von Erastin unspezifisch gehemmt werden könnte. Des Weiteren wird für Erastin beschrieben, dass es auch VDAC2 und 3 hemmen kann, die als porenartige Ionen Kanäle an der mitochondrialen Membran verankert und durchlässig für hydrophile Moleküle sind. Eine weitere Erklärung wäre, dass die GSH Verminderung durch andere Signalwege kompensiert werden könnte. Hierzu zählt der Nrf2 Signalweg, der durch einen erhöhten oxidativen Stress aktiviert wird. Dies führt zu einer erhöhten Transkription von spezifischen Zielgenen, die an der GSH Synthese beteiligt sind, um dem oxidativen Stress entgegen zu wirken. Des Weiteren könnten weitere Signalwege, die Cystine anderweitig zur Verfügung stellen, ebenfalls die durch Erastin ausgelöste GSH Verringerung in der Zelle kompensieren.

Da ALL Zellen nur in Bezug auf RSL3 als ein ferroptotisches Modellsystem Verwendung fanden, handelt der dritte Teil der Studie von einem neuen ferroptotischen Modellsystem, in dem RSL3 aber insbesondere Erastin Ferroptose auslösen. Hierfür wurden Rhabdomyosarkom (RMS) Zellen verwendet, welches das am häufigsten diagnostizierte Weichteilsarkom im Kindesalter darstellt. Diese Tumorzellen sind dafür bekannt, eine erhöhte Anzahl an Antioxidantien aufzuweisen, da sie aufgrund ihres mesenchymalen Ursprungs eine erhöhte Metabolismusrate aufweisen, die eine vermehrte

ROS Bildung zur Folge hat. Daher sollen RMS gegenüber Redox-basierten Therapieansätzen sensitiv sein. Generell werden RMS histologisch in zwei Subklassen unterteilt, zum einen in das embryonale RMS (eRMS) und zum anderen in das alveoläre RMS (aRMS). Diese Subklassen unterscheiden sich im Detail durch ihr genetisches Profil. Das eRMS zeichnet sich durch den für das Tumorwachstum begünstigenden Verlust der Heterozygotie auf Chromosom 11p15.5 aus, wobei aRMS durch die ebenfalls proliferationsfördernde Expression des konstitutiv aktiven Fusionsproteins PAX3/7-FOXO1 charakterisiert werden. Die Standardtherapie von RMS umfasst eine Kombination aus Chemotherapeutika mit Vincristin, Actinomycin D und Cyclophosphamid (VAC), Strahlentherapie sowie der chirurgischen Entfernung des Tumors. Für rezidive und metastasierende RMS jedoch fehlt es an neuen Therapieansätzen, die von Nöten sind, da die Überlebensrate dieser Patienten verschwindend gering ist.

In einem vorangegangenen Screening wurden neun verschiedene RMS Zelllinien hinsichtlich ihrer Sensitivität gegenüber Erastin getestet. Von diesen Zelllinien weisen vier Zelllinien einen RAS mutierten (RD, RH36, TE381.T, T174) und fünf Zelllinien (RH30, RH41, Kym-1, TE441.T, RH18), einen Wildtyp (WT) RAS Status auf. Die Auswahl an RAS mutierten und RAS WT RMS wurde getroffen, da sowohl Erastin als auch RSL3 dazu entwickelt wurden, RAS mutierte Zellen gezielt zu eliminieren, da dieses Gen häufig in bösartigen Tumoren mutiert ist. Im Allgemeinen löste die Zugabe von Erastin in embryonalen und alveolären RMS in einer dosis- und zeitabhängigen Weise, hingegen unabhängig von ihrem RAS Status, Zelltod aus. Nur in zwei Zelllinien, Kym-1 und TE441.T (RAS WT), wurde weder durch hohe Konzentrationen noch nach einer erhöhten Inkubationszeit von Erastin Zelltod induziert. Demnach wurde untersucht, ob eine Abhängigkeit zwischen der Sensitivität der Zellen gegenüber Erastin und dem Expressionslevel von xCT bestand, einer funktionellen Untergruppe des Cystine/Glutamat -Antiporters x_c^- , an dem Erastin irreversibel bindet. Eine Korrelation dieser zwei Faktoren wurde jedoch nicht eindeutig nachgewiesen. Auffällig war, dass RAS mutierte Zelllinien normalisiert zu RD ein erhöhtes Expressionsniveau an xCT im Vergleich zu RAS WT Zellen aufwiesen.

Um zu prüfen, ob es sich bei dem induzierten Zelltod durch Erastin um Ferroptose handelte, wurden spezifische Ferroptose Inhibitoren (Lip-1 und Fer-1), ein Eisenchelator (DFO) und α -Tocopherol als generelles Antioxidans verwendet. Zudem wurde GSH, ein wichtiges Antioxidans und Cofaktor von GPX4 getestet. Hierfür wurden nur

noch RD und RH30 als Modellzelllinien und RH36 als zusätzliche Zelllinie verwendet. All diese Inhibitoren waren in der Lage, den durch Erastin hervorgerufenen Zelltod in RD und RH30 zu supprimieren. Des Weiteren wurden ROS Inhibitoren hinzugefügt (DPI und GKT137381), die NADPH Oxydasen (NOX) in ihrer enzymatischen Funktion, ROS in den Zellen zu produzieren, inhibieren. DPI ist bekannt als NOX Inhibitor, der generell Flavoproteine hemmt, wobei GKT137381 eine Selektivität gegenüber NOX1 und NOX4 zugeschrieben wird. Auch diese Inhibitoren hemmten den Erastin induzierten Zelltod in RD und RH30 Zellen. In RH36 Zellen wirkten sowohl Fer-1, DFO als auch GKT137381 inhibierend auf den durch Erastin ausgelösten Zelltod. Auch RSL3 induzierter Zelltod konnte in RD und RH30 als Ferroptose charakterisiert werden, welche durch die Zugabe von GKT137381 gehemmt wurde. Hierbei wurde angenommen, dass NOX am ferroptotischen Signalweg beteiligt sein könnte.

Da Erastin über die Hemmung des membranständigen Cystine/Glutamat-Antiporters x_c^- wirkt, wurden GSH Level, ROS Produktion und die Oxidation von Lipiden nach Erastin Stimulation bestimmt. Nach sechs Stunden Erastin Behandlung wurde eine Verringerung des basalen GSH Levels in der Zelle nachgewiesen. Darauffolgend, wurden ROS Produktion und Lipidperoxidation nach 12 Stunden, vor Eintreten des Zelltods, detektiert. Die Akkumulation von ROS und Lipidperoxidation wurde durch die Addition von Fer-1, Lip-1, DFO sowie GSH, α -Tocopherol, DPI und GKT137381 verringert. Demnach wurde bestätigt, dass ROS Produktion und die Akkumulation an oxidierten Lipiden maßgebend für die Induktion des ferroptotischen Zelltods in RMS waren und NOX als ROS produzierendes Enzym an diesen ferroptotischen Ereignissen beteiligt sein könnte. Da NOX4 Level im höheren Maße als NOX1 in RD und RH30 exprimiert war, wurde NOX4 genetisch durch ein siRNA basierendes Knockdown Verfahren inhibiert. Aufgrund des Mangels an einer geeigneten zweiten Sequenz, wurde nur anhand einer siRNA Sequenz gezeigt, dass NOX4 am Erastin ausgelösten Zelltod involviert war. Generell ist NOX ein komplexes Enzym, das aus verschiedenen Untereinheiten besteht und über verschiedene Mechanismen aktiviert wird. Die Aktivierung erfolgt entweder über eine erhöhte Expression des Enzyms, über regulatorische Untereinheiten oder über Phosphorylierung.

Beispielsweise aktivieren unterschiedliche Proteinkinasen C (PKC) durch Phosphorylierung spezifische NOX Isoformen. Aus diesem Grund wurden in dieser Studie ein nicht selektiver, genereller PKC Inhibitor Bisindolylmaleimide I (Bim1) und ein für PKC α

und β Isoform selektiver Inhibitor (Gö6976) verwendet, um die Beteiligung von PKC am ferroptotischen Zelltod zu überprüfen. Die von Erastin hervorgerufene Lipidperoxidation und ebenso der ausgelöste Zelltod wurden signifikant von beiden Inhibitoren verhindert. Nur hinsichtlich der ROS Produktion lieferten die Inhibitoren unterschiedliche Ergebnisse. Bim1 inhibierte die durch Erastin erzeugte ROS Produktion, wobei Gö6976 keinen Effekt auf diese zeigte. Dieser unterschiedliche Effekt könnte ROS spezifisch sein. Neben der Aktivierung durch Diacylglycerol (DAG), Phorbol-12-Myristate-13-Acetate (PMA) oder Calcium, werden PKC auch durch ROS aktiviert, da sie Redox-sensitive Cysteine in ihrer Zinkfingerdomäne besitzen. ROS kann aber auch zu einer Inaktivierung führen, sobald der C-Terminus oxidiert wird. Somit werden PKC über ROS aktiviert und deaktiviert, fördern jedoch auch die Produktion von ROS, indem sie NOX aktivieren. Man beschreibt diesen Prozess auch als ROS induzierte ROS Produktion, der ein kompliziertes Zusammenspiel aus ROS Quellen und Redox-sensitiven Proteinen darstellt. Um zu klassifizieren, welche PKC Isoformen einen wichtigen Anteil in der Induktion von Ferroptose in RMS besitzen, wurde auf mRNA Ebene das Expressionslevel von PKC α , β , ϵ und δ ermittelt. Im Vergleich zu allen anderen Isoformen wurde PKC α vermehrt exprimiert. Folglich wurde PKC α genetisch durch einen siRNA-basierenden Knockdown inhibiert. Diese genetische Inhibition zeigte, dass PKC α durchaus an dem durch Erastin induzierten Zelltod beteiligt war, da der Knockdown den durch Erastin hervorgerufenen Zelltod hemmte. Es könnte aber durchaus sein, dass nicht nur PKC α , sondern auch andere Isoformen ebenso am ferroptotischen Zelltod Mechanismus beteiligt sein könnten.

Zusammenfassend lässt sich sagen, dass in RMS sowohl durch die Zugabe von Erastin als auch durch die Zugabe von RSL3 Ferroptose ausgelöst wird. Des Weiteren wurde in dieser Studie der molekulare Wirkmechanismus von Ferroptose insbesondere in RMS charakterisiert, in dem PKC und NOX eine zentrale Rolle in der ROS Produktion spielen könnten. Dies könnte nützlich für neue Redox-basierte Therapieansätze sein, um beispielsweise rezidive und metastasierende RMS behandeln zu können.

References

1. Gerl, R. and D.L. Vaux, *Apoptosis in the development and treatment of cancer*. Carcinogenesis, 2005. **26**(2): p. 263-70.
2. Weinberg, R.A., *How cancer arises*. Sci Am, 1996. **275**(3): p. 62-70.
3. Pui, C.H. and W.E. Evans, *Acute lymphoblastic leukemia*. N Engl J Med, 1998. **339**(9): p. 605-15.
4. Pui, C.-H., L.L. Robison, and A.T. Look, *Acute lymphoblastic leukaemia*. The Lancet, 2008. **371**(9617): p. 1030-1043.
5. Buffler, P., et al., *Environmental and Genetic Risk Factors for Childhood Leukemia: Appraising the Evidence*. Cancer Investigation, 2005. **23**(1): p. 60-75.
6. Pui, C.H., M.V. Relling, and J.R. Downing, *Acute lymphoblastic leukemia*. N Engl J Med, 2004. **350**(15): p. 1535-48.
7. Terwilliger, T. and M. Abdul-Hay, *Acute lymphoblastic leukemia: a comprehensive review and 2017 update*. Blood Cancer J, 2017. **7**(6): p. e577.
8. Harris, N.L., et al., *World Health Organization classification of neoplastic diseases of the hematopoietic and lymphoid tissues: report of the Clinical Advisory Committee meeting-Airlie House, Virginia, November 1997*. J Clin Oncol, 1999. **17**(12): p. 3835-49.
9. Hunger, S.P., et al., *Improved survival for children and adolescents with acute lymphoblastic leukemia between 1990 and 2005: a report from the children's oncology group*. J Clin Oncol, 2012. **30**(14): p. 1663-9.
10. Bassan, R. and D. Hoelzer, *Modern therapy of acute lymphoblastic leukemia*. J Clin Oncol, 2011. **29**(5): p. 532-43.
11. Miller, R.W., J.L. Young, Jr., and B. Novakovic, *Childhood cancer*. Cancer, 1995. **75**(1 Suppl): p. 395-405.
12. Ferrari, A., et al., *Rhabdomyosarcoma in adults. A retrospective analysis of 171 patients treated at a single institution*. Cancer, 2003. **98**(3): p. 571-80.
13. Parham, D.M., R. Alaggio, and C.M. Coffin, *Myogenic tumors in children and adolescents*. Pediatr Dev Pathol, 2012. **15**(1 Suppl): p. 211-38.
14. Weber, C.O.V., R., *Archiv f. pathol. Anat.* 1854. **7**(1): p. 115-125.
15. Stout, A.P., *Rhabdomyosarcoma of the Skeletal Muscles*. Ann Surg, 1946. **123**(3): p. 447-72.
16. Radzikowska, J., et al., *Rhabdomyosarcoma of the head and neck in children*. Wspolczesna Onkologia-Contemporary Oncology, 2015. **19**(2): p. 98-107.
17. Heij, H.A., et al., *Urogenital Rhabdomyosarcoma in Children: Is a Conservative Surgical Approach Justified?* The Journal of Urology, 1993. **150**(1): p. 165-168.
18. Newton, W.A., Jr., et al., *Classification of rhabdomyosarcomas and related sarcomas. Pathologic aspects and proposal for a new classification--an Intergroup Rhabdomyosarcoma Study*. Cancer, 1995. **76**(6): p. 1073-85.
19. Li, F.P. and J.F. Fraumeni, Jr., *Soft-tissue sarcomas, breast cancer, and other neoplasms. A familial syndrome?* Ann Intern Med, 1969. **71**(4): p. 747-52.
20. Diller, L., et al., *Germline p53 mutations are frequently detected in young children with rhabdomyosarcoma*. J Clin Invest, 1995. **95**(4): p. 1606-11.
21. Zhan, S., D.N. Shapiro, and L.J. Helman, *Activation of an imprinted allele of the insulin-like growth factor II gene implicated in rhabdomyosarcoma*. J Clin Invest, 1994. **94**(1): p. 445-8.

22. Nishimura, R., et al., *Characterization of genetic lesions in rhabdomyosarcoma using a high-density single nucleotide polymorphism array*. *Cancer Sci*, 2013. **104**(7): p. 856-64.
23. Dagher, R. and L. Helman, *Rhabdomyosarcoma: an overview*. *Oncologist*, 1999. **4**(1): p. 34-44.
24. Minniti, C.P., et al., *Specific expression of insulin-like growth factor-II in rhabdomyosarcoma tumor cells*. *Am J Clin Pathol*, 1994. **101**(2): p. 198-203.
25. Ognjanovic, S., et al., *Trends in childhood rhabdomyosarcoma incidence and survival in the United States, 1975-2005*. *Cancer*, 2009. **115**(18): p. 4218-26.
26. Xia, S.J., J.G. Pressey, and F.G. Barr, *Molecular Pathogenesis of Rhabdomyosarcoma*. *Cancer Biology & Therapy*, 2014. **1**(2): p. 97-104.
27. Gaiger, A.M., E.H. Soule, and W.A. Newton, *Pathology of rhabdomyosarcoma: experience of the Intergroup Rhabdomyosarcoma Study, 1972-78*. National Cancer Institute monograph, 1981(56): p. 19-27.
28. Bennicelli, J.L., et al., *Wild type PAX3 protein and the PAX3-FKHR fusion protein of alveolar rhabdomyosarcoma contain potent, structurally distinct transcriptional activation domains*. *Oncogene*, 1995. **11**(1): p. 119-130.
29. Barr, F.G., *Gene fusions involving PAX and FOX family members in alveolar rhabdomyosarcoma*. *Oncogene*, 2001. **20**(40): p. 5736-46.
30. Davicioni, E., et al., *Gene expression profiling for survival prediction in pediatric rhabdomyosarcomas: a report from the children's oncology group*. *J Clin Oncol*, 2010. **28**(7): p. 1240-6.
31. Dasgupta, R., J. Fuchs, and D. Rodeberg, *Rhabdomyosarcoma*. *Semin Pediatr Surg*, 2016. **25**(5): p. 276-283.
32. O'Brien, D., et al., *Advances in pediatric rhabdomyosarcoma characterization and disease model development*. *Histol Histopathol*, 2012. **27**(1): p. 13-22.
33. Egas-Bejar, D. and W.W. Huh, *Rhabdomyosarcoma in adolescent and young adult patients: current perspectives*. *Adolesc Health Med Ther*, 2014. **5**: p. 115-25.
34. Crist, W.M., et al., *Intergroup rhabdomyosarcoma study-IV: results for patients with nonmetastatic disease*. *J Clin Oncol*, 2001. **19**(12): p. 3091-102.
35. Gorrini, C., I.S. Harris, and T.W. Mak, *Modulation of oxidative stress as an anticancer strategy*. Nature Publishing Group, 2013. **12**(12): p. 931-947.
36. Cairns, R.A., I.S. Harris, and T.W. Mak, *Regulation of cancer cell metabolism*. *Nat Rev Cancer*, 2011. **11**(2): p. 85-95.
37. Glasauer, A. and N.S. Chandel, *Targeting antioxidants for cancer therapy*. *Biochem Pharmacol*, 2014. **92**(1): p. 90-101.
38. Barnham, K.J., C.L. Masters, and A.I. Bush, *Neurodegenerative diseases and oxidative stress*. *Nat Rev Drug Discov*, 2004. **3**(3): p. 205-14.
39. Sugamura, K. and J.F. Keane, Jr., *Reactive oxygen species in cardiovascular disease*. *Free Radic Biol Med*, 2011. **51**(5): p. 978-92.
40. Schieber, M. and N.S. Chandel, *ROS function in redox signaling and oxidative stress*. *Curr Biol*, 2014. **24**(10): p. R453-62.
41. Rhee, S.G., *Cell signaling. H₂O₂, a necessary evil for cell signaling*. *Science*, 2006. **312**(5782): p. 1882-3.
42. Finkel, T., *Signal transduction by reactive oxygen species*. *J Cell Biol*, 2011. **194**(1): p. 7-15.
43. Gupta, A., S.F. Rosenberger, and G.T. Bowden, *Increased ROS levels contribute to elevated transcription factor and MAP kinase activities in malignantly progressed mouse keratinocyte cell lines*. *Carcinogenesis*, 1999. **20**(11): p. 2063-73.

44. Torres, M., *Mitogen-activated protein kinase pathways in redox signaling*. Front Biosci, 2003. **8**: p. d369-91.
45. Ranjan, P., et al., *Redox-dependent expression of cyclin D1 and cell proliferation by Nox1 in mouse lung epithelial cells*. Antioxid Redox Signal, 2006. **8**(9-10): p. 1447-59.
46. Benhar, M., D. Engelberg, and A. Levitzki, *ROS, stress-activated kinases and stress signaling in cancer*. EMBO Rep, 2002. **3**(5): p. 420-5.
47. Leslie, N.R., et al., *Redox regulation of PI 3-kinase signalling via inactivation of PTEN*. EMBO J, 2003. **22**(20): p. 5501-10.
48. Lee, S.R., et al., *Reversible inactivation of protein-tyrosine phosphatase 1B in A431 cells stimulated with epidermal growth factor*. J Biol Chem, 1998. **273**(25): p. 15366-72.
49. Xu, D., Rovira, II, and T. Finkel, *Oxidants painting the cysteine chapel: redox regulation of PTPs*. Dev Cell, 2002. **2**(3): p. 251-2.
50. Weinberg, F., et al., *Mitochondrial metabolism and ROS generation are essential for Kras-mediated tumorigenicity*. Proc Natl Acad Sci U S A, 2010. **107**(19): p. 8788-93.
51. Davis, M.F., D. Vigil, and S.L. Campbell, *Regulation of Ras proteins by reactive nitrogen species*. Free Radic Biol Med, 2011. **51**(3): p. 565-75.
52. Adachi, Y., et al., *Oncogenic Ras upregulates NADPH oxidase 1 gene expression through MEK-ERK-dependent phosphorylation of GATA-6*. Oncogene, 2008. **27**(36): p. 4921-32.
53. Paulsen, C.E. and K.S. Carroll, *Cysteine-mediated redox signaling: Chemistry, biology, and tools for discovery*. Chemical Reviews, 2013. **113**(7): p. 4633-4679.
54. Cooke, M.S., et al., *Oxidative DNA damage: mechanisms, mutation, and disease*. FASEB J, 2003. **17**(10): p. 1195-214.
55. Radi, R., et al., *Peroxynitrite-induced membrane lipid peroxidation: the cytotoxic potential of superoxide and nitric oxide*. Arch Biochem Biophys, 1991. **288**(2): p. 481-7.
56. Stadtman, E.R. and R.L. Levine, *Protein oxidation*. Ann N Y Acad Sci, 2000. **899**: p. 191-208.
57. Galadari, S., et al., *Reactive oxygen species and cancer paradox: to promote or to suppress?* Free Radical Biology and Medicine, 2017.
58. Li, X., et al., *Targeting mitochondrial reactive oxygen species as novel therapy for inflammatory diseases and cancers*. J Hematol Oncol, 2013. **6**: p. 19.
59. Xu, X. and E.A. Arriaga, *Qualitative determination of superoxide release at both sides of the mitochondrial inner membrane by capillary electrophoretic analysis of the oxidation products of triphenylphosphonium hydroethidine*. Free Radic Biol Med, 2009. **46**(7): p. 905-13.
60. Murphy, M.P., *How mitochondria produce reactive oxygen species*. The Biochemical journal, 2009. **417**(1): p. 1-13.
61. Zeeshan, H.M., et al., *Endoplasmic Reticulum Stress and Associated ROS*. Int J Mol Sci, 2016. **17**(3): p. 327.
62. Malhotra, J.D. and R.J. Kaufman, *Endoplasmic reticulum stress and oxidative stress: a vicious cycle or a double-edged sword?* Antioxid Redox Signal, 2007. **9**(12): p. 2277-93.
63. Laurindo, F.R., L.A. Pescatore, and C. Fernandes Dde, *Protein disulfide isomerase in redox cell signaling and homeostasis*. Free Radic Biol Med, 2012. **52**(9): p. 1954-69.

64. Perez-Vizcaino, F., et al., *Postnatal maturation in nitric oxide-induced pulmonary artery relaxation involving cyclooxygenase-1 activity*. *Am J Physiol Lung Cell Mol Physiol*, 2002. **283**(4): p. L839-48.
65. Zangar, R.C., D.R. Davydov, and S. Verma, *Mechanisms that regulate production of reactive oxygen species by cytochrome P450*. *Toxicol Appl Pharmacol*, 2004. **199**(3): p. 316-31.
66. Kim, C., J.Y. Kim, and J.H. Kim, *Cytosolic phospholipase A(2), lipoxygenase metabolites, and reactive oxygen species*. *BMB Rep*, 2008. **41**(8): p. 555-9.
67. Maccarrone, M., G. Melino, and A. Finazzi-Agro, *Lipoxygenases and their involvement in programmed cell death*. *Cell Death Differ*, 2001. **8**(8): p. 776-84.
68. Gaschler, M.M. and B.R. Stockwell, *Lipid peroxidation in cell death*. *Biochem Biophys Res Commun*, 2017. **482**(3): p. 419-425.
69. Shah, R., M.S. Shchepinov, and D.A. Pratt, *Resolving the Role of Lipoxygenases in the Initiation and Execution of Ferroptosis*. *ACS Central Science*, 2018.
70. Shah, R., K. Margison, and D.A. Pratt, *The Potency of Diarylamine Radical-Trapping Antioxidants as Inhibitors of Ferroptosis Underscores the Role of Autoxidation in the Mechanism of Cell Death*. *ACS Chem Biol*, 2017. **12**(10): p. 2538-2545.
71. Winterbourn, C.C., *Toxicity of iron and hydrogen peroxide: the Fenton reaction*. *Toxicol Lett*, 1995. **82-83**: p. 969-74.
72. Repetto, M., J. Semprine, and A. Boveris, *Lipid Peroxidation: Chemical Mechanism, Biological Implications and Analytical Determination*. 2012.
73. Fransen, M., et al., *Role of peroxisomes in ROS/RNS-metabolism: implications for human disease*. *Biochim Biophys Acta*, 2012. **1822**(9): p. 1363-73.
74. Bonekamp, N.A., et al., *Reactive oxygen species and peroxisomes: struggling for balance*. *Biofactors*, 2009. **35**(4): p. 346-55.
75. Ma, M.W., et al., *NADPH oxidase in brain injury and neurodegenerative disorders*. *Mol Neurodegener*, 2017. **12**(1): p. 7.
76. Altenhofer, S., et al., *The NOX toolbox: validating the role of NADPH oxidases in physiology and disease*. *Cell Mol Life Sci*, 2012. **69**(14): p. 2327-43.
77. Brandes, R.P., N. Weissmann, and K. Schroder, *Nox family NADPH oxidases: Molecular mechanisms of activation*. *Free Radic Biol Med*, 2014. **76**: p. 208-26.
78. Brandes, R.P. and K. Schroder, *NOXious phosphorylation: Smooth muscle reactive oxygen species production is facilitated by direct activation of the NADPH oxidase Nox1*. *Circ Res*, 2014. **115**(11): p. 898-900.
79. Serrander, L., et al., *NOX4 activity is determined by mRNA levels and reveals a unique pattern of ROS generation*. *Biochem J*, 2007. **406**(1): p. 105-14.
80. Martyn, K.D., et al., *Functional analysis of Nox4 reveals unique characteristics compared to other NADPH oxidases*. *Cell Signal*, 2006. **18**(1): p. 69-82.
81. Xie, Z.-Z., Y. Liu, and J.-S. Bian, *Hydrogen Sulfide and Cellular Redox Homeostasis*. *Oxidative medicine and cellular longevity*, 2016. **2016**: p. 6043038-6043038.
82. Waris, G. and H. Ahsan, *Reactive oxygen species: role in the development of cancer and various chronic conditions*. *J Carcinog*, 2006. **5**: p. 14.
83. Copin, J.C., Y. Gasche, and P.H. Chan, *Overexpression of copper/zinc superoxide dismutase does not prevent neonatal lethality in mutant mice that lack manganese superoxide dismutase*. *Free Radic Biol Med*, 2000. **28**(10): p. 1571-6.

84. Fukai, T. and M. Ushio-Fukai, *Superoxide dismutases: role in redox signaling, vascular function, and diseases*. *Antioxid Redox Signal*, 2011. **15**(6): p. 1583-606.
85. Schrader, M. and H.D. Fahimi, *Peroxisomes and oxidative stress*. *Biochim Biophys Acta*, 2006. **1763**(12): p. 1755-66.
86. Reczek, C.R. and N.S. Chandel, *ScienceDirect ROS-dependent signal transduction*. *Current Opinion in Cell Biology*, 2015. **33**: p. 8-13.
87. Wood, Z.A., et al., *Structure, mechanism and regulation of peroxiredoxins*. *Trends Biochem Sci*, 2003. **28**(1): p. 32-40.
88. Rhee, S.G., H.Z. Chae, and K. Kim, *Peroxiredoxins: a historical overview and speculative preview of novel mechanisms and emerging concepts in cell signaling*. *Free Radic Biol Med*, 2005. **38**(12): p. 1543-52.
89. Rhee, S.G., et al., *Peroxiredoxin functions as a peroxidase and a regulator and sensor of local peroxides*. *J Biol Chem*, 2012. **287**(7): p. 4403-10.
90. Scheerer, P., et al., *Structural basis for catalytic activity and enzyme polymerization of phospholipid hydroperoxide glutathione peroxidase-4 (GPx4)*. *Biochemistry*, 2007. **46**(31): p. 9041-9.
91. Brigelius-Flohé, R. and M. Maiorino, *Glutathione peroxidases*. *Biochimica et Biophysica Acta (BBA) - General Subjects*, 2013. **1830**(5): p. 3289-3303.
92. Thomas, J.P., et al., *Enzymatic reduction of phospholipid and cholesterol hydroperoxides in artificial bilayers and lipoproteins*. *Biochim Biophys Acta*, 1990. **1045**(3): p. 252-60.
93. Lu, S.C., *Glutathione synthesis*. *Biochim Biophys Acta*, 2013. **1830**(5): p. 3143-53.
94. Townsend, D.M. and K.D. Tew, *The role of glutathione-S-transferase in anti-cancer drug resistance*. *Oncogene*, 2003. **22**(47): p. 7369-75.
95. Qiao, Y.L., et al., *Total and cancer mortality after supplementation with vitamins and minerals: follow-up of the Linxian General Population Nutrition Intervention Trial*. *J Natl Cancer Inst*, 2009. **101**(7): p. 507-18.
96. Traber, M.G. and J.F. Stevens, *Vitamins C and E: beneficial effects from a mechanistic perspective*. *Free Radic Biol Med*, 2011. **51**(5): p. 1000-13.
97. Frei, B., *Reactive oxygen species and antioxidant vitamins: mechanisms of action*. *Am J Med*, 1994. **97**(3A): p. 5S-13S; discussion 22S-28S.
98. Rayman, M.P., *Selenoproteins and human health: insights from epidemiological data*. *Biochim Biophys Acta*, 2009. **1790**(11): p. 1533-40.
99. Dolma, S., et al., *Identification of genotype-selective antitumor agents using synthetic lethal chemical screening in engineered human tumor cells*. *Cancer Cell*, 2003. **3**(3): p. 285-96.
100. Yang, W.S. and B.R. Stockwell, *Synthetic Lethal Screening Identifies Compounds in Oncogenic-RAS-Harboring Cancer Cells*. 2008(March): p. 234-245.
101. Dixon, S.J., et al., *Ferroptosis: An Iron-Dependent Form of Nonapoptotic Cell Death*. *Cell*, 2012. **149**(5): p. 1060-1072.
102. Dixon, S.J., et al., *Pharmacological inhibition of cystine–glutamate exchange induces endoplasmic reticulum stress and ferroptosis*. *eLife*, 2014. **3**: p. 1-25.
103. Sato, M., et al., *The ferroptosis inducer erastin irreversibly inhibits system xc- and synergizes with cisplatin to increase cisplatin's cytotoxicity in cancer cells*. *Sci Rep*, 2018. **8**(1): p. 968.
104. Yang, Wan S., et al., *Regulation of Ferroptotic Cancer Cell Death by GPX4*. *Cell*, 2014. **156**(1-2): p. 317-331.

105. Yagoda, N., et al., *RAS-RAF-MEK-dependent oxidative cell death involving voltage-dependent anion channels*. Nature, 2007. **447**(7146): p. 864-8.
106. Reed, J.C. and M. Pellecchia, *Ironing Out Cell Death Mechanisms*. Cell, 2012. **149**(5): p. 963-965.
107. Wilhelm, S., et al., *Discovery and development of sorafenib: a multikinase inhibitor for treating cancer*. Nat Rev Drug Discov, 2006. **5**(10): p. 835-44.
108. Wilhelm, S.M., et al., *BAY 43-9006 exhibits broad spectrum oral antitumor activity and targets the RAF/MEK/ERK pathway and receptor tyrosine kinases involved in tumor progression and angiogenesis*. Cancer Res, 2004. **64**(19): p. 7099-109.
109. Abou-Alfa, G.K., et al., *Phase II study of sorafenib in patients with advanced hepatocellular carcinoma*. J Clin Oncol, 2006. **24**(26): p. 4293-300.
110. Kane, R.C., et al., *Sorafenib for the treatment of advanced renal cell carcinoma*. Clin Cancer Res, 2006. **12**(24): p. 7271-8.
111. Walter, I., et al., *Human osteosarcoma cells respond to sorafenib chemotherapy by downregulation of the tumor progression factors S100A4, CXCR4 and the oncogene FOS*. Oncol Rep, 2014. **31**(3): p. 1147-56.
112. Coriat, R., et al., *Sorafenib-induced hepatocellular carcinoma cell death depends on reactive oxygen species production in vitro and in vivo*. Mol Cancer Ther, 2012. **11**(10): p. 2284-93.
113. Zhu, A.X., et al., *SEARCH: a phase III, randomized, double-blind, placebo-controlled trial of sorafenib plus erlotinib in patients with advanced hepatocellular carcinoma*. J Clin Oncol, 2015. **33**(6): p. 559-66.
114. Grignani, G., et al., *A phase II trial of sorafenib in relapsed and unresectable high-grade osteosarcoma after failure of standard multimodal therapy: an Italian Sarcoma Group study*. Ann Oncol, 2012. **23**(2): p. 508-16.
115. Fulda, S. and D. Vucic, *Targeting IAP proteins for therapeutic intervention in cancer*. Nature reviews. Drug discovery, 2012. **11**(2): p. 109-24.
116. Varfolomeev, E., et al., *IAP antagonists induce autoubiquitination of c-IAPs, NF-kappaB activation, and TNFalpha-dependent apoptosis*. Cell, 2007. **131**(4): p. 669-81.
117. Opel, D., et al., *Targeting inhibitor of apoptosis proteins by Smac mimetic elicits cell death in poor prognostic subgroups of chronic lymphocytic leukemia*. Int J Cancer, 2015. **137**(12): p. 2959-70.
118. Belz, K., et al., *Smac mimetic and glucocorticoids synergize to induce apoptosis in childhood ALL by promoting ripoptosome assembly*. Blood, 2014. **124**(2): p. 240-50.
119. Schumacker, Paul T., *Reactive Oxygen Species in Cancer: A Dance with the Devil*. Cancer Cell, 2015. **27**(2): p. 156-157.
120. Du, M.Q., P.L. Carmichael, and D.H. Phillips, *Induction of activating mutations in the human c-Ha-ras-1 proto-oncogene by oxygen free radicals*. Mol Carcinog, 1994. **11**(3): p. 170-5.
121. Hussain, S.P., et al., *Oxy-radical induced mutagenesis of hotspot codons 248 and 249 of the human p53 gene*. Oncogene, 1994. **9**(8): p. 2277-81.
122. Salmeen, A., et al., *Redox regulation of protein tyrosine phosphatase 1B involves a sulphenyl-amide intermediate*. Nature, 2003. **423**(6941): p. 769-73.
123. Seth, D. and J. Rudolph, *Redox regulation of MAP kinase phosphatase 3*. Biochemistry, 2006. **45**(28): p. 8476-87.
124. Klaunig, J.E., L.M. Kamendulis, and B.A. Hocevar, *Oxidative stress and oxidative damage in carcinogenesis*. Toxicol Pathol, 2010. **38**(1): p. 96-109.

125. Gao, P., et al., *HIF-dependent antitumorigenic effect of antioxidants in vivo*. *Cancer Cell*, 2007. **12**(3): p. 230-8.
126. Finch, J.S., et al., *Catalase reverses tumorigenicity in a malignant cell line by an epidermal growth factor receptor pathway*. *Free Radic Biol Med*, 2006. **40**(5): p. 863-75.
127. Weydert, C.J., et al., *Overexpression of manganese or copper-zinc superoxide dismutase inhibits breast cancer growth*. *Free Radic Biol Med*, 2006. **41**(2): p. 226-37.
128. Aykin-Burns, N., et al., *Increased levels of superoxide and H₂O₂ mediate the differential susceptibility of cancer cells versus normal cells to glucose deprivation*. *Biochem J*, 2009. **418**(1): p. 29-37.
129. Madesh, M. and G. Hajnoczky, *VDAC-dependent permeabilization of the outer mitochondrial membrane by superoxide induces rapid and massive cytochrome c release*. *J Cell Biol*, 2001. **155**(6): p. 1003-15.
130. Ye, Y.C., et al., *RIP1-mediated mitochondrial dysfunction and ROS production contributed to tumor necrosis factor alpha-induced L929 cell necroptosis and autophagy*. *Int Immunopharmacol*, 2012. **14**(4): p. 674-82.
131. Hengartner, M.O., *The biochemistry of apoptosis*. *Nature*, 2000. **407**: p. 770.
132. Schweichel, J.U. and H.J. Merker, *The morphology of various types of cell death in prenatal tissues*. *Teratology*, 1973. **7**(3): p. 253-66.
133. Zhang, D.W., et al., *RIP3, an energy metabolism regulator that switches TNF-induced cell death from apoptosis to necrosis*. *Science*, 2009. **325**(5938): p. 332-6.
134. Berghe, T.V., et al., *Regulated necrosis: the expanding network of non-apoptotic cell death pathways*. *Nature Reviews Molecular Cell Biology*, 2014. **15**(2): p. 135-147.
135. Berghe, T.V., et al., *Molecular crosstalk between apoptosis, necroptosis and survival signaling*. *Molecular & Cellular Oncology*, 2015. **3556**(July 2015): p. 00-00.
136. Yang, W.S. and B.R. Stockwell, *Ferroptosis : Death by Lipid Peroxidation*. *Trends in Cell Biology*, 2015. **xx**: p. 1-12.
137. Neitemeier, S., et al., *BID links ferroptosis to mitochondrial cell death pathways*. *Redox Biology*, 2017.
138. Gout, P.W., et al., *Sulfasalazine, a potent suppressor of lymphoma growth by inhibition of the x(c)- cystine transporter: a new action for an old drug*. *Leukemia*, 2001. **15**(10): p. 1633-40.
139. Louandre, C., et al., *The retinoblastoma (Rb) protein regulates ferroptosis induced by sorafenib in human hepatocellular carcinoma cells*. *Cancer Letters*, 2015. **356**(2): p. 971-977.
140. Griffith, O.W. and A. Meister, *Potent and specific inhibition of glutathione synthesis by buthionine sulfoximine (S-n-butyl homocysteine sulfoximine)*. *J Biol Chem*, 1979. **254**(16): p. 7558-60.
141. Seiler, A., et al., *Glutathione Peroxidase 4 Senses and Translates Oxidative Stress into 12/15-Lipoxygenase Dependent- and AIF-Mediated Cell Death*. *Cell Metabolism*, 2008. **8**(3): p. 237-248.
142. Yant, L.J., et al., *The selenoprotein GPX4 is essential for mouse development and protects from radiation and oxidative damage insults*. *Free Radical Biology and Medicine*, 2003. **34**(4): p. 496-502.
143. Conrad, M., et al., *what ' s so special about it ? Glutathione peroxidase 4 (Gpx4) and ferroptosis : what ' s so special about it ?* 2015. **3556**(October): p. 0-3.

144. Linkermann, A., et al., *Synchronized renal tubular cell death involves ferroptosis*. Proceedings of the National Academy of Sciences, 2014. **111**(47): p. 16836-16841.
145. Eling, N., et al., *Identification of artesunate as a specific activator of ferroptosis in pancreatic cancer cells*. Oncoscience, 2015. **2**(5): p. 517-32.
146. Ooko, E., et al., *Artemisinin derivatives induce iron-dependent cell death (ferroptosis) in tumor cells*. Phytomedicine, 2015. **22**(11): p. 1045-1054.
147. Liu, Y., et al., *The 5-Lipoxygenase Inhibitor Zileuton Confers Neuroprotection against Glutamate Oxidative Damage by Inhibiting Ferroptosis*. Biological and Pharmaceutical Bulletin, 2015. **38**(8): p. 1234-1239.
148. Gao, M., et al., *Glutaminolysis and Transferrin Regulate Ferroptosis*. Molecular Cell, 2015. **59**(2): p. 298-308.
149. Barradas, M.A., et al., *Iron chelators inhibit human platelet aggregation, thromboxane A2 synthesis and lipoxygenase activity*. FEBS Lett, 1989. **245**(1-2): p. 105-9.
150. Conlon, M. and S.J. Dixon, *Ferroptosis-like death in plant cells*. Mol Cell Oncol, 2017. **4**(3): p. e1302906.
151. Skouta, R., et al., *Ferrostatis inhibit oxidative lipid damage and cell death in diverse disease models*. Journal of the American Chemical Society, 2014. **136**(12): p. 4551-4556.
152. Cheng, Z. and Y. Li, *What is responsible for the initiating chemistry of iron-mediated lipid peroxidation: an update*. Chem Rev, 2007. **107**(3): p. 748-66.
153. Yang, W.S., et al., *Peroxidation of polyunsaturated fatty acids by lipoxygenases drives ferroptosis*. Proceedings of the National Academy of Sciences, 2016: p. 201603244-201603244.
154. Doll, S., et al., *ACSL4 dictates ferroptosis sensitivity by shaping cellular lipid composition*. Nature Chemical Biology, 2016(November).
155. Kagan, V.E., et al., *Oxidized arachidonic and adrenergic PEs navigate cells to ferroptosis*. Nature Chemical Biology, 2016(November).
156. Angeli, J.P.F., et al., *Ferroptosis Inhibition: Mechanisms and Opportunities*. Trends Pharmacol Sci, 2017. **38**(5): p. 489-498.
157. Cao, J.Y. and S.J. Dixon, *Mechanisms of ferroptosis*. Cellular and Molecular Life Sciences, 2016.
158. Xie, Y., et al., *Ferroptosis : process and function*. 2016: p. 1-11.
159. Yu, H., et al., *Ferroptosis, a new form of cell death, and its relationships with tumourous diseases*. J Cell Mol Med, 2016.
160. Hayano, M., et al., *Loss of cysteinyl-tRNA synthetase (CARS) induces the transsulfuration pathway and inhibits ferroptosis induced by cystine deprivation*. Cell Death and Differentiation, 2015: p. 1-9.
161. Sun, X., et al., *HSPB1 as a novel regulator of ferroptotic cancer cell death*. Oncogene, 2015. **34**(45): p. 5617-25.
162. Dixon, S.J., et al., *Human Haploid Cell Genetics Reveals Roles for Lipid Metabolism Genes in Nonapoptotic Cell Death*. ACS Chemical Biology, 2015. **10**(7): p. 1604-1609.
163. Jiang, L., et al., *Ferroptosis as a p53-mediated activity during tumour suppression*. Nature, 2015. **520**(7545): p. 57-62.
164. Xie, Y., et al., *The Tumor Suppressor p53 Limits Ferroptosis by Blocking DPP4 Activity*. Cell Rep, 2017. **20**(7): p. 1692-1704.
165. Iglehart, J.K., et al., *Cystine requirement of continuous human lymphoid cell lines of normal and leukemic origin*. J Biol Chem, 1977. **252**(20): p. 7184-91.

166. McBean, G.J., *The transsulfuration pathway: a source of cysteine for glutathione in astrocytes*. *Amino Acids*, 2012. **42**(1): p. 199-205.
167. Yu, X. and Y.C. Long, *Crosstalk between cystine and glutathione is critical for the regulation of amino acid signaling pathways and ferroptosis*. *Scientific reports*, 2016. **6**: p. 30033-30033.
168. Shimada, K., et al., *Global survey of cell death mechanisms reveals metabolic regulation of ferroptosis*. *Nature Chemical Biology*, 2016. **12**(May): p. 1-10.
169. Viswanathan, V.S., et al., *Dependency of a therapy-resistant state of cancer cells on a lipid peroxidase pathway*. *Nature*, 2017. **547**(7664): p. 453-457.
170. Zhu, S., et al., *HSPA5 Regulates Ferroptotic Cell Death in Cancer Cells*. *Cancer Res*, 2017. **77**(8): p. 2064-2077.
171. Sun, X., et al., *Activation of the p62-Keap1-NRF2 pathway protects against ferroptosis in hepatocellular carcinoma cells*. *Hepatology*, 2016. **63**(1): p. 173-184.
172. Chen, D., et al., *NRF2 Is a Major Target of ARF in p53-Independent Tumor Suppression*. *Mol Cell*, 2017. **68**(1): p. 224-232 e4.
173. Sehm, T., et al., *Temozolomide toxicity operates in a xCT / SLC7a11 dependent manner and is fostered by ferroptosis*. 2016.
174. Yu, Y., et al., *The ferroptosis inducer erastin enhances sensitivity of acute myeloid leukemia cells to chemotherapeutic agents*. *Molecular & Cellular Oncology*, 2015. **2**(4): p. e1054549-e1054549.
175. Kim, S.E., et al., *Ultrasmall nanoparticles induce ferroptosis in nutrient-deprived cancer cells and suppress tumour growth*. *Nat Nanotechnol*, 2016. **11**(11): p. 977-985.
176. Hambright, W.S., et al., *Ablation of ferroptosis regulator glutathione peroxidase 4 in forebrain neurons promotes cognitive impairment and neurodegeneration*. *Redox Biol*, 2017. **12**: p. 8-17.
177. Irwin, M.E., N. Rivera-Del Valle, and J. Chandra, *Redox control of leukemia: from molecular mechanisms to therapeutic opportunities*. *Antioxid Redox Signal*, 2013. **18**(11): p. 1349-83.
178. Chen, X., et al., *Targeting oxidative stress in embryonal rhabdomyosarcoma*. *Cancer cell*, 2013. **24**(6): p. 710-24.
179. Lee, E.W., et al., *The roles of FADD in extrinsic apoptosis and necroptosis*. *BMB Reports*, 2012. **45**(9): p. 496-508.
180. Probst, L., et al., *Lipoxygenase inhibitors protect acute lymphoblastic leukemia cells from ferroptotic cell death*. *Biochem Pharmacol*, 2017. **140**: p. 41-52.
181. Lemaire, C., et al., *Inhibition of caspase activity induces a switch from apoptosis to necrosis*. *FEBS Lett*, 1998. **425**(2): p. 266-70.
182. Degtarev, A., J.L. Maki, and J. Yuan, *Activity and specificity of necrostatin-1, small-molecule inhibitor of RIP1 kinase*. *Cell Death Differ*, 2013. **20**(2): p. 366.
183. Deschamps, J.D., V.A. Kenyon, and T.R. Holman, *Baicalein is a potent in vitro inhibitor against both reticulocyte 15-human and platelet 12-human lipoxygenases*. *Bioorg Med Chem*, 2006. **14**(12): p. 4295-301.
184. Salari, H., P. Braquet, and P. Borgeat, *Comparative effects of indomethacin, acetylenic acids, 15-HETE, nordihydroguaiaretic acid and BW755C on the metabolism of arachidonic acid in human leukocytes and platelets*. *Prostaglandins Leukot Med*, 1984. **13**(1): p. 53-60.
185. Rossi, A., et al., *The 5-lipoxygenase inhibitor, zileuton, suppresses prostaglandin biosynthesis by inhibition of arachidonic acid release in macrophages*. *Br J Pharmacol*, 2010. **161**(3): p. 555-70.

186. Sendobry, S.M., et al., *Attenuation of diet-induced atherosclerosis in rabbits with a highly selective 15-lipoxygenase inhibitor lacking significant antioxidant properties*. Br J Pharmacol, 1997. **120**(7): p. 1199-206.
187. Dächert, J., et al., *RSL3 and Erastin differentially regulate redox signaling to promote Smac mimetic-induced cell death*. 2016: p. 1-14.
188. Schoeneberger, H., et al., *Impairment of antioxidant defense via glutathione depletion sensitizes acute lymphoblastic leukemia cells for Smac mimetic-induced cell death*. Oncogene, 2015. **34**(31): p. 4032-43.
189. Arranz, L., et al., *The glutathione precursor N-acetylcysteine improves immune function in postmenopausal women*. Free Radic Biol Med, 2008. **45**(9): p. 1252-62.
190. Zhang, M., C.M. Linardic, and D.G. Kirsch, *RAS and ROS in rhabdomyosarcoma*. Cancer cell, 2013. **24**(6): p. 689-91.
191. Do Van, B., et al., *Ferroptosis, a newly characterized form of cell death in Parkinson's disease that is regulated by PKC*. Neurobiol Dis, 2016. **94**: p. 169-78.
192. Dolgikh, N., et al., *NRAS-Mutated Rhabdomyosarcoma Cells Are Vulnerable to Mitochondrial Apoptosis Induced by Coinhibition of MEK and PI3Kalpha*. Cancer Res, 2018.
193. Aldieri, E., et al., *Classical inhibitors of NOX NAD(P)H oxidases are not specific*. Curr Drug Metab, 2008. **9**(8): p. 686-96.
194. Aoyama, T., et al., *Nicotinamide adenine dinucleotide phosphate oxidase in experimental liver fibrosis: GKT137831 as a novel potential therapeutic agent*. Hepatology, 2012. **56**(6): p. 2316-27.
195. Cosentino-Gomes, D., N. Rocco-Machado, and J.R. Meyer-Fernandes, *Cell signaling through protein kinase C oxidation and activation*. Int J Mol Sci, 2012. **13**(9): p. 10697-721.
196. Komander, D., et al., *Interactions of LY333531 and other bisindolyl maleimide inhibitors with PDK1*. Structure, 2004. **12**(2): p. 215-26.
197. Martiny-Baron, G., et al., *Selective inhibition of protein kinase C isozymes by the indolocarbazole Go 6976*. J Biol Chem, 1993. **268**(13): p. 9194-7.
198. Stanulla, M. and M. Schrappe, *Treatment of childhood acute lymphoblastic leukemia*. Semin Hematol, 2009. **46**(1): p. 52-63.
199. Fulda, S., *Tumor resistance to apoptosis*. International Journal of Cancer, 2009. **124**(3): p. 511-515.
200. Peters-Golden, M. and T.G. Brock, *5-lipoxygenase and FLAP*. Prostaglandins Leukot Essent Fatty Acids, 2003. **69**(2-3): p. 99-109.
201. Li, C.T., et al., *Oxygen-glucose deprivation activates 5-lipoxygenase mediated by oxidative stress through the p38 mitogen-activated protein kinase pathway in PC12 cells*. J Neurosci Res, 2009. **87**(4): p. 991-1001.
202. Werz, O., et al., *Arachidonic acid promotes phosphorylation of 5-lipoxygenase at Ser-271 by MAPK-activated protein kinase 2 (MK2)*. J Biol Chem, 2002. **277**(17): p. 14793-800.
203. Jones, G.D., et al., *Role of Lipid Hydroperoxides in the Activation of 15-Lipoxygenase*. Biochemistry, 1996. **35**(22): p. 7197-7203.
204. Schnurr, K., et al., *The Selenoenzyme Phospholipid Hydroperoxide Glutathione Peroxidase Controls the Activity of the 15-Lipoxygenase with Complex Substrates and Preserves the Specificity of the Oxygenation Products*. Journal of Biological Chemistry, 1996. **271**(9): p. 4653-4658.
205. Doll, S. and M. Conrad, *Iron and ferroptosis: A still ill-defined liaison*. IUBMB Life, 2017.

206. Dixon, S.J. and B.R. Stockwell, *The role of iron and reactive oxygen species in cell death*. Nat Chem Biol, 2014. **10**(1): p. 9-17.
207. Li, Y., P. Maher, and D. Schubert, *A role for 12-lipoxygenase in nerve cell death caused by glutathione depletion*. Neuron, 1997. **19**(2): p. 453-63.
208. Matsushita, M., et al., *T cell lipid peroxidation induces ferroptosis and prevents immunity to infection*. Journal of Experimental Medicine, 2015. **212**(4): p. 555-568.
209. Friedmann, et al., *Inactivation of the ferroptosis regulator Gpx4 triggers acute renal failure in mice*. Nature cell biology, 2014. **3**(August): p. 1-9.
210. Wenzel, S.E., et al., *PEBP1 Wardens Ferroptosis by Enabling Lipoxygenase Generation of Lipid Death Signals*. Cell, 2017. **171**(3): p. 628-641 e26.
211. Fulda, S., *Inhibitor of Apoptosis Proteins in Pediatric Leukemia: Molecular Pathways and Novel Approaches to Therapy*. Frontiers in oncology, 2014. **4**(January): p. 3-3.
212. Fulda, S., *Molecular Pathways : Targeting Inhibitor of Apoptosis Proteins in Cancer — From Molecular Mechanism to Therapeutic Application*. 2014(3): p. 289-296.
213. DeHart, D.N., et al., *Opening of voltage dependent anion channels promotes reactive oxygen species generation, mitochondrial dysfunction and cell death in cancer cells*. Biochem Pharmacol, 2017. **148**: p. 155-162.
214. Maldonado, E.N., et al., *Voltage-dependent anion channels modulate mitochondrial metabolism in cancer cells: regulation by free tubulin and erastin*. The Journal of biological chemistry, 2013. **288**(17): p. 11920-9.
215. Maldonado, E.N., *VDAC–Tubulin, an Anti-Warburg Pro-Oxidant Switch*. Frontiers in Oncology, 2017. **7**(January): p. 4-4.
216. Shoshan-Barmatz, V., et al., *VDAC, a multi-functional mitochondrial protein regulating cell life and death*. Mol Aspects Med, 2010. **31**(3): p. 227-85.
217. Vandenabeele, P., et al., *Molecular mechanisms of necroptosis: an ordered cellular explosion*. Nat Rev Mol Cell Biol, 2010. **11**(10): p. 700-14.
218. Canli, Ö., et al., *Glutathione peroxidase 4 prevents necroptosis in mouse erythroid precursors*. Blood, 2015. **127**(1): p. 139-149.
219. Zhang, D., J. Lin, and J. Han, *Receptor-interacting protein (RIP) kinase family*. Cellular and Molecular Immunology, 2010. **7**(4): p. 243-249.
220. Silke, J., J.A. Rickard, and M. Gerlic, *The diverse role of RIP kinases in necroptosis and inflammation*. Nat Immunol, 2015. **16**(7): p. 689-697.
221. Banjac, A., et al., *The cystine/cysteine cycle: a redox cycle regulating susceptibility versus resistance to cell death*. Oncogene, 2008. **27**(11): p. 1618-28.
222. Bannai, S., et al., *Induction of cystine transport activity in human fibroblasts by oxygen*. J Biol Chem, 1989. **264**(31): p. 18480-4.
223. Habib, E., et al., *Expression of xCT and activity of system xc(-) are regulated by NRF2 in human breast cancer cells in response to oxidative stress*. Redox Biol, 2015. **5**: p. 33-42.
224. Kanai, Y. and H. Endou, *Functional properties of multispecific amino acid transporters and their implications to transporter-mediated toxicity*. J Toxicol Sci, 2003. **28**(1): p. 1-17.
225. Kakazu, E., et al., *Plasma L-cystine/L-glutamate imbalance increases tumor necrosis factor-alpha from CD14+ circulating monocytes in patients with advanced cirrhosis*. PLoS One, 2011. **6**(8): p. e23402.
226. Conrad, M., et al., *Regulated necrosis: disease relevance and therapeutic opportunities*. Nature Reviews Drug Discovery, 2016.

227. Hochwald, S.N., et al., *Elevation of glutathione and related enzyme activities in high-grade and metastatic extremity soft tissue sarcoma*. *Ann Surg Oncol*, 1997. **4**(4): p. 303-9.
228. Seitz, G., et al., *Inhibition of glutathione-S-transferase as a treatment strategy for multidrug resistance in childhood rhabdomyosarcoma*. *Int J Oncol*, 2010. **36**(2): p. 491-500.
229. Maruwge, W., et al., *Sorafenib inhibits tumor growth and vascularization of rhabdomyosarcoma cells by blocking IGF-1R-mediated signaling*. *OncoTargets and therapy*, 2008. **1**: p. 67-78.
230. Kim, A., et al., *Phase 2 trial of sorafenib in children and young adults with refractory solid tumors: A report from the Children's Oncology Group*. *Pediatric blood & cancer*, 2015. **62**(9): p. 1562-6.
231. Habermann, K.J., et al., *Targeting redox homeostasis in rhabdomyosarcoma cells: GSH-depleting agents enhance auranofin-induced cell death*. *Cell Death Dis*, 2017. **8**(10): p. e3067.
232. Latunde-Dada, G.O., *Ferroptosis: Role of lipid peroxidation, iron and ferritinophagy*. *Biochim Biophys Acta*, 2017. **1861**(8): p. 1893-1900.
233. Dixon, S.J., et al., *Pharmacological inhibition of cystine-glutamate exchange induces endoplasmic reticulum stress and ferroptosis*. *Elife*, 2014. **3**: p. e02523.
234. Rousset, F., et al., *Heme oxygenase-1 regulates matrix metalloproteinase MMP-1 secretion and chondrocyte cell death via Nox4 NADPH oxidase activity in chondrocytes*. *PLoS One*, 2013. **8**(6): p. e66478.
235. Kleniewska, P., et al., *The NADPH oxidase family and its inhibitors*. *Arch Immunol Ther Exp (Warsz)*, 2012. **60**(4): p. 277-94.
236. Takac, I., et al., *The E-loop is involved in hydrogen peroxide formation by the NADPH oxidase Nox4*. *J Biol Chem*, 2011. **286**(15): p. 13304-13.
237. Petry, A., et al., *NOX2 and NOX4 mediate proliferative response in endothelial cells*. *Antioxid Redox Signal*, 2006. **8**(9-10): p. 1473-84.
238. Block, K., Y. Gorin, and H.E. Abboud, *Subcellular localization of Nox4 and regulation in diabetes*. *Proc Natl Acad Sci U S A*, 2009. **106**(34): p. 14385-90.
239. Egea, J., et al., *European contribution to the study of ROS: A summary of the findings and prospects for the future from the COST action BM1203 (EU-ROS)*. *Redox Biol*, 2017. **13**: p. 94-162.
240. Altenhöfer, S., et al., *Evolution of NADPH Oxidase Inhibitors: Selectivity and Mechanisms for Target Engagement*. *Antioxidants & redox signaling*, 2015. **23**(5): p. 406-427.
241. Jiang, J.X., et al., *Liver fibrosis and hepatocyte apoptosis are attenuated by GKT137831, a novel NOX4/NOX1 inhibitor in vivo*. *Free Radic Biol Med*, 2012. **53**(2): p. 289-96.
242. Li, Q., et al., *NADPH oxidase subunit p22(phox)-mediated reactive oxygen species contribute to angiogenesis and tumor growth through AKT and ERK1/2 signaling pathways in prostate cancer*. *Biochim Biophys Acta*, 2013. **1833**(12): p. 3375-85.
243. Meitzler, J.L., et al., *Decoding NADPH oxidase 4 expression in human tumors*. *Redox Biol*, 2017. **13**: p. 182-195.
244. Sumimoto, H., *Structure, regulation and evolution of Nox-family NADPH oxidases that produce reactive oxygen species*. *FEBS J*, 2008. **275**(13): p. 3249-77.
245. Helmcke, I., et al., *Identification of structural elements in Nox1 and Nox4 controlling localization and activity*. *Antioxid Redox Signal*, 2009. **11**(6): p. 1279-87.

246. Rastogi, R., et al., *NOX Activation by Subunit Interaction and Underlying Mechanisms in Disease*. Front Cell Neurosci, 2016. **10**: p. 301.
247. Jiang, F., Y. Zhang, and G.J. Dusting, *NADPH oxidase-mediated redox signaling: roles in cellular stress response, stress tolerance, and tissue repair*. Pharmacol Rev, 2011. **63**(1): p. 218-42.
248. Kodama, R., et al., *ROS-generating oxidases Nox1 and Nox4 contribute to oncogenic Ras-induced premature senescence*. Genes Cells, 2013. **18**(1): p. 32-41.
249. Colston, J.T., et al., *H₂O₂ activates Nox4 through PLA2-dependent arachidonic acid production in adult cardiac fibroblasts*. FEBS Lett, 2005. **579**(11): p. 2533-40.
250. Leusen, J.H., A.J. Verhoeven, and D. Roos, *Interactions between the components of the human NADPH oxidase: intrigues in the phox family*. J Lab Clin Med, 1996. **128**(5): p. 461-76.
251. Bey, E.A., et al., *Protein Kinase C Is Required for p47phox Phosphorylation and Translocation in Activated Human Monocytes*. The Journal of Immunology, 2004. **173**(9): p. 5730-5738.
252. Lewis, E.M., et al., *Phosphorylation of p22phox on threonine 147 enhances NADPH oxidase activity by promoting p47phox binding*. J Biol Chem, 2010. **285**(5): p. 2959-67.
253. Giorgi, C., et al., *Redox control of protein kinase C: cell- and disease-specific aspects*. Antioxid Redox Signal, 2010. **13**(7): p. 1051-85.
254. Cenni, V., et al., *Regulation of novel protein kinase C epsilon by phosphorylation*. Biochem J, 2002. **363**(Pt 3): p. 537-45.
255. Almeida-Amaral, E.E., et al., *Leishmania amazonensis: PKC-like protein kinase modulates the (Na⁺⁺K⁺)ATPase activity*. Exp Parasitol, 2007. **116**(4): p. 419-26.
256. DelCarlo, M. and R.F. Loeser, *Chondrocyte cell death mediated by reactive oxygen species-dependent activation of PKC-beta1*. Am J Physiol Cell Physiol, 2006. **290**(3): p. C802-11.
257. Marengo, B., et al., *PKCdelta sensitizes neuroblastoma cells to L-buthionine-sulfoximine and etoposide inducing reactive oxygen species overproduction and DNA damage*. PLoS One, 2011. **6**(2): p. e14661.
258. Kim, Y.A., M.Y. Kim, and Y.S. Jung, *Glutathione Depletion by L-Buthionine-S,R-Sulfoximine Induces Apoptosis of Cardiomyocytes through Activation of PKC-delta*. Biomol Ther (Seoul), 2013. **21**(5): p. 358-63.
259. Lin, Y.L., et al., *The evolutionarily conserved zinc finger motif in the largest subunit of human replication protein A is required for DNA replication and mismatch repair but not for nucleotide excision repair*. J Biol Chem, 1998. **273**(3): p. 1453-61.
260. Lin, D. and D.J. Takemoto, *Oxidative activation of protein kinase Cgamma through the C1 domain. Effects on gap junctions*. J Biol Chem, 2005. **280**(14): p. 13682-93.
261. Daiber, A., *Redox signaling (cross-talk) from and to mitochondria involves mitochondrial pores and reactive oxygen species*. Biochim Biophys Acta, 2010. **1797**(6-7): p. 897-906.
262. Zorov, D.B., M. Juhaszova, and S.J. Sollott, *Mitochondrial reactive oxygen species (ROS) and ROS-induced ROS release*. Physiol Rev, 2014. **94**(3): p. 909-50.

263. Rathore, R., et al., *Hypoxia activates NADPH oxidase to increase [ROS]_i and [Ca²⁺]_i through the mitochondrial ROS-PKCε signaling axis in pulmonary artery smooth muscle cells*. *Free Radic Biol Med*, 2008. **45**(9): p. 1223-31.

Appendix

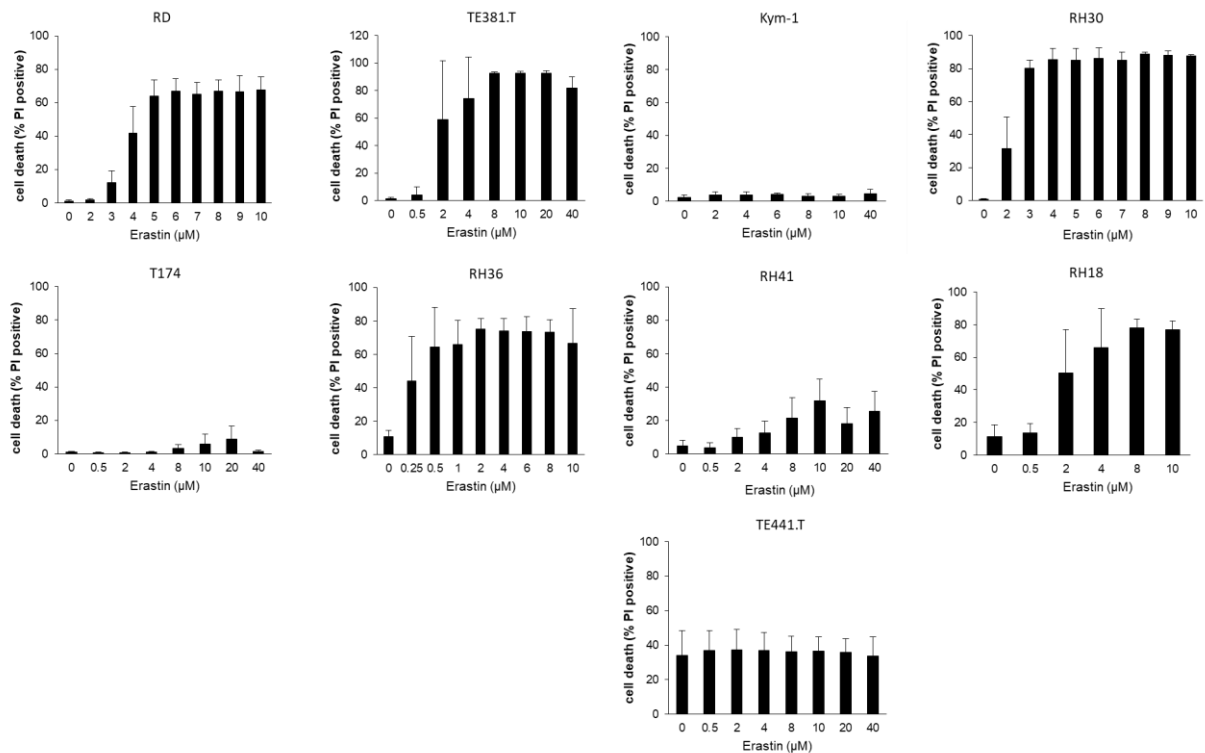


Figure 34: Detailed cell death induction of RMS after 24 hours of Erastin treatment.

Cell death of either RAS mutated (first and second) or RAS WT (third and fourth) after 24 hours of Erastin treatment. PI-positive cells were determined using PI/Hoechst-staining and the fluorescence microscope. Mean and SD of at least three experiments performed in triplicates are shown

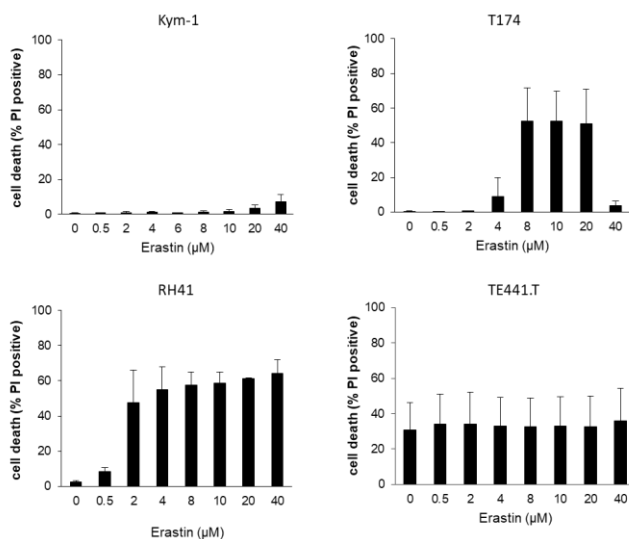


Figure 35: Detailed cell death induction of RMS after 48 hours of Erastin treatment.

Cell death of either RAS mutated (T174) or RAS WT (RH41, TE441.T) after 48 hours of Erastin treatment. PI-positive cells were determined using PI/Hoechst-staining and the fluorescence microscope. Mean and SD of at least three experiments performed in triplicates are shown.

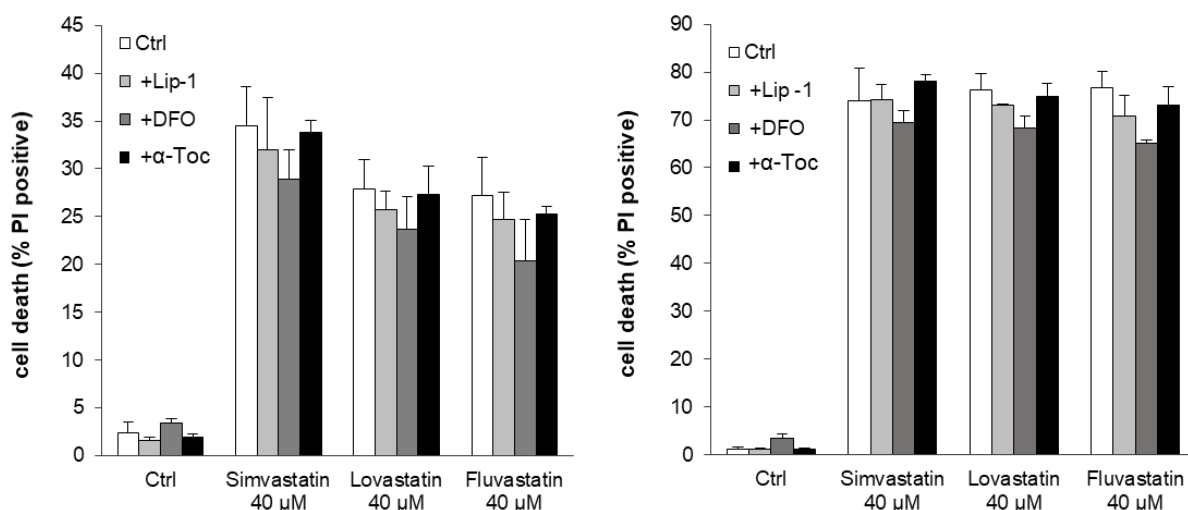


Figure 36: Statins do not induce ferroptosis.

RD (left) and RH30 cells (right) were treated with Simva-, Lova- and Fluvastatin for 48 hours in the presence or absence of Lip-1 (25 nM) and DFO (25 μM), which were added two hours before. PI-positive cells were determined using PI/Hoechst-staining and the fluorescence microscope. Erastin treatment was used as positive control. Mean and SD of three experiments performed in triplicates are shown.

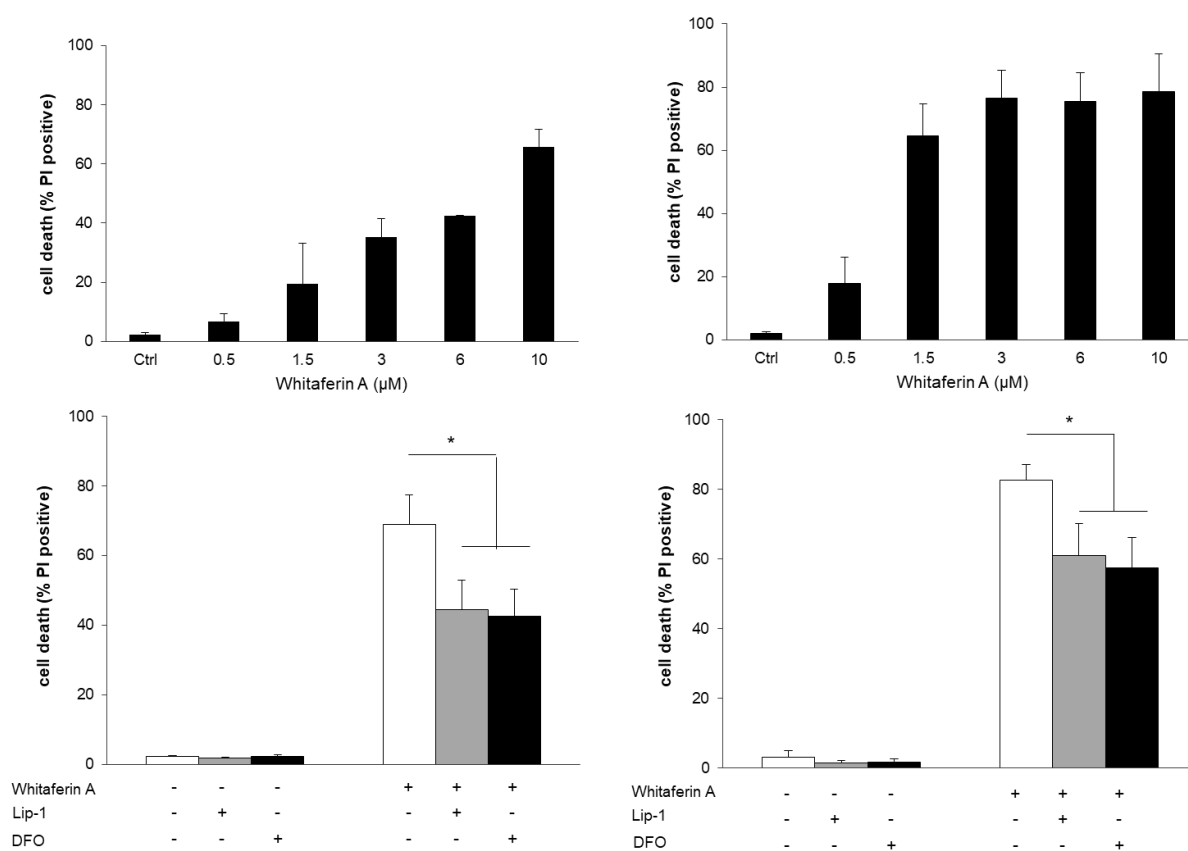


Figure 37: Whitaferin A does not trigger classical ferroptosis.

RMS cells (RD left, RH30 right) were treated for 24 hours with indicated Whitaferin A concentrations (upper panel). RD and RH30 were treated with Whitaferin A (RD: 10 μM; RH30: 3 μM) for 24 hours in the presence or absence of Lip-1 (25 nM) and DFO (25 μM) (lower panel), which were added two hours prior treatment. PI-positive cells were determined using PI/Hoechst-staining and the fluorescence microscope. Erastin treatment was used as positive control. Mean and SD of three experiments performed in triplicates are shown; *, $P < 0.05$.

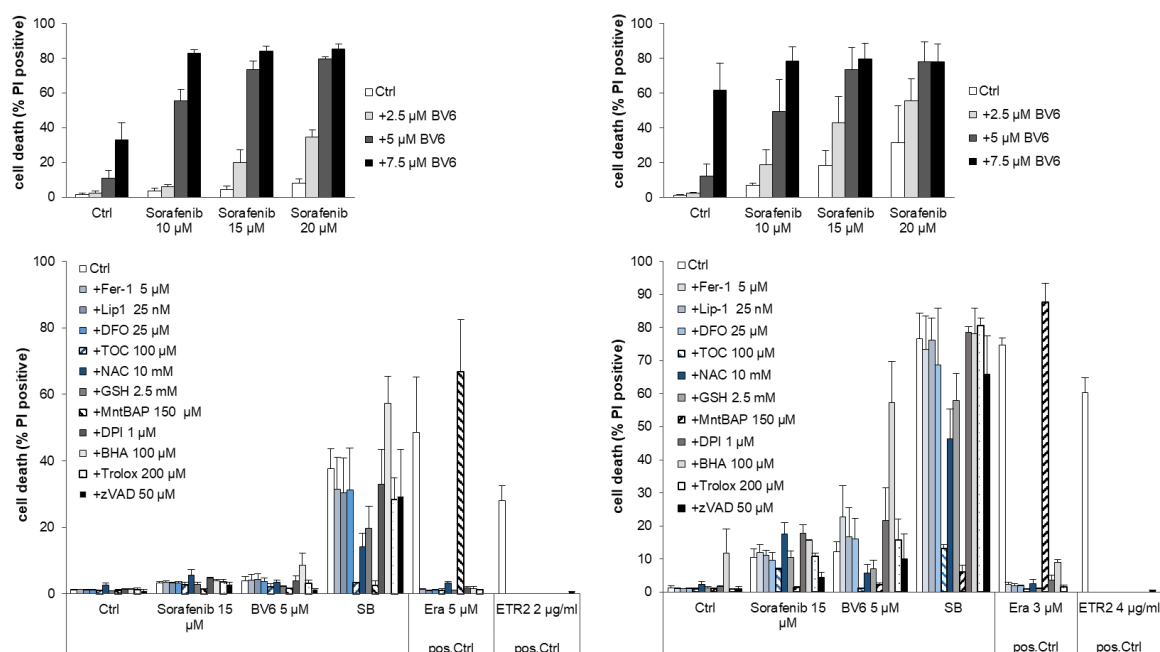


Figure 38: Sorafenib and BV6 in combination stimulate oxidative stress that is independent of ferroptosis. RD (left) and RH30 cells (right) were treated with indicated Sorafenib and BV6 concentrations for 24hours. Erastin was used as positive control for two hours preincubated ferroptosis inhibitors, DFO, α -Tocopherol, NAC, GSH, BHA, Trolox in indicated concentration, whereas ETR2 was used as positive control for zVAD in indicated concentrations. Cell death was diminished significantly through α -Tocopherol (RD, RH30: ***, $P < 0.001$.), NAC (RD: **, RH30: *, $P < 0.05$; ** $P < 0.01$), GSH (RD, RH30:*, $P < 0.05$) and MnTBAP (RD, RH30:***, **** $P < 0.001$). PI-positive cells were determined using PI/Hoechst-staining and the fluorescence microscope. Mean and SD of at least three experiments performed in triplicates are shown; *, $P < 0.05$; **, $P < 0.01$; ***, $P < 0.001$.

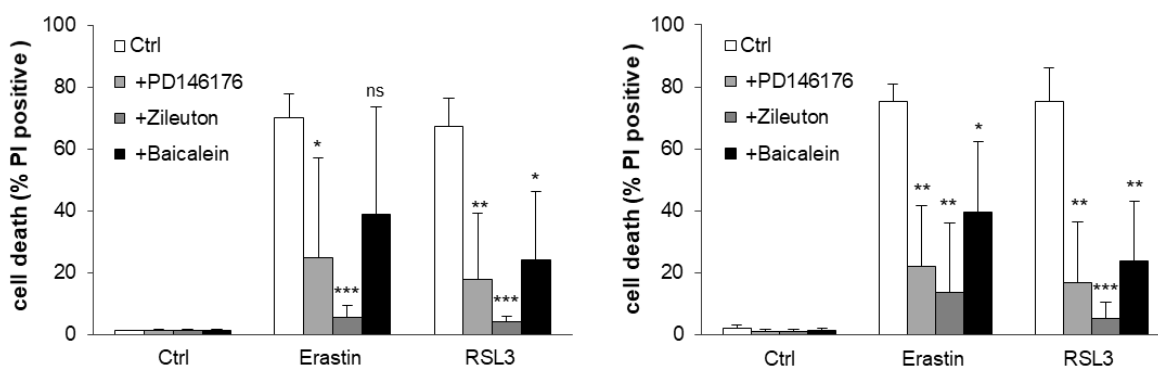


Figure 39: Different LOX inhibitors rescue from Erastin- and RSL3-induced ferroptosis in RMS. RMS cells (RD left, RH30 right) were treated with Erastin for 24 hours (RD 5 μ M, RH30 3 μ M) and RSL3 (RD 1 μ M, RH30 0.4 μ M) in the presence or absence of LOX inhibitors (PD146176 1 μ M, Zileuton 5 μ M, Baicalein 2 μ M) which were added two hours before. PI-positive cells were determined using PI/Hoechst-staining and the fluorescence microscope. Erastin treatment was used as positive control. Mean and SD of at least three experiments performed in triplicates are shown; *, $P < 0.05$; **, $P < 0.01$; ***, $P < 0.001$.

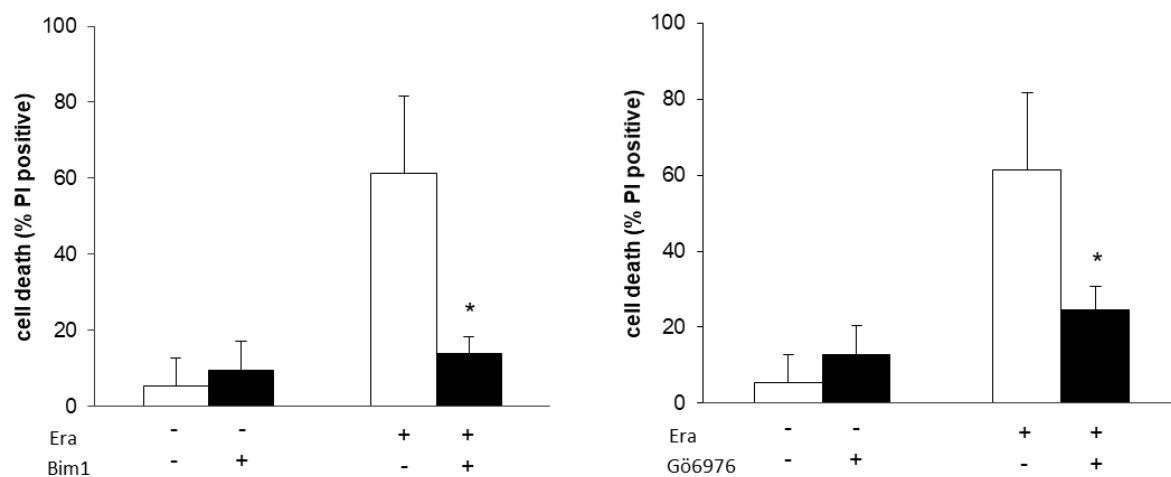


Figure 40: PKC inhibitors rescue from Erastin-induced cell death in RH36.

RH36 cells were treated with Erastin for 24 hours in the presence of absence of broad spectrum PKC inhibitor Bim1 and α and β selective PKC inhibitor Gö6976, which were added two hours before treatment. PI-positive cells were determined using PI/Hoechst-staining and the fluorescence microscope. Mean and SD of three experiments performed in triplicates are shown; *, $P < 0.05$; **, $P < 0.01$; ***, $P < 0.001$.

Acknowledgement

First of all, I would like to thank Prof. Dr. Simone Fulda for providing me the possibility to perform my PhD thesis in the well-equipped laboratory of the institute for experimental cancer research in pediatrics and for her support, discussions and advices during my thesis.

Also, I thank Prof. Dr. Volker Dötsch from the institute of biophysical chemistry for taking on the responsibility of supervising my project and for evaluating this thesis.

I also like to thank the Frankfurter Stiftung für krebskranke Kinder and all the generous donors for supporting our research, especially this study.

A big thanks goes to Christina Hugenberg, for her goodness and sympathetic ear, as well as for her advices to solve bureaucratic and non-bureaucratic problems.

Thanks to all former and current lab members for your never ending humour, good vibes, discussions, input and support. I also thank Daniela Brücher, Sonja Smith and the „Rhabdo-Crew“ for all the support and help in the lab and Katharina Belz for supervising me in my first year. Also I want to highlight a few people, which enriched my life during the last years. A big thank you goes to Karoline, Lara, Tanja, Svenja, Anna, Nadine, Michael, Sebastian, Florian and Sjoerd, for fruitful discussions, proofreading my manuscript and all the amazing moments we shared in- and outside the lab. Thanks to Vanessa, for being the nicest and active fosterling.

And finally, I would like to say thank you to all my friends, my whole family and especially Kolja for always supporting me in every decision I made, for the help, for your belief in me, for your endless motivations to go on and for always being there for me whenever I need you.

Eidesstattliche Versicherung

Ich erkläre hiermit an Eides Statt, dass ich die vorgelegte Dissertation mit dem Titel „Oxidative stress-induced cell death in paediatric cell lines“ selbstständig angefertigt und mich anderer Hilfsmittel als der in ihr angegebenen nicht bedient habe, insbesondere, dass alle Entlehnungen aus anderen Schriften mit Angabe der betreffenden Schrift gekennzeichnet sind.

Ich versichere, nicht die Hilfe einer kommerziellen Promotionsvermittlung in Anspruch genommen, sowie die Grundsätze der guten wissenschaftlichen Praxis beachtet zu haben.

Frankfurt am Main, den 14.06.2018

Curriculum Vitae

Personal Data:

Name: Jasmin Dächert

Address: Rebstöcker Straße 16, 60326 Frankfurt

E-Mail: j.daechert@gmx.de

Phone: 0176 32469929

Date of birth: 10.08.1989

Place of birth: Seeheim-Jugenheim

Academic education:

11/2014 – 05/2018

Goethe-Universität Frankfurt

Institute for experimental cancer research in pediatrics

Course of study: Biochemistry

Degree: Dr. phil. nat. (prospective)

10/2012 – 09/2014

Philipps-Universität Marburg

Course of study: Human biology

Degree: Master of Science (1.3)

10/2009 – 09/2012

Johannes Gutenberg-Universität Mainz

Course of study: Molecular biology

Degree: Bachelor of Science (1.5)

08/2000 – 09/2009

Edith-Stein-Schule Darmstadt (Gymnasium)

Qualification: Abitur (1.9)

Publications

05/2018

Oncotagret (under revision 05/2018)

Targeting ferroptosis in rhabdomyosarcoma cells (Dächert et al. 2018)

09/2017

Biochemical Pharmacology

Lipoxygenase inhibitors protect acute lymphoblastic leukemia cells from ferroptotic cell death (Probst et al. 2017, shared first authorship)

09/2016**Oncotarget**

RSL3 and Erastin differentially regulate redox signaling to promote Smac mimetic-induced cell death (Dächert et al. 2016, shared first authorship)

Conferences (Poster presentation)**10/2017**8th UCT Science Day**03/2017**19th International AEK Cancer Congress**10/2016**7th UCT Science Day**08/2015**4th Talented Academy of Paediatric Oncology**Special skills****Languages**

German: native language

English: Business fluent

French: good knowledge

Spanish: basic knowledge

Computer skills

Microsoft Office

Laboratory-based (FlowJo, FACSDiva,

Image-Xpress, ImageJ)

Writing-based (Endnote, Mendeley, Citavi)

Frankfurt am Main, June 2018

Jasmin Dächert